

ABSTRACT

TWO-DIMENSIONAL NONLINEAR ANISOTROPIC ELASTIC AND
IN-VIVO PHYSIOLOGIC PROPERTIES OF THE STEER
THORACIC AORTA BASED ON IN-VITRO BIAXIAL TESTING

By

Joseph J. Manak

Master of Science in Engineering

Youngstown State University, 1977

Submitted in Partial Fulfillment of the Requirements

for the Degree of

Master of Science in Engineering

in the

Mechanical Engineering

Program

Lloyd E. Morris 4-11-77
Advisor Date

Allen Rand 5/16/77
Dean of the Graduate School Date

YOUNGSTOWN STATE UNIVERSITY

June, 1977

ABSTRACT

TWO-DIMENSIONAL NONLINEAR ANISOTROPIC ELASTIC AND
IN-VIVO PHYSIOLOGIC PROPERTIES OF THE STEER
THORACIC AORTA BASED ON IN-VITRO BIAXIAL TESTING

Joseph J. Manak

Master of Science in Engineering

Youngstown State University, 1977

A Biaxial Test Program was conducted for the purpose of determining the in-vitro stress-strain-elasticity relationships of the steer thoracic aorta blood vessel material under the condition of plane stress (two-dimensional) loading. The non-linear anisotropic properties of the incompressible material are described in Chapter VI. Applying the in-vitro properties of the material to the in-vivo or physiologic condition of normal blood vessel pulsatile pressure and longitudinal tethering loadings, the functional characteristics of the blood vessel are determined for the in-vivo state. Physiologic predictions of vessel wall distensibility, wall stresses and strains, modulus of elasticity, and hemodynamic characteristics, are made based on the in-vitro properties of the aorta material. These analytical predictions are compared with the in-vitro and in-vivo experimental findings of other investigators and are found to be in good agreement.

TABLE OF CONTENTS

	PAGE
ABSTRACT	ii
TABLE OF CONTENTS	iii
LIST OF SYMBOLS	vi
LIST OF FIGURES	viii
LIST OF TABLES	x
CHAPTER	
I. INTRODUCTION	1
Introduction	1
II. RHEOLOGY OF LARGE BLOOD VESSELS	4
Introduction	4
Material Composition	5
Physiologic Loading and Geometry	7
Elastic Symmetry	9
Vessel Wall Thickness	11
Incompressibility	11
Wall Stress Equations	12
Definitions of Strain	14
III. AXIAL SPECIMEN TESTING	20
Introduction	20
Thoracic Aorta Specimen-Location and Data	20
Testing	25
True Stress	27
Test Results and Discussion	28

	PAGE
IV. DETERMINATION OF THE TANGENTIAL EXTENSION RATIOS FOR IN-VIVO SIMULATION-BIAXIAL TESTING	37
Introduction	37
Determination of the Strain Energy Coefficients.	39
Calculation of λ_{\ominus} Values	41
Conclusion	43
V. BIAXIAL TESTING	45
Introduction	45
Test Specimen, Set-up, Instrumentation	45
Test Procedure	52
Test Data	53
VI. ANALYSIS AND RESULTS OF BIAXIAL TESTING	58
Introduction	58
Analysis	58
Strain Energy Gradient	58
Stress-Strain Relations	63
Comparison-Biaxial and Axial σ - λ Results	66
Strain-Stress Relations	69
Modulus of Elasticity	71
Summary and Discussion of Results	75
Stress-Strain	78
Modulus of Elasticity	81
Conclusions	85

	PAGE
VII. PHYSIOLOGIC ANALYSIS	88
Introduction	88
Analysis	89
Physiologic Analysis Summaries	93
Discussion of the Physiologic Results	100
λ_e Comparison - Biaxial Test vs In-Vivo	100
Incompressibility-Accuracy	102
Vessel Wall Thinness	103
Hemodynamic Observations	104
Longitudinal Characteristics	106
Tangential Stress and Strain	113
Wall Deformation and Distensibility	117
In-Vivo Modulus of Elasticity	120
Conclusion	125
VIII. SUMMARY	127
BIBLIOGRAPHY	130

Strain Energy Density Function g/cm^2

Longitudinal Location cm

Stress (Kirchhoff) ca/cm

Strain (Cauchy) ca/cm

Stress (Nenky) cm/cm

True Stress gm/cm^2

Mean True Stress gm/cm^2

Distension Ratio cm/cm

LIST OF SYMBOLS

SYMBOL	DEFINITION	UNITS
a	Longitudinal Length	cm
b	Tangential Length	cm
d	Mean Wall Diameter	cm
E	Tangent Modulus of Elasticity	gm/cm ²
F	Longitudinal Force	gm, gm/cm
h	Wall Thickness	cm
L	Length	cm
p	Pressure	cm H ₂ O
P	Applied Load	gm
q	Fluid Flow Parameter	cm ² , cm ³
\bar{q}	Shear Force per unit of Longitudinal Length	gm/cm
r	Radius, Correlation Coefficient	cm, None
SD	Standard Deviation	
SEM	Standard Deviation of the Mean	
w	Width of Specimen	cm
W	Strain Energy Density Function	gm/cm ²
Z	Longitudinal Location	cm
ϵ	Strain (Kirchhoff)	cm/cm
$\bar{\epsilon}$	Strain (Cauchy)	cm/cm
$\bar{\epsilon}'$	Strain (Hencky)	cm/cm
σ	True Stress	gm/cm ²
$\bar{\sigma}$	Mean True Stress	gm/cm ²
λ	Extension Ratio	cm/cm

LIST OF SYMBOLS - Continued

SYMBOL	DEFINITION	PAGE
	- Subscripts -	
A	Cross-Sectional Area	19
m	Mean Value or Midwall	21
n	(r, θ , z) directional notation	24
o	Unstressed Condition, In-vitro or In-vivo	29
r, θ , z	Radial, Tangential, Longitudinal directions	29
s	Shear	30
t	Tension	31
v	Volume per Unit of Longitudinal Length	31
	9. Variation of σ vs r Properties of the Upper Site	37
	10. Variation of σ vs r Properties at the Middle Site	38
	11. Variation of σ vs r Properties at the Lower Site	39
	12. Diagram of Biaxial Test Set-Up	46
	13. Biaxial Test Specimen and Extension (r / Gage)	47
	14. Photographs of Specimen and Biaxial Test Set-Up	48
	15. Strain Energy Gradient $dW/d\epsilon_2$ vs-Tangential Strain ϵ_2	60
	16. Strain Energy Gradient $dW/d\epsilon_2$ vs-Longitudinal Strain ϵ_2	61
	17. True Tangential Stress-vs-Tangential Strain	64
	18. True Longitudinal Stress-vs-Longitudinal and Tangential Strain	65
	19. Comparison of Biaxial Test Stress-Strain Equations with Axial Test Specimen Data	67
	20. Tangential and Longitudinal Modulus of Elasticity-vs-Strain	74

LIST OF FIGURES

FIGURE	PAGE
1. Loading and Geometry of an Arterial Segment	7
2. Prismatic Strain Element	15
3. Comparison of Strain Measures	19
4. Steer Thoracic Aorta-In-Vitro: Specimen Site Location, Geometry, and Nomenclature	21
5. Unstressed Circumference and Wall Thickness-Vs-Thoracic Location-In-Vitro	24
6. Comparison of Axial Directional Stress-Strain Properties at Three Aorta Sites	29
7. Tangential σ vs λ Characteristics Relative to Site Location	30
8. Longitudinal σ vs λ Characteristics Relative to Site Location	31
9. Variation of σ vs λ Properties at the Upper Site	32
10. Variation of σ vs λ Properties at the Middle Site	33
11. Variation of σ vs λ Properties at the Lower Site	34
12. Diagram of Biaxial Test Set-Up	46
13. Biaxial Test Specimen and Extension (λ) Gage	47
14. Photographs of Specimen and Biaxial Test Set-Up	48
15. Strain Energy Gradient $dW/d\epsilon_e$ -vs-Tangential Strain ϵ_e .	60
16. Strain Energy Gradient $dW/d\epsilon_z$ -vs-Longitudinal Strain ϵ_z	61
17. True Tangential Stress-vs-Tangential Strain	64
18. True Longitudinal Stress-vs-Longitudinal and Tangential Strain	65
19. Comparison of Biaxial Test Stress-Strain Equations with Axial Test Specimen Data	67
20. Tangential and Longitudinal Modulus of Elasticity-vs- Strain	74

FIGURE	PAGE
21. Tangential Stress-Strain-vs-Thoracic Aorta Location . . .	79
22. Longitudinal Stress-Strain-vs-Thoracic Aorta Location . .	80
23. Tangential Modulus of Elasticity-vs-Thoracic Aorta Location	82
24. Longitudinal Modulus of Elasticity-vs-Thoracic Aorta Location	84
25. Variation of Initial Modulus-vs-Aorta Longitudinal Location	86
26. Thick Wall Cylinder Tangential Stress Correction Factor K	92
27. Physiologic Data at Upper Aorta Location-vs-Internal Pressure	96
28. Physiologic Data at Middle Aorta Location-vs-Internal Pressure	97
29. Physiologic Data at Lower Aorta Location-vs-Internal Pressure	98
30. Thoracic Aorta Distensibility Curves: In-Vivo	99
31. Longitudinal Loading of the Descending Thoracic Aorta . .	109
32. Physiologic Modulus of Elasticity-vs-Aorta Longitudinal Position	121

LIST OF TABLES

TABLE	PAGE
1. Animal Data and Aorta Specimen Thickness and Circumference (Unstressed-In-Vitro)	23
2. Principal Extension Ratio Combinations for Biaxial Specimen Testing	44
3. Biaxial Stress Data, Middle Location, Z = 12 cm	56
4. Biaxial σ/ϵ_n Data, Middle Location, Z = 12 cm	57
5. Summary of Coefficients for Polynomial Equation (38)	76
6. Summary of Coefficients for Polynomial Equation (39)	77
7. Summary of Initial Modulus and Aorta Location	83
8. Summary of Physiologic Data	94

smooth membrane muscle, including the major blood vessels of the venous, pulmonary, and arterial systems. The principles of fluid mechanics have been used to determine preliminary flow characteristics through tapered vessels of both large and blood cell size vessels, through bifurcations, and even within the major organs such as the ventricles and valves of the heart, chambers of the lungs, and the functioning of the kidneys. The results of such research are contained in the writings of Fung², Bergel³, and Kirshy⁴.

During this period, most of the work conducted in the area of determining basic material properties and characteristics has been limited to uniaxial type of testing. It has long been realized that the two or three-dimensional material properties of biological tissues under conditions of normal physiologic loading strains must eventually be defined. The non-linear and viscoelastic nature of biological materials under the influence

CHAPTER I

INTRODUCTION

In the past thirty years the application of engineering principals to the understanding of the human body and to the design of artificial limbs and organs has been dramatic. In this time period much research and experimental work has focused on the basic principals underlying muscle mechanics (stratified and cardiac), the biological tissue material properties of skin and smooth membrane muscle, including the major blood vessels of the venous, pulmonary, and arterial systems. The principals of fluid mechanics have been used to determine preliminary flow characteristics through tapered vessels of both large and blood cell size vessels, through bifurcations, and even within the major organs such as the ventricles and valves of the heart, chambers of the lungs, and the functioning of the kidneys. The results of such research are contained in the writings of Fung², Bergel³, and Mirsky⁸.

During this period, most of the work conducted in the area of determining basic material properties and characteristics has been limited to uniaxial type of testing. It has long been realized that the two or three-dimensional material properties of biological tissues under conditions of normal physiologic loading strains must eventually be defined. The non-linear and viscoelastic nature of biological materials under the influence

of natural state(pre-stress) and physiologic pressure loading results in finite or large deformations(20 to 70% elongations) under normal physiological conditions. The effects of hypertension, hypertrophy, drugs, disease, and nervous system activity cannot be assessed until the normal state of the tissue, muscle, or blood vessel material is accurately defined. The determination of the two or three-dimensional material properties of the major blood vessels will lead to:

1. An improved understanding of the static and dynamic properties and characteristics of the material involved under the influence of interacting stresses and deformations in the in-vivo state.
2. The design and development of improved materials for prosthesis or artificial organs which more closely simulates the in-vivo or natural state of the organ or tissue.
3. A more accurate description of the fluid flow static and dynamic boundary conditions to be used in the solution of hemodynamic problems at such locations as bifurcations, heart valves, and throughout the wide ranging arterial and venous systems.

The purpose of this thesis is to report the results and findings of a biaxial test program conducted during the summer of 1976 by the writer at the Pennsylvania State University Engineering Science and Mechanics Department. During this period a relatively simple and inexpensive biaxial test set-up was designed, assembled, and used to determine the two-dimensional (plane stress) material properties of the Steer Thoracic Aorta at three longitudinal locations along its length. The tests were conducted in-vitro. From the test results the two-dimensional constitutive equations of stress vs strain, modulus of elasticity vs strain, and other material characteristics can be derived.

Using such equations, which describe the passive or steady state characteristics of the aorta material in-vitro, the functional physiological characteristics of the vessel in-vivo, such as diameter changes, principal stresses and strains, and volume can be estimated without the need for performing in-vivo tests. The two-dimensional material properties and the resulting physiologic analysis is contained within Chapters VI and VII respectively.

The tests conducted in this study, and the resulting analysis and findings, represent a "first time" successful accomplishment in the area of major blood vessel or biological tissue rheology. Lanir and Fung¹⁵ in 1974 reported the design of a very intricate and expensive biaxial test apparatus for similar investigative purposes. Using their apparatus and working with rabbit skin Lanir and Fung¹⁶ reported the results of some preliminary two-dimensional materials properties. For some unknown reason no attempt was made to conduct the tests under varying combinations of two-dimensional tension strains which would facilitate the determination of the constants in the constitutive equations for the material.

CHAPTER II

RHEOLOGY OF LARGE BLOOD VESSELS

Introduction

The large blood vessels of the animal body are generally classified as being those vessels which either supply blood to the heart(venous system) or which returns the blood from the heart(arterial system) to the various body organs and tissues. Excluded from this classification are the small arteries, capillaries, and the small veins. Thus, "large vessels" herein refer to the ascending and descending aorta(thoracic aorta) artery which supply the major organs and arteries of the body with fresh oxygenated blood under pulsatile flow conditions as supplied by the left ventricle of the heart during the period of systole.

At the instant of aortic valve opening, the heart ejects blood at a pressure of 80 to 100 mm Hg. The cardiac muscle then contracts with increasing muscle fiber shortening velocity thereby ejecting the fluid with increasing pressure and high velocity with final peak pressure build-up being in the range of 120 to 140 mm Hg. At the completion of ejection the aortic valve closes, the muscle relaxes for a short period, and refilling(diastole) of the ventricle begins. Thus, the heart is an intermittent pump which releases blood to the arterial system at a frequency of 70 to 80 cycles per minute. The blood ejected into the ascending and thoracic

aorta is in the condition of pulsatic flow rate and pressure. If the heart released such flow into a relatively stiff vessel the benefits of the high velocity pulsatile flow would be diminished in terms of forcing the blood efficiently into the smaller arteries of the body. Thus, the ascending and thoracic aorta is a flexible tube which due to its low and varying longitudinal elasticity characteristics aids in the transmission of the pressure wave thru the arterial system in a most efficient manner.

Discussed in the following paragraphs is information pertaining to the rheology of blood flow thru the large vessels. While the basic purpose of the thesis concerns itself with the thoracic or descending region of the steer aorta, the information is applicable to all large blood vessels in general. The basic characteristics of such blood vessels are that they display non-linear passive and non-linear viscoelastic material properties under the influence of in-vivo environmental loadings. This thesis concerns itself with obtaining knowledge relative to the in-vitro passive properties of the aorta tissue, i.e.: constitutive equations of the material under the influence of steady state or near steady state loading, and the behavior of the in-vivo vessel under the condition of pulsatile loading.

Material Composition

Like most biological tissues, the blood vessel tissue is composed of a complex parallel assembly of collagen fibers wound loosely around the less stiff elastin fibers which lay within a gelatinous matrix of smooth muscle tissue having high liquid

content. Further complicating the physical properties of the composite material is the fact that both the directional arrangement and the relative quantities of the collagen and elastin constituents vary with longitudinal position along the length of the vessel. This is particularly true for the ascending and thoracic regions. Thus, while the tissue material can be considered as being homogeneous at a given location, or for a particle, it is non-homogeneous over a short distance of its length.

Bergel⁹ summarizes the elastic modulus(E) of the arterial wall constituents as being:

collagen	100-1000	(dynes/cm ² X 10 ⁶)
elastin	5-10	"
smooth muscle	0.1-2.5	"

As we shall see in Chapter III the wide range in the elastic moduli of the fibers(as indicated above), the relative size of the fiber diameters, and the fact that the collagen fibers are initially loose(not taut relative to the smaller diameter elastin fibers) all contribute to the non-linearity displayed in the material stress-strain relationship. Thus, the material displays non-Hookean response, i.e.: stress is not linearly related to strain through a proportionality constant called the modulus of elasticity(E), or: $\sigma \neq E\epsilon$. This same characteristic can also be found in such engineering materials as rubber(natural and synthetic) and most soft polymers.

Physiologic Loading and Geometry

The blood vessels can be considered to be hollow tubes transmitting flow under constant or pulsatile pressure(p) causing diametrical or tangential deformation and wall stresses. They are also subjected to a longitudinal tethering force(F). Figure 1 shows the loading of an arterial segment, its geometry, and the principal stress element of the wall material. The sign convention for positive forces, stresses, and directions is shown.

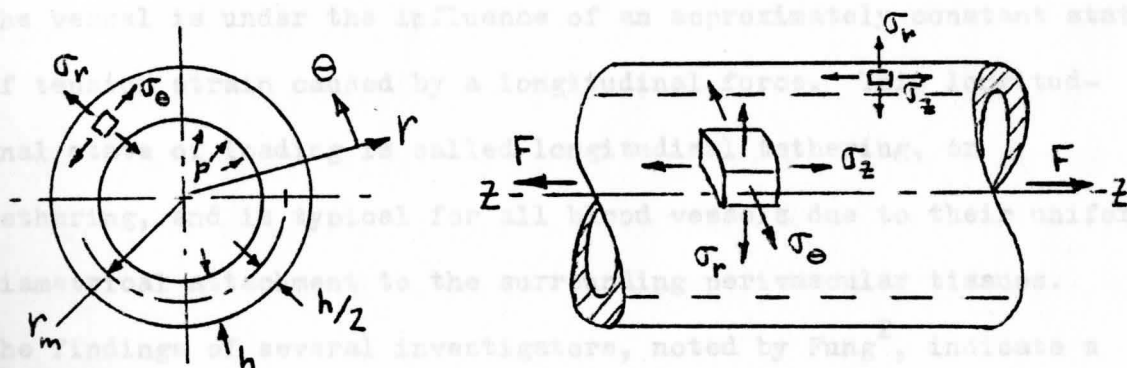


Figure 1 - Loading and Geometry of an Arterial Segment

Pressure Loading - The internal pressure of the blood for normal, healthy animals in the thoracic aorta locale is pulsatile having a mean pressure of approximately 150 to 160 cm H₂O and a pulse pressure variation ranging from 20 to 40 cm H₂O in magnitude. Dukes¹ states that the normal resting steer aorta pressures are approximately 143, 156, and 169 cm H₂O for the minimum, mean, and maximum pressure values. Values of 140, 155, and 170 cm H₂O will

be used in the following chapters. Under the abnormal physiologic conditions of hypertension and hypertrophy the above values of pressure would not be valid. The fluid pressure acting on an element of the tissue produces radial (σ_r) and tangential (σ_θ) stresses within the material. Thus, deformations of the wall material are principally radial and circumferential in nature.

Longitudinal Loading - When a blood vessel is excised during in-vivo experiments the vessel is found to contract a significant amount causing the cut edges to become separated from each other. This indicates that in the natural state (in-vivo) the vessel is under the influence of an approximately constant state of tension strain caused by a longitudinal force. This longitudinal state of loading is called longitudinal tethering, or tethering, and is typical for all blood vessels due to their uniform diametrical attachment to the surrounding perivascular tissues. The findings of several investigators, noted by Fung², indicate a percent contraction of the excised vessel ranging from 25-34% for both dog and man. Thus, the in-vivo stretch or extension ratio of the vessel is approximately $\lambda_z = 1.30$ under normal steady state conditions. The longitudinal extension ratio is defined as follows:

$$\lambda_z = \frac{\text{in-vivo length(stressed)}}{\text{in-vitro length(unstressed)}} = \frac{L}{L_0}$$

Patel and Fry¹⁰ carried out experiments (static and dynamic) both in-vivo and in-vitro which studied the properties of longitudinal tethering of the dog aorta under the physiologic influence of both steady state and pulsatile pressures. Their findings show that for normal physiologic pulsatile pressure loading, the static

and dynamic properties are essentially linear and approximately constant due to the small cyclic strains caused by the internal fluid friction forces and the viscous nature of the perivascular inertia forces. The characteristics of tethering could be mathematically modeled using a spring-mass-damper system which verified that the static and dynamic modulus of the wall tissue is linear with only a small phase angle ($< 10^{\circ}$) lag in the 1 to 10 Hertz range. The linearity of the tissue properties in the longitudinal direction was again verified by Patel, et al.¹¹, in their investigations which were conducted to verify the "incremental theory", reference Bergel³.

Since this investigation is concerned with the in-vitro simulation of in-vivo loading of the aorta material the tethering force (F) was simulated by applying constant longitudinal extension (strain) ratios of $\lambda_z = 1.25, 1.30, \text{ and } 1.35$ to the biaxial test specimens.

Elastic Symmetry

Due to the nature of the material constituents of the aortic blood vessel wall, previously described, the question was raised as to whether there exists significant internal shear stresses within the tissue and thus whether the geometric axes (r, θ , z) could be considered to be the principal stress-strain axis for the material under the physiologic loading of internal pressure and tethering force. The significant variation of the material constituents relative to site location along the aorta

tree, at first glance, would indicate that the directional or orthotropic properties would result in significant shear strains and thus the principal strain axis would not coincide with the geometric or loading axis. For this purpose Patel and Fry¹² conducted ingenious tests using long segments of the descending aorta, abdominal aorta, and of the common carotid artery under physiologic ranges of pressure and simulated tethering forces. The tests consisted of measuring circumferential and longitudinal strains including shear strains (angle of rotation) in the longitudinal-circumferential and the radial-circumferential directions under conditions of varying pressure and longitudinal forces. Their results show that under normal physiologic loading ($p < 180 \text{ cm H}_2\text{O}$) the shear strains are not zero in magnitude, but are definitely an order of magnitude less than the circumferential and longitudinal strains. They conclude that blood vessels can be considered to be cylindrically orthotropic tubes having elastic symmetry about the planes perpendicular to the r , θ , and z directions. Thus, the principal stresses and directions, as shown in Figure 1, are applicable and represent the only significant stresses which act within the vessel wall material. Thus, elastic symmetry will be assumed in this work.

The significance of these findings is that torsional deformation of the interior (lumen) surface is minimal, wall surface and wall nutrition is not compromised, and that geometric torsional disfiguration and fluid friction forces are minimal at conduit geometries such as bifurcations and small artery branches found at

various locations along the length of the major blood vessels.

Vessel Wall Thickness

While the longitudinal stress, σ_z , is a function of the wall radius and thickness, calculation of the tangential wall stress, σ_θ , requires that the vessel wall be classified as being either a thin or thick wall cylinder. Bergel⁹ and Learoyd¹³ report that the physiologic in-vivo ratio of mid-wall radius to wall thickness (r_m/h) ranges from approximately 7.1 to 16.6 for the thoracic aorta of man and dog. Thus, the aorta wall can be classified as "thin wall" meaning that the tangential and longitudinal stress distributions across its thickness are approximately constant. This assumption will be used in subsequent chapters but when necessary it will be corrected for any significant deviation from the thin wall theory which is applicable for ratios of $r_m/h \geq 10$.

Incompressibility

It is generally recognized that rubberlike materials, Treloar⁴, which are capable of sustaining large and non-linear deformations (as large as 100 to 600% elongation) exhibit a very low degree of compressibility. This is contrary to most engineering materials, ferrous and non-ferrous, which exhibit the property of being a compressible material within their elastic range. Prior to 1968 extensive experimental investigations of biological materials left the question of incompressibility in a state of

confusion. Carew¹⁴ conducted extensive tests along the aortic tree, pulmonary artery, and the common carotid artery and concluded that "for most practical purposes arteries may be considered incompressible." The findings of Carew essentially settled the question and have since been recognized as being conclusive. Thus, the aorta wall material will be considered to have infinite resistance to material volume change under a state of deformation. This means that for a cube of material having sides of unit length in the undeformed condition that in the deformed condition the product of its three principal stretch ratios, or lengths, will be equal to unity. This will subsequently be shown below and in Figure 2. The condition of material incompressibility simplifies theoretical and experimental work whether we classify strain in the biological engineering sense as extension ratios(λ), or as per large deformation theory(ϵ).

Wall Stress Equations

If a longitudinal plane containing the z and r-axis is passed thru the arterial segment of Figure 1 and a free body diagram of the cut thin wall segment is drawn we obtain from equilibrium considerations the relationship for the true tangential wall stress, σ_{θ} , as being

$$\sigma_{\theta} = pr_m/h, \quad \text{gm/cm}^2 \quad (1)$$

where: p = internal pressure, cm H₂O.

r_m = mid-wall radius in the stressed condition, cm.

h = wall thickness in the stressed condition, cm.

Equation (1) represents the true tangential wall stress based on the deformed geometry of the blood vessel wall.

Similarly, by passing a vertical plane through the segment containing the Θ and r-axis we obtain the relationship for longitudinal wall stress, σ_z , as:

$$\sigma_z = F/2 \pi r_m h, \quad \text{gm/cm}^2 \quad (2)$$

where: F = longitudinal force, grams

for an open vessel with an applied tethering force, or:

$$\sigma_z = F/2 \pi r_m h + pr_m/2h \quad (3)$$

for a closed end vessel with an applied tethering force, as is usually required in the testing of vessel segments in-vitro. Equation (2) represents the in-vivo state of longitudinal stress.

The radial stress is simply defined as

$$\sigma_r = -p/2 \quad (4)$$

which is simply the average pressure acting on the inner and outer wall of the thin wall vessel. Normally the value of σ_r is of the magnitude of 70 to 90 gm/cm² which is an order of magnitude less than that of σ_Θ and σ_z which normally exceeds 1000 gm/cm² in the physiologic state. Thus, σ_r is normally assumed to be negligible and is deleted for analytical simplification purposes. For biaxial testing, Chapter V, a plane stress condition exists such that $\sigma_\Theta, \sigma_z > 0$ and $\sigma_r = 0$.

It is important to point out at this time that equations (1) through (3) represent true stresses based on the deformed geometry of the blood vessel under the influence of longitudinal and

pressure loading. This is pertinent because the deformations of the aorta wall material during in-vivo loading are not linear or infinitesimal in magnitude. Instead, the material response to loading is nonlinear and the deformations are finite and significant. Thus, principal stresses based on the original, or unstressed geometry, are both misleading and inaccurate. Use of unstressed dimensions, designated by the subscript "o", will be used, but will be corrected to the deformed state in all cases.

Definitions of Strain

Strain is the measure of deformation of a material relative to some reference dimension such as initial length, volume, or angle. As such, there is no unique measure of strain. Three different measures of strain are the Cauchy measure, Kirchoff measure, and Hencky measure, each of which have its merits.

Figure 2a shows an initially undeformed prismatic element having edge lengths as defined and orientated in the directions of the principal axes, z , θ , and r . This element is deformed (due to loading in the principal directions) into a prismatic element having edge lengths of L_z , L_θ , and L_r and is in the state of zero shear deformation, Figure 2b.

often referred to as "engineering" or "conventional" strain.

The ratio of the deformed length to the original or unstressed length in the direction of loading or deformation

$$\lambda = L/L_0$$

(6)

is commonly referred to as the extension ratio. This measure of

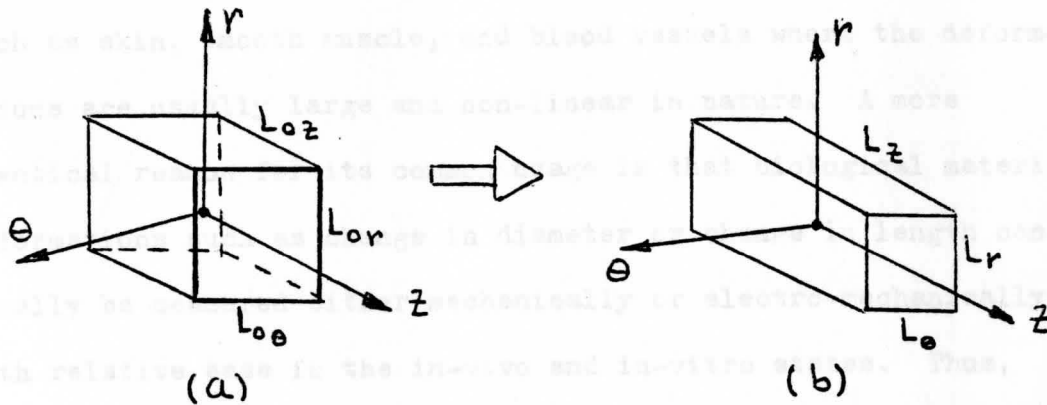


Figure 2 - Prismatic Strain Element

Assuming that the strain is infinitesimal, the strain or elongation per unit of original length in the n th direction is:

$$\bar{\epsilon}_n = \frac{L_n - L_{0n}}{L_{0n}} = \frac{L_n}{L_{0n}} - 1 = \lambda_n - 1 \quad (5)$$

where: $n = z, \theta, r$ principal directions

This measure of strain is called the Cauchy measure and is used for conditions of linear and infinitesimal deformations experienced by most engineering materials including biological materials such as cardiac and skeletal muscle where deformations are usually limited to 3 to 5% of muscle length. Equation (5) is often referred to as "engineering" or "conventional" strain.

The ratio of the deformed length to the original or unstressed length in the direction n of loading or deformation

$$\lambda_n = L_n / L_{0n} \quad (6)$$

is commonly referred to as the extension ratio. This measure of

strain is generalized for finite deformations and is most often used for the measure of strain or deformation of biological tissues such as skin, smooth muscle, and blood vessels where the deformations are usually large and non-linear in nature. A more practical reason for its common usage is that biological material deformations such as change in diameter or change in length can usually be measured either mechanically or electro-mechanically with relative ease in the in-vivo and in-vitro states. Thus, equation (6) will be used hereafter as a unit of measure of strain of the aorta wall tissue during axial and biaxial specimen testing.

Applying equation (6), the extension ratios for the principal stress element of Figure 1(arterial segment) in the three principal directions of element loading can be defined as:

$$\lambda_z = L/L_0 \quad (7a)$$

$$\lambda_e = c/c_0 = d/d_0 = r_m/r_0 \quad (7b)$$

$$\lambda_r = h/h_0 \quad (7c)$$

where: L and L_0 , c and c_0 , d and d_0 , r_m and r_0 , h and h_0 are defined as the stressed and unstressed length, circumference, diameter, radius, and wall thickness of the blood vessel or test specimen.

Note that the stretch ratios exceed the corresponding conventional or Cauchy strains by unity, i.e. $\lambda_n = \bar{\epsilon}_n + 1$, and that:

- a) for the unstressed condition - $\lambda_n = 1.0$, $\bar{\epsilon}_n = 0$
- b) for tensile loading or strain - $\lambda_n > 1.0$, $\bar{\epsilon}_n > 0$
- c) for compressive loading or strain - $\lambda_n < 1, \neq 0$, $\bar{\epsilon}_n < 0$

From the definition of incompressibility given on page 12

we can state mathematically that:

$$\lambda_z \lambda_e \lambda_r = 1.0 \quad (8)$$

The significance of the "Incompressibility Equation", equation (8), is that if any two values of the extension ratio or the strain are known the third value can be conveniently determined. In the case of blood vessels the change in both length and diameter can be measured but the accurate measurement of wall thickness is almost an impossibility both for in-vivo and in-vitro situations. Thus, the incompressibility equation facilitates the determination of λ_r or wall thickness values in both experimental and theoretical analysis.

As we shall see in the following chapters the material stress-extension (σ_n vs λ_n) curves for both the axial and biaxial loading conditions are highly non-linear in character and the physiologic strains exceed $\lambda_n > 1.20$. Such curves show an approximately initial linear region followed by a gradual and finally a sharp exponential relationship of true stress vs strain. For such highly non-linear elastic materials which also display viscoelastic properties the development of a non-linear theory advanced by Rivlin⁶ and Vaishnav¹⁸ proposes the use of the Kirchhoff measure of strain defined as:

$$\epsilon_n = \frac{1}{2}(\lambda_n^2 - 1) \quad (9)$$

which is often referred to as the Green-St. Venant strain. This measure of strain has the distinct advantage of considering non-linearity of the material and has the tendency to linearize the stress-strain equations and thus facilitate ease of calculation.

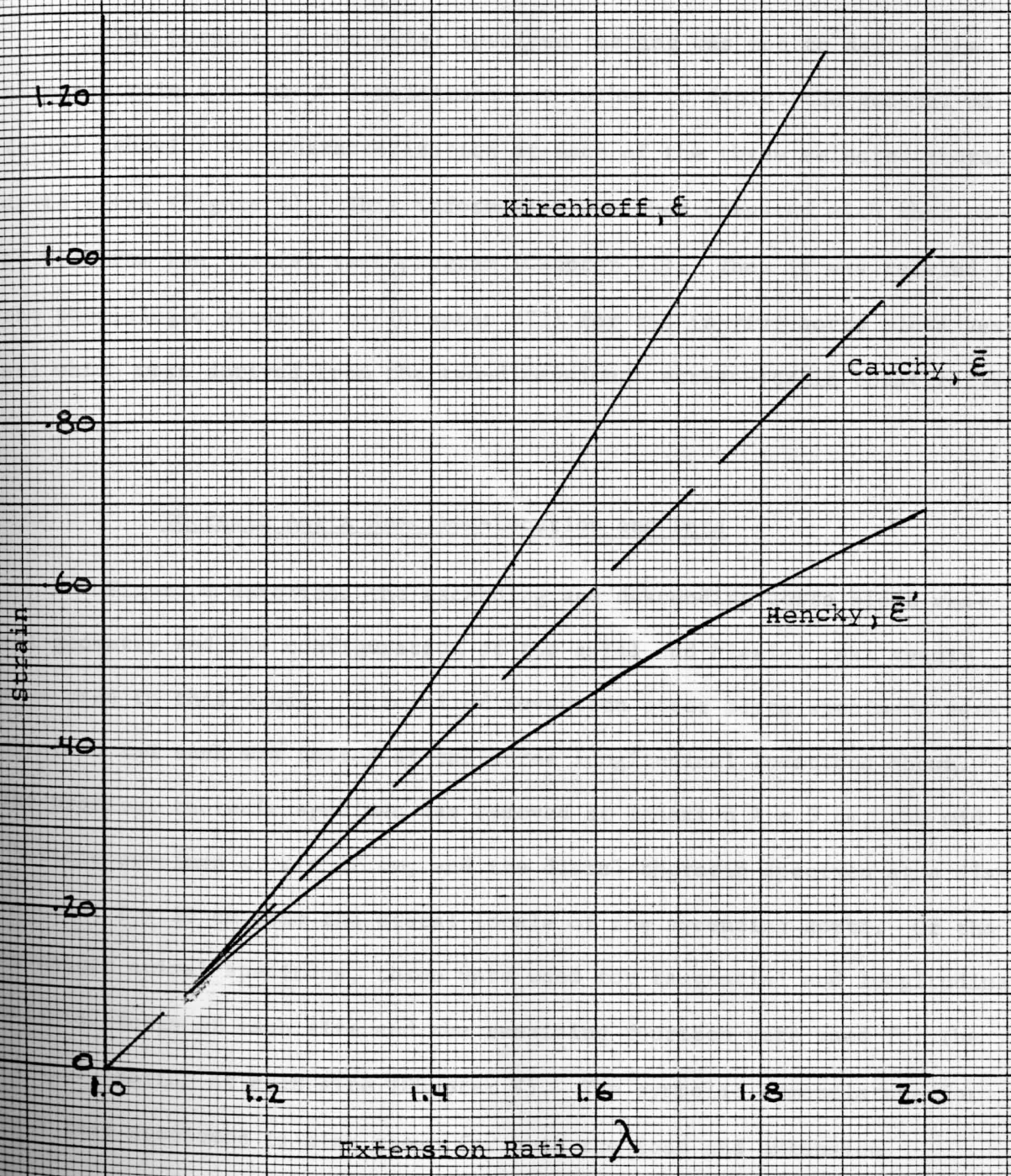
Equation (9) will be used extensively in this study of the thoracic aorta wall material properties.

A comparison of equation (5), linear theory, and equation (9), non-linear theory, is shown in Figure 3 which also includes the sometimes used Hencky or Natural strain measure defined as:

$$\bar{\epsilon}'_n = \int_{L_0}^{L_n} \frac{dL_n}{L_n} = \ln(\lambda) \quad (10)$$

Note that all three measures of strain are identical when the stretch ratio is equal to unity (unstressed), i.e. $\bar{\epsilon}_n = \epsilon_n = \bar{\epsilon}'_n = 0$ at $\lambda_n = 1.0$.

Figure 3 - Comparison of Strain Measures



CHAPTER III

AXIAL SPECIMEN TESTING

Introduction

The purpose of the axial specimen testing was not to define the stress-strain (σ vs λ) relations but rather to depict the general material behavior and characterization at each of the three selected thoracic aorta sites (Figure 4). This information was then compared with that observed from the biaxial test program (Chapter VI). Then it was related to the physiologic predictions (Chapter VII) for the in-vivo aorta blood vessel which were derived from the two-dimensional stress-strain constitutive equations.

Thoracic Aorta Specimen-Location and Data

Figure 4 describes the ascending and descending aorta blood vessel geometry and the configuration of the axial and biaxial test specimens used in this study. A total of seventeen steer aorta specimens were obtained and each was tested at the three longitudinal locations shown. The proximal thoracic specimen was removed at location $Z = 5$ cm, the mid thoracic specimen at $Z = 12$ cm, and the distal thoracic specimen at a distance of $Z = 20$ cm from the distal locale of the ascending aorta. Of the seventeen animal specimens, three were used for tangential and longitudinal uniaxial tests at each site and the remaining fourteen were used for the biaxial testing at each site (Chapter V). The symbolic nomenclature for both test specimens is also shown for both the load and extension

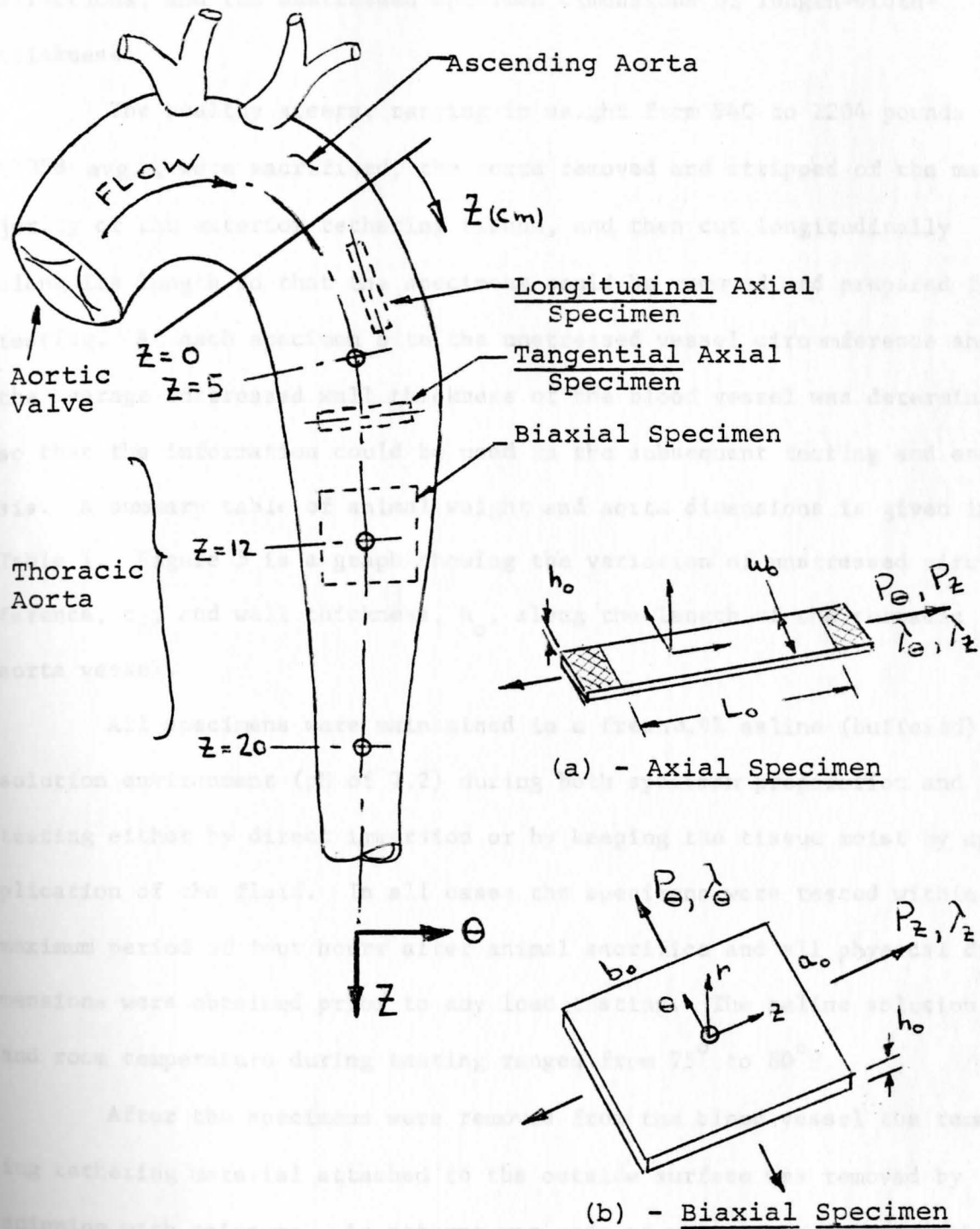


Figure 4 Steer Thoracic Aorta-in-vitro: Specimen Site Location, Aorta Geometry, and Nomenclature

directions, and the unstressed specimen dimensions of length-width-thickness.

The healthy steers, ranging in weight from 940 to 1204 pounds (1058 avg.), were sacrificed, the aorta removed and stripped of the majority of the exterior tethering tissue, and then cut longitudinally along its length so that the specimens could be removed and prepared for testing. At each specimen site the unstressed vessel circumference and the average unstressed wall thickness of the blood vessel was determined so that the information could be used in the subsequent testing and analysis. A summary table of animal weight and aorta dimensions is given in Table 1. Figure 5 is a graph showing the variation of unstressed circumference, c_o , and wall thickness, h_o , along the length of the thoracic aorta vessel.

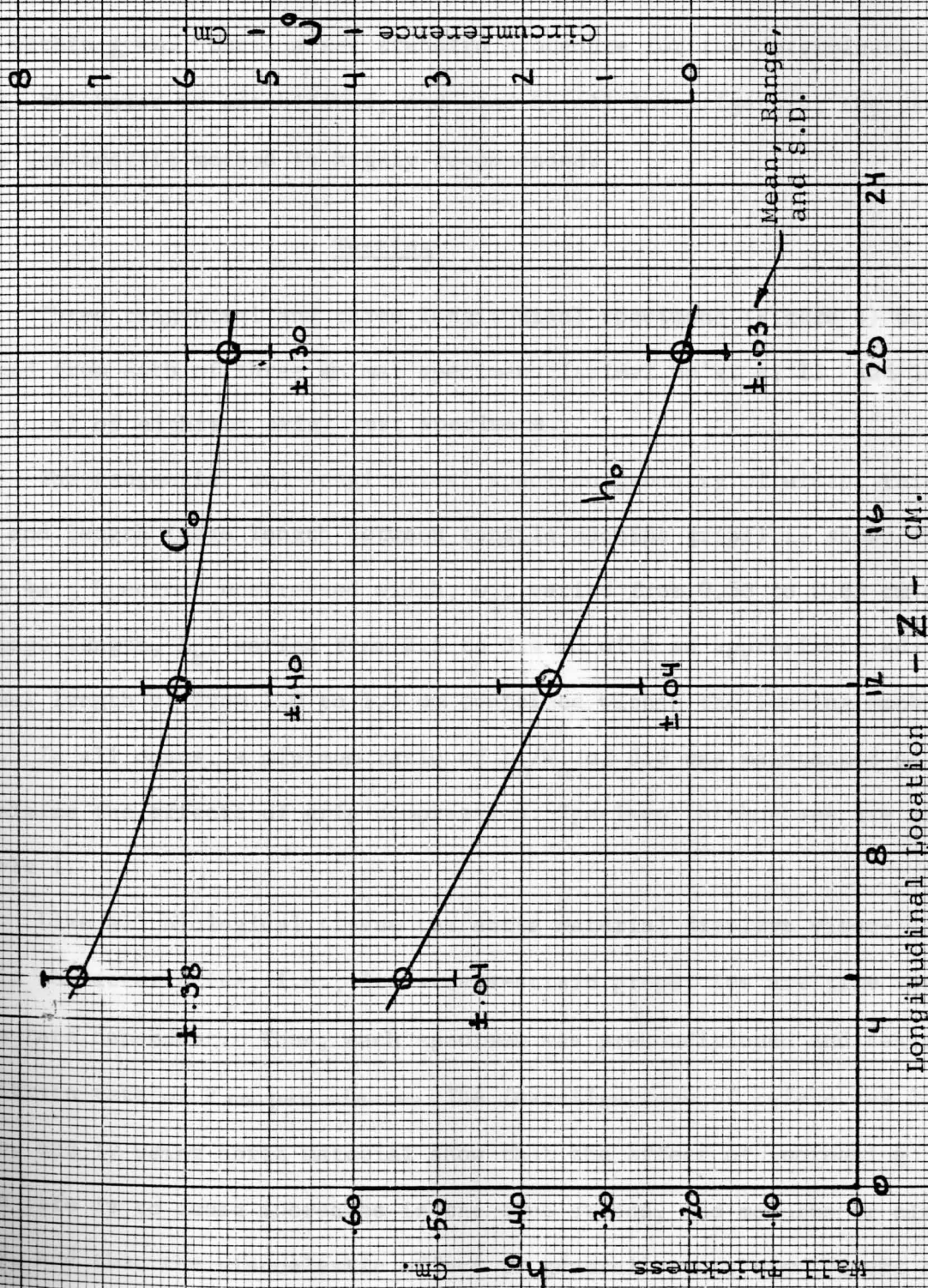
All specimens were maintained in a fresh 0.9% saline (buffered) solution environment (pH of 7.2) during both specimen preparation and testing either by direct immersion or by keeping the tissue moist by application of the fluid. In all cases the specimens were tested within a maximum period of four hours after animal sacrifice and all physical dimensions were obtained prior to any load testing. The saline solution and room temperature during testing ranged from 75° to 80°F.

After the specimens were removed from the blood vessel the remaining tethering material attached to the outside surface was removed by snipping with scissors. An attempt was made to measure vessel wall thickness (specimen thickness), h_o , using hand calipers, but it was found that under slight variations of surface pressure the variation in thickness readings at any one location on the specimens was wide ranging and yielded a measurement variation of approximately $\pm 17\%$. The high liquid content

TABLE 1 - Animal Data & Aorta Specimen Thickness and Circumference (unstressed-in-vitro)

SPECIMAN No.	ANIMAL WEIGHT (LBS)	THICKNESS - h_0 (cm)			CIRCUMFERENCE - C_0 (cm)		
		Z=5	Z=12	Z=20	Z=5	Z=12	Z=20
1	1016	0.59	0.36	0.20	7.7	6.3	5.8
2	964	.48	.26	.17	7.5	6.1	6.0
3	1174	.55	.36	—	6.2	5.0	—
4	1020	—	—	—	—	—	—
5	940	.55	.41	.22	7.5	6.5	5.9
6	1162	.58	.39	.19	7.5	6.0	5.3
7	994	.52	.39	.24	7.2	6.2	5.3
8	874	.48	.38	.20	7.3	6.2	5.2
9	986	.48	.34	.21	7.2	6.3	5.5
10	992	.54	.41	.24	7.3	6.2	5.5
11	1070	.55	.39	.23	7.7	6.4	5.5
12	1022	.55	.34	.16	7.0	5.6	5.4
13	1150	—	—	—	—	—	—
14	1174	.60	—	.25	7.5	—	5.2
15	960	.56	.43	.20	7.2	6.0	5.0
16	1204	—	—	—	—	—	—
17	1180	0.59	0.40	0.16	7.7	6.4	5.8
N	17	14	13	13	14	13	13
MEAN	1058	0.54	0.37	0.21	7.3	6.1	5.5
SEM	23	0.01	0.01	0.01	0.10	0.11	0.08
SD	94	0.04	0.04	0.03	0.38	0.40	0.30
MEAN	MID-WALL RADIUS - r_{m_0} (cm)	—	—	—	1.16	0.97	0.88

Figure 5 - Unstressed Circumference and Wall Thickness VS Thoracic Location - in-vitro



Longitudinal Location - Z - cm.

Wall Thickness - cm.

Circumference - C_0 - cm.

Mean, Range, and S.D.

and the extreme softness of the tissue dictated that a gravimetric method be used. Thus, after measuring the length and width of the specimen the specimens were then weighed in both air (after light blotting of the tissue) and in saline solution, the tissue volume calculated, and the wall thickness was then determined. The accuracy by this method was assessed to be within $\pm 4\%$. Until a set standard procedure for the determination of wall thickness is established, and used by all investigators, the use of the gravimetric method is highly recommended.

Testing

Three tangential and three longitudinal specimens (Figure 4) were obtained from each of three animal specimens (animal no's. 4, 13, and 16) for a total of eighteen axial test specimens.

The tangential and longitudinal specimen geometry of width, thickness, and length (gage length between tensile machine grips) is shown in Figure 4a. Specimen unstressed width, w_0 , varied from 0.50 to 0.85 cm and test gage length, L_0 , varied from 2.5 to 3.4 cm with an approximate additional length of from 1.0 to 1.5 cm contained within the loading machine grips. In all cases, a minimum ratio of L_0/w_0 of 3.0 was maintained so as to minimize the effects of grip compression. Specimen thicknesses are given in Table 1.

Like all biological tissue the aorta material displays viscoelastic characteristics, i.e., its stress-strain properties are time and strain rate dependent. Thus, each specimen was preconditioned and tested at a strain rate of 2 cm per minute. The investigations of references 2, 11, 12, 16, and 17 using aorta material show that the effect of increasing strain rate is to cause increases in the true stress, and modulus of elasticity, and that the viscoelastic effect is generally most significant at

extension ratios greater than 1.50 where the collagen fibers become most effective and cause the so-called "knee" of the σ vs λ curves. A value of 2 cm/minute is recommended as a reasonable value.

Most investigators recommend, but do not specifically define, a preconditioning of test specimens consisting of three cycles of loading prior to the conducting of the axial tests. The purpose of the preconditioning is to achieve an approximate state of equilibrium for the tissue prior to the conducting of the axial load tests. Preliminary testing of several specimens indicated that the following procedure should be used prior to axial load testing.

Tangential specimens - 3 cycles of loading to	$\lambda_e = 1.70$
2 minutes relaxation at	$\lambda_e = 1.00$
Static test to	$\lambda_e = 2.00$

Longitudinal specimens - 4 cycles of loading to	$\lambda_z = 1.70$
2 minutes relaxation at	$\lambda_z = 1.00$
Static test to	$\lambda_z = 2.00$

While the above preconditioning and test sequence cannot claim to be infallible, due to the very nature of the material, it did yield repeatable results on those specimens which were used to develop the procedure. The hysteresis of the axial test specimens was minimized as evidenced by the fact that all specimens showed a permanent deformation of less than $0.04 L_0$ (maximum value recorded) after two minutes following the static test.

The test equipment consisted of the following equipment:

- UTM- II Tensilon test machine
load cells - 1000 and 2000 grams
strain rate - 2 cm/minute
- SS - 105D - 13 - UTM Recorder
paper speed - 10 cm/minute

Vernier calipers - measurement of specimen gage length, L_0 .

True Stress

For uni-axial loading, the extension ratio, λ_n , in the direction of loading is greater than unity and from the incompressibility equation, equation (8), the extension (contraction) ratio in the two mutually perpendicular unloaded directions is

$$\lambda_1 = \frac{1}{\sqrt{\lambda_n}} \quad (11)$$

Thus, the true stress, measured in terms of the deformed geometry, as a function of the initial or unstressed geometry is:

$$\sigma_n = P_n / [w_o (\lambda_1) (h_o (\lambda_1))] = (P_n / A_o) \lambda_n$$

$$\text{or } \sigma_e = (P_e / A_o) \lambda_e \quad \text{and} \quad \sigma_z = \sigma_r = 0 \quad (12)$$

$$\text{or } \sigma_z = (P_z / A_o) \lambda_z \quad \text{and} \quad \sigma_e = \sigma_r = 0$$

where: $A_o =$ unstressed cross-sectional area = $w_o h_o$, cm^2

Test Results and Discussion

The test results in the form of stress-extension ratio graphs are given in Figures 6 thru 11 (pages 29 thru 34) and are discussed in the following paragraphs.

Figure 6 - Figure 6 gives an approximate overall view of the longitudinal and tangential stress-strain (σ vs λ) curves at each of the three longitudinal aorta locations using animal specimen No. 16, live weight = 1204 pounds. Of special interest is the close similarity of each of the σ - λ diagrams for the loading in the two mutually perpendicular directions at each of the three specimen aorta locations. This similarity, but distinct difference, in the shape of the σ_e and σ_z curves confirms the anisotropic nature of the aorta material. If the material were isotropic σ_e and σ_z , would be identical, i.e., no directional material variation of stress vs strain. Also, the direct similarity of the low initial slope of the curves followed by an increasing slope for not only each loading direction at a particular site, but at each of the stress site locations tested, indicates that the material exhibits orthotropic symmetry with respect to the two principal directions of loading. Thus, as was discussed in Chapter II, the aorta tissue displays both anisotropic and orthotropic behavior due to both fiber directional orientation and the varying relative quantities of its elastin and collagen fibers longitudinally along the thoracic tree. The progressive change in the shape of the σ vs λ curves from the upper to the lower site shows evidence of the increasing collagen fiber content which causes increasing stiffness (or elasticity) as we progress along the thoracic tree to the abdominal aorta locale. This observation has been confirmed by many investigators^{2,11,12,17} using axial test specimens, or arterial segments, and will also be dis-

Figure 6 - Comparison of Axial Directional Stress-Strain Properties at Three Aorta Sites

Specimen #16

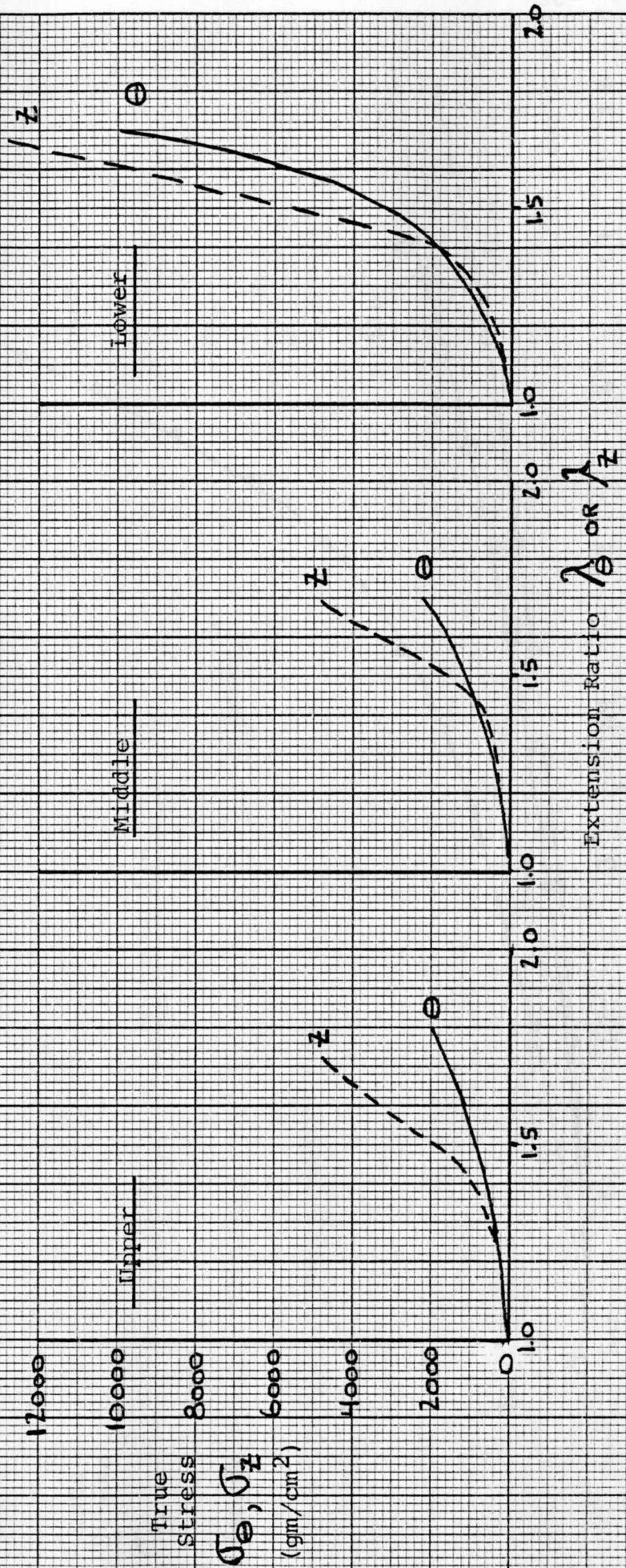


Figure 7 - Tangential σ vs λ Characteristics Relative to Site Location

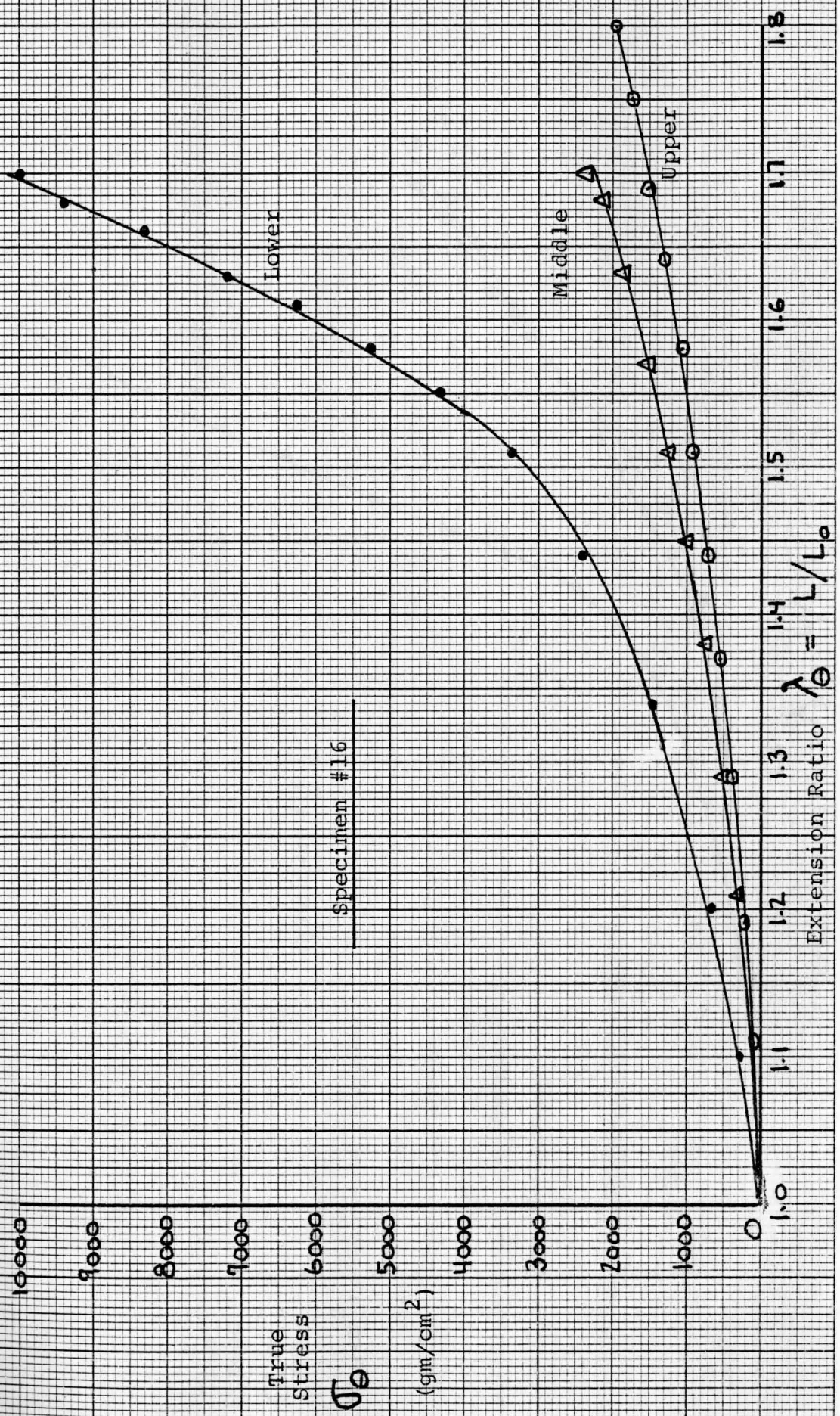


Figure 8 - Longitudinal σ_z vs λ_z Characteristics Relative to Site Location

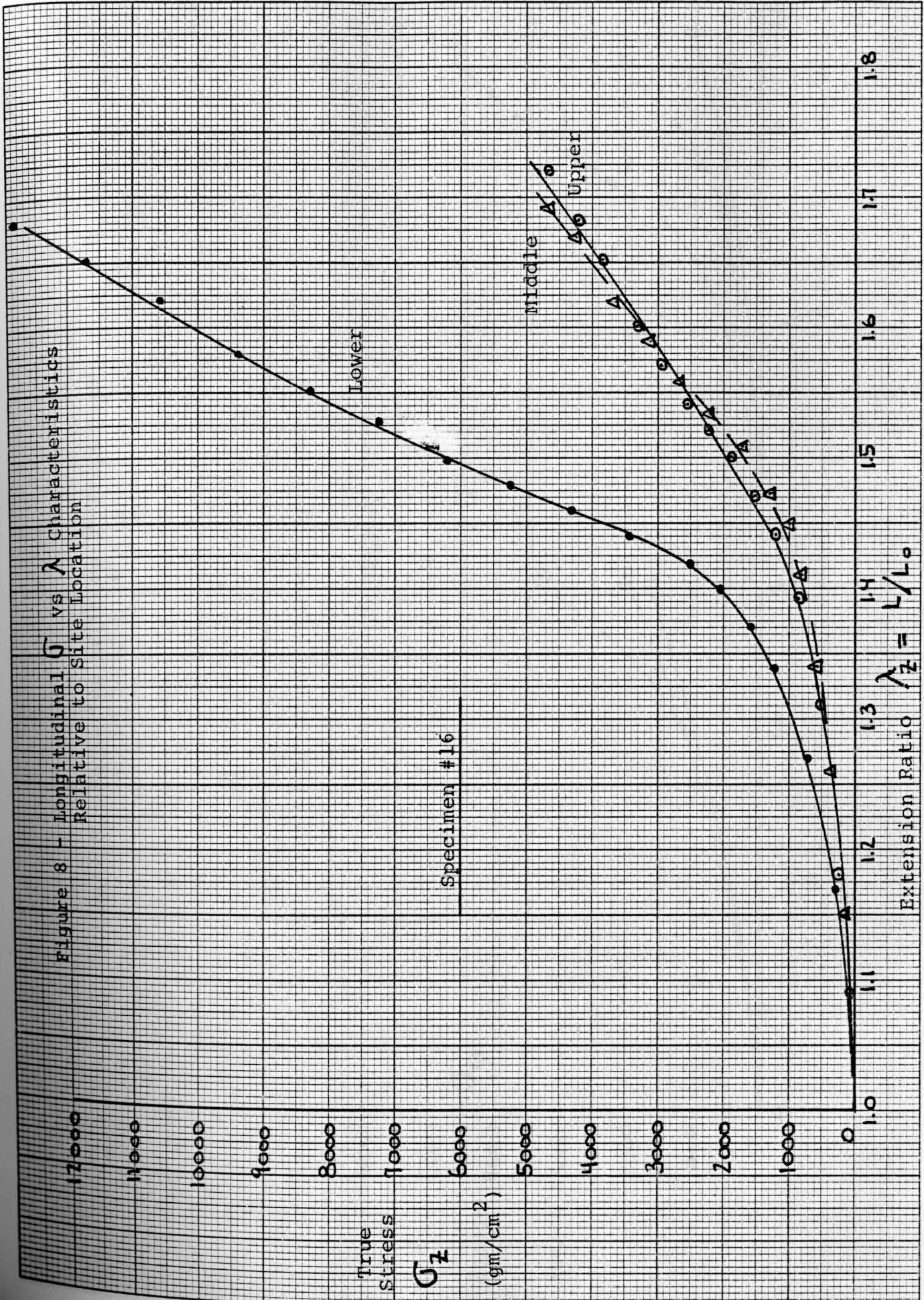
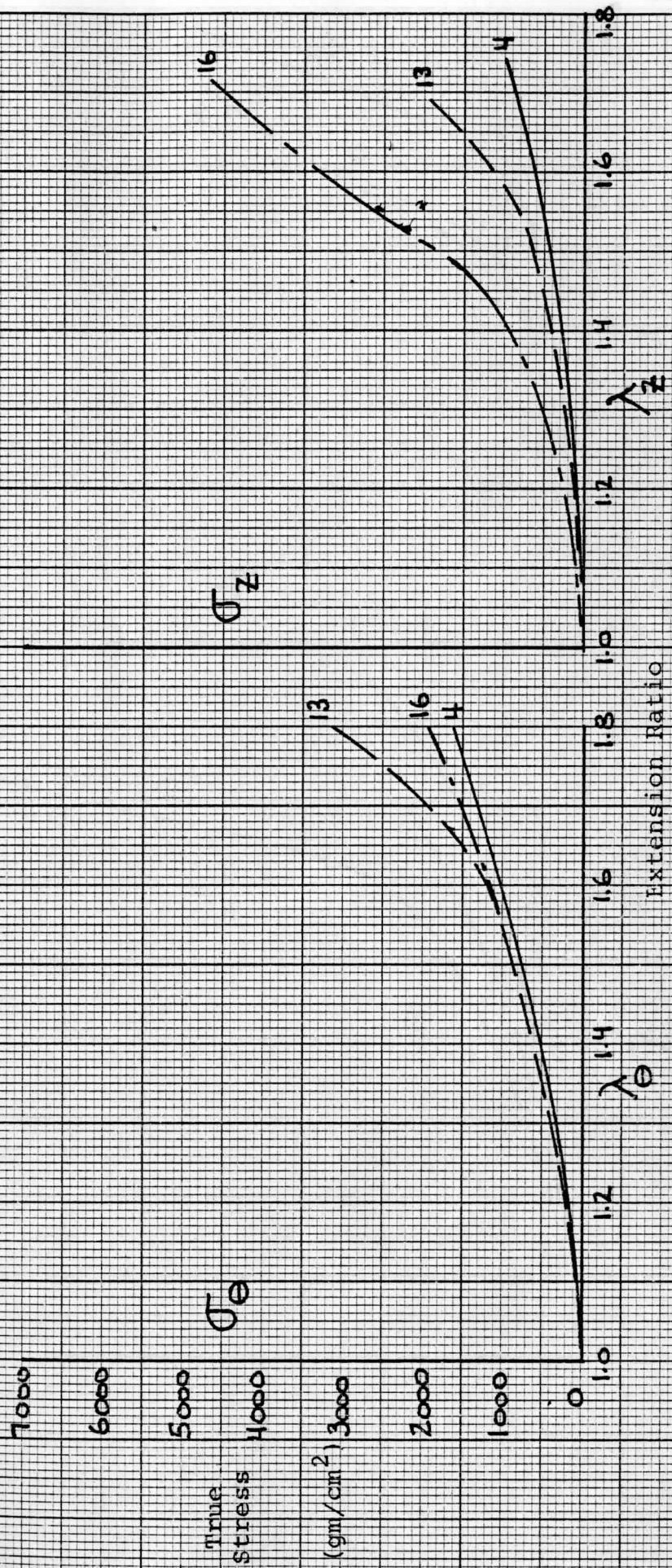


Figure 9 - Variation of σ vs λ Properties at the Upper Site

Specimens #4, 13, 16



True Stress (σ_e)
(gm/cm^2)

Extension Ratio

σ_z

λ_z

λ_e

Figure 10 - Variation of σ vs λ Properties at the Middle Site

Specimen #4, 13, 16

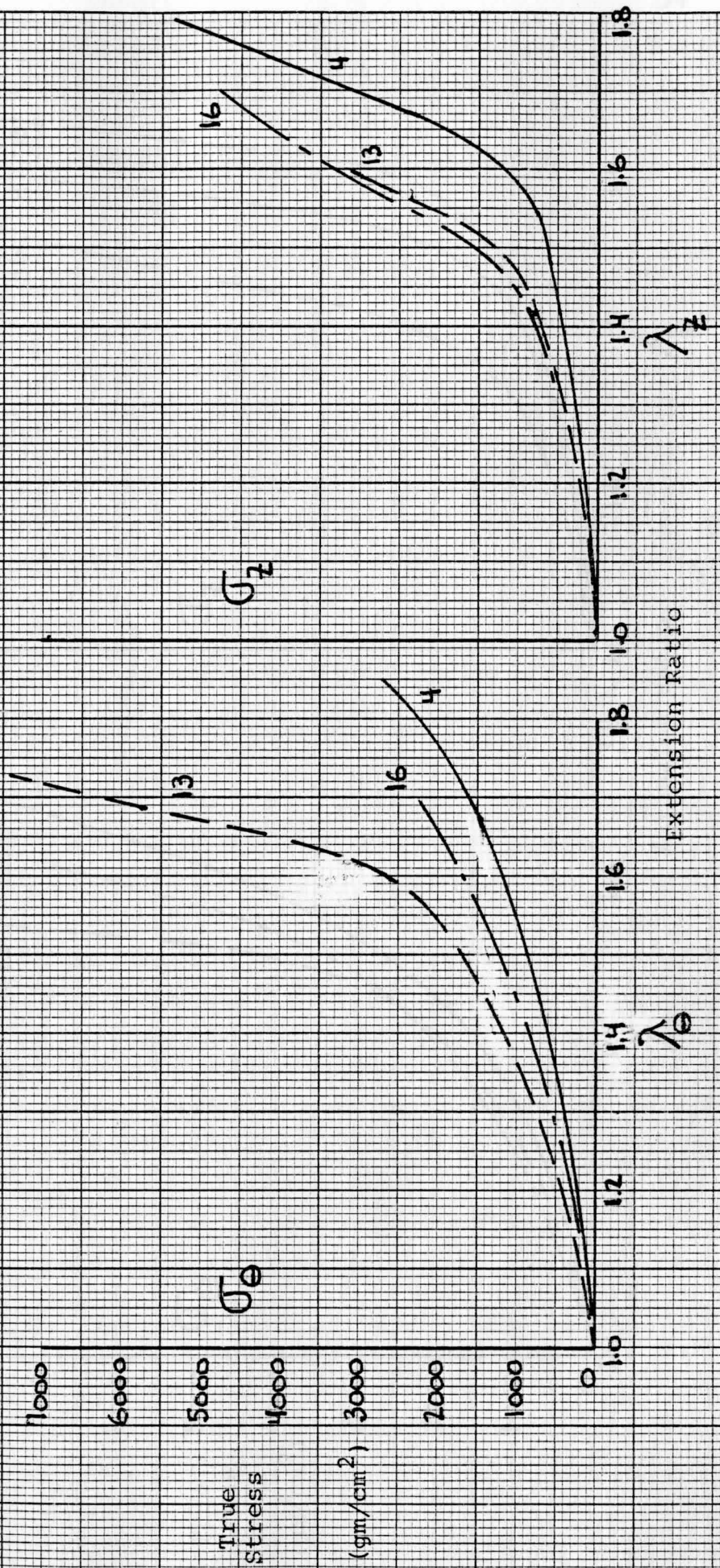
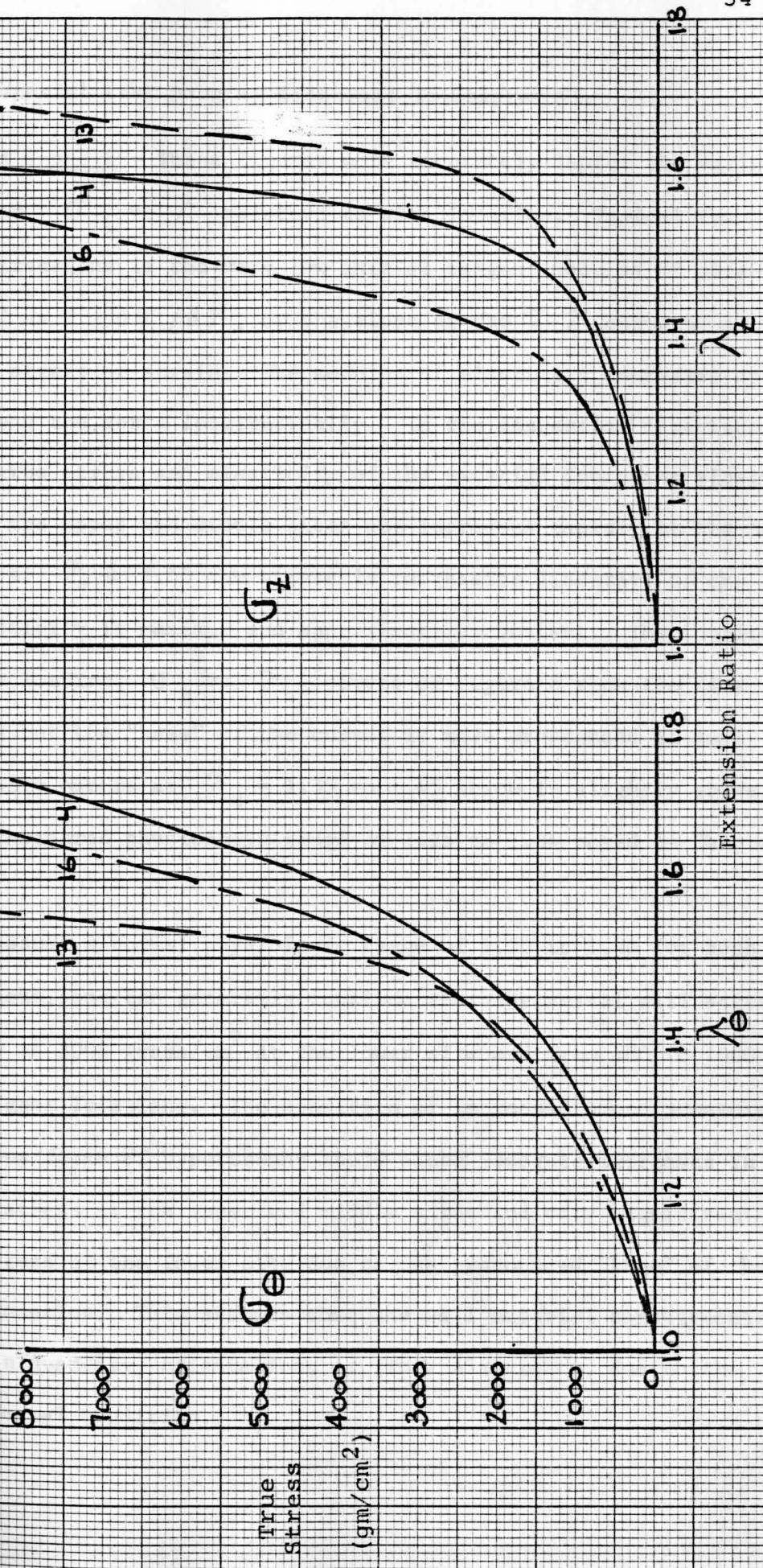


Figure 11 - Variation of σ vs λ Properties at the Lower Site

Specimen #4, 13, 16



played in the biaxial test program discussed in Chapter VI.

Figures 7 and 8 - These figures more accurately depict the variation of σ_{θ} and σ_z vs λ relative to site location. Typical for both loading directions is the very low initial tangent modulus of elasticity, defined as $E = d\sigma / d\lambda$, or the slope of the σ - λ curve at a given point of stress or strain. The modulus of elasticity increases as we progress along the aorta longitudinally. In the tangential direction, Figure 7, the true stress and elasticity of the material increases slowly with strain at the upper and middle sites but increases rapidly at the lower site where at $\lambda_{\theta} \geq 1.55$ the stress is increasing linearly, or the modulus of elasticity is maximum and approximately constant. The longitudinal direction loading, σ_z vs λ_z , curves of Figure 8 show the same characteristics but the "knee" of the curves is more pronounced at each site and generally occurs at $\lambda_z = 1.35$ to 1.45 which is slightly above the normally considered physiologic range of 1.25 to 1.34 noted in Chapter II.

If we assume a normal physiologic range of 1.20 to 1.40 for both loading directions, one can generally conclude that the vessel wall stress ranges from 500 to 2000 grams/cm² at the lower site and from 500 to 1000 grams/cm² at higher locations. The condition of increased blood pressure caused by various forms of hypertrophy would cause moderate increases in the tangential stress at the upper and middle sites and very significant increases in stress at the lower site due to the pronounced "knee" of the curve at this location. This assumes that the wall material constituents are unaltered in quantity, orientation, or fiber elasticity, due to the physiologic abnormal condition.

Figures 6 thru 8 demonstrate the nonlinear material response to deformation and its increased resistance (stiffness) relative to increasing deformation. The stress-strain curves further show the trend of exponential characterization which is contrary to the linear or power curve characterization which sometimes is used to simulate the stress-strain response of most engineering materials.

Figures 9 thru 11 - These graphs show the animal-to-animal tangential and longitudinal variation of the mechanical properties at each site for animals No. 4, 13, and 16 having live weights of 1020, 1150, and 1204 pounds, respectively. Some of this variation can be attributed to age, if one assumes that animal age is directly related to weight. Also, some variation could be attributed to specimen pre-conditioning which in itself does not necessarily reflect that a definite equilibrium state has been achieved by the wall tissue. At values of λ_e and $\lambda_z \leq 1.40$ only moderate variation in stress is evident at each location and thus age and preconditioning are not necessarily significant factors. However, at increasing values of strain, $\lambda_n > 1.40$, the variation in material properties (σ and E) is dramatic due again to the exponential "knee" of the stress-strain curves. As an example, at $\lambda_e = \lambda_z = 1.60$, the variation in stress ranges from a 200 to 400% variation with magnitudes ranging from 1000 to 10,000 grams/cm². With such high magnitudes of stress and possible variations of wall material stress, one can only hope, for the sake of tissue life, that the physiologic in-vivo range of strain is below $\lambda_n = 1.60$. As we shall see in Chapter VII, this is fortunately the case for the condition of normal pulsatile flow in healthy animals.

CHAPTER IV

DETERMINATION OF THE TANGENTIAL EXTENSION RATIOS FOR
IN-VIVO SIMULATION - BIAXIAL TESTINGIntroduction

As stated in Chapter I, the purpose of this work is to determine the two-dimensional (plane stress) constitutive equations for the thoracic aorta material at three longitudinal locations along its length based on the results of in-vitro biaxial tests. From such experimental findings, the state of wall stress and the deformation of the blood vessel in-vivo can be then approximated without the need of conducting in-vivo experiments. The question posed for the biaxial test program is essentially: "What values and combinations of values of the principal extension ratios, λ_z and λ_e , should be used in the conducting of such a test program so that the in-vivo deformation of the tissue is reasonably approximated?" Obviously, values of λ_z and λ_e ranging from 1.10 to 2.00 could be used and that a near infinite combination of these values would yield a complete (but not necessarily efficient) description of the stress-strain characterization of the material. To minimize the number of test specimens to the value of nine normally used for statistical reasons, and especially to minimize the critical testing time for each specimen, a method must be developed which yields both an efficient test program (cost and time-wise) and representative of in-vivo simulation.

In Chapter II, the findings of other investigators were discussed regarding the in-vivo longitudinal state of loading or deformation. It

was concluded that λ_z values of 1.25, 1.30, and 1.35 should be used in the biaxial test program and would be representative of the in-vivo tethering state. Thus, one part of the question posed has been answered.

In Chapter III, axial test results and discussion, it was observed that the stress-strain characterization of the material is approximately exponential in form. Thus, the material strain energy function must also be exponential and will be a function of the strains or the strain tensor invariants. A strain energy function (W) will be determined, assuming that $\lambda_z = 1.30$. This function represents a first approximation of the aorta material tangential properties at each of the three aorta sites. It will be based on the tangential stress-strain properties presented in Figures 9 thru 11 of Chapter III. After having determined the form of W , and the applicable coefficients for the material, this information can then be substituted into the three dimensional stress equations and then be equated with the in-vivo principal stress equations of Chapter II. This will yield an approximation of the values for the tangential extension ratios applicable to the in-vivo pulsatile flow pressures of 140, 155, and 170 cm H₂O, reference Chapter II. Accordingly, the biaxial testing at each site can be reduced to fewer λ_e values (and combinations of λ_z and λ_e) which approximate the in-vivo states. After the completion of the biaxial and the subsequent physiologic analysis, based on the biaxial test results, a check will be made to see if the above described method has been satisfactory at each aorta site.

The method outlined above and developed in the following paragraphs is based on the experimental and theoretical work of Rivlin¹⁹ and Treloar⁴ working with natural and synthetic rubber. Such material also displays finite nonlinear deformation and the exponential stress-strain

characteristics similar to that of biological materials. However, while rubber can also be assumed to be incompressible, its directional properties in the unstressed and stressed state are isotropic. The stress equations (axial and biaxial) used below are based on the Statistical and Kinetic Theory of Large Deformations as developed by Rivlin and are used for the aorta material which is anisotropic. It is for this reason that the method used is an approximation.

Determination of the Strain Energy Coefficients

For an elastic and initially isotropic material, the strain energy function (W) is a unique function of the state of strain and is defined as the amount of stored energy per unit volume. The values of the three principal extension ratios, λ_z , λ_e , λ_r , specify the state of strain (shear strains are assumed negligible) and for an incompressible material (volume constancy):

$$\lambda_z \lambda_e \lambda_r = 1.0 \quad (10)$$

which also implies that W is a function of the strain tensor invariants defined as:

$$I_1 = \lambda_z^2 + \lambda_e^2 + \lambda_r^2 \quad (11a)$$

$$I_2 = \lambda_z^2 \lambda_e^2 + \lambda_e^2 \lambda_r^2 + \lambda_r^2 \lambda_z^2 \quad (11b)$$

$$I_3 = \lambda_z^2 \lambda_e^2 \lambda_r^2 = 1.0 \quad (11c)$$

Note that equation (10) implies that only two of the three extension ratios are independent by virtue of volume constancy and that equations (11a) and (11b) are equal to 3.0 at zero stress state, i.e., $\lambda_z = \lambda_e = \lambda_r = 1.0$, and that the value of I_3 is constant for an incompressible material based on equation (10). Thus, the strain energy function is a

function of the invariants I_1 and I_2 only. Fung² suggests the use of a polynomial or exponential form for W and tests on aorta tissue conducted by Sharma¹⁷ indicates that an exponential-polynomial form can be used for the aorta material in the form of

$$W = C_1 \left[e^{m(I_1-3)} - 1 \right] - C_2 (I_2-3)^n$$

which can be further simplified to

$$W = Ae^{m(I_1-3)} \quad (12)$$

since at low to moderate values of λ_e (≤ 1.50) the coefficients C_2 and n (Sharma¹⁷) make the term $C_2(I_2-3)^n$ small in magnitude. Thus, equation (12) will be used to approximate the form of the strain energy function for the non-isotropic material. The coefficients A and m remain to be determined.

From Rivlin¹⁹ and Treloar⁴, the principal stress for uni-axial loading in the tangential direction can be expressed as

$$\sigma_e = 2 \left(\lambda_e^2 - \frac{1}{\lambda_e} \right) \left[\frac{dW}{dI_1} + \frac{1}{\lambda_e} \frac{dW}{dI_2} \right]$$

which, using equation (12), can be reduced to

$$\begin{aligned} \sigma_e &= 2 \left(\lambda_e^2 - \frac{1}{\lambda_e} \right) \frac{dW}{dI_1} \\ &= 2 \left(\lambda_e^2 - \frac{1}{\lambda_e} \right) A m e^m (I_1-3) \end{aligned} \quad (13)$$

Taking the logarithm of equation (13) and rearranging, we obtain:

$$\text{Log} \frac{\sigma_e}{2 \left(\lambda_e^2 - \frac{1}{\lambda_e} \right)} = \text{Log}(Am) + m(I_1-3) \text{Log} \quad (14)$$

Thus, using $\lambda_z = 1.30$ and the tangential axial stress-strain data* of Chapter III (Figures 9 thru 11) a graph of equation (14) can be plotted (on semi-log paper) of the left side of equation (14) vs (I_1-3) . The intercept and slope of the resulting curves at each aorta location can be

*Actual testing was conducted to $\lambda_e = 2.0$. Data was plotted for the full range and to larger scale for improved accuracy.

determined so that the coefficients A and m at each site can be calculated. The values of the coefficients for use in equations (12) and (13) are listed below.

	UPPER (Z = 5 cm)	MIDDLE (Z = 12 cm)	LOWER (Z = 20 cm)	
A =	380	250	240	; gm/cm ²
m =	0.45	0.92	1.50	; non-dimensional

Calculation of λ_e Values

Having determined the values of A and m for the strain energy function, the approximate in-vivo tangential extension ratios can be determined at each thoracic site for the biaxial or plane stress condition of loading at the physiologic blood pressures of P = 140, 155, and 170 cm H₂O under the influence of a longitudinal strain of $\lambda_z = 1.30$.

Using the three-dimensional stress-strain equations derived by Rivlin and in Treloar⁴ (page 156) which are based on their theory of large deformations (incompressible - isotropic material) the equations reduce to

$$\sigma_e = 2 \left(\lambda_e^2 - \frac{1}{\lambda_e^2 \lambda_z^2} \right) \frac{dW}{dI_1}$$

$$\sigma_z = 2 \left(\lambda_z^2 - \frac{1}{\lambda_e^2 \lambda_z^2} \right) \frac{dW}{dI_1}$$

for the plane stress case where $\sigma_r = 0$. Using equation (12), we obtain

$$\sigma_e = 2Am \left(\lambda_e^2 - \frac{1}{\lambda_e^2 \lambda_z^2} \right) e^{m(I_1 - 3)} \quad (15a)$$

$$\sigma_z = 2Am \left(\lambda_z^2 - \frac{1}{\lambda_e^2 \lambda_z^2} \right) e^{m(I_1 - 3)} \quad (15b)$$

where A and m have been determined above and I_1 is defined by equation (11a).

Since the in-vivo tethering or longitudinal extension ratio is assumed to be equal to 1.30, equation (15a) can be solved for the corresponding values of λ_e by equating this equation to the in-vivo equation for

the tangential stress (σ_e), equation (1) repeated below:

$$\sigma_e = pr_m/h \quad (1)$$

This equation presents a problem since the in-vivo (physiologic) values of the midwall radius (r_m) and wall thickness (h) are unknown. This situation can be rectified by expressing r_m and h as functions of the unstressed values r_o and h_o , respectively, (known from Table 1) using equations (7b) and (7c), and by expressing λ_r as a function of λ_z and λ_e using the incompressibility equation, equation (8). Thus, equation (1) reduces to:

$$\sigma_e = (pr_o/h_o) \lambda_z \lambda_e^2 \quad (16)$$

Equating equation (15a) and (16) gives:

$$(pr_o/h_o) \lambda_z \lambda_e^2 = 2Am \left(\lambda_e^2 - \frac{1}{\lambda_z^2 \lambda_e^2} \right) e^{m(I_1-3)} \quad (17)$$

Using equation (11a) and recognizing that

$$\lambda_r^2 = 1/\lambda_z^2 \lambda_e^2$$

from equation (10), the strain invariant I_1 can be expressed as

$$I_1 = \lambda_e^2 + \lambda_z^2 + 1/\lambda_e^2 \lambda_z^2$$

which upon substituting $\lambda_z = 1.30$ reduces to

$$I_1 = \lambda_e^2 + .592/\lambda_e^2 + 1.69 \quad (18)$$

Substituting $\lambda_z = 1.30$ and equation (18) into equation (17)

yields:

$$1.3(pr_o/h_o) \lambda_e^2 = 2Am (\lambda_e^2 - .592/\lambda_e^2) \text{Exp} \left[m(\lambda_e^2 + .592/\lambda_e^2 - 1.31) \right]$$

and upon dividing both sides of the equation by $(2Am \lambda_e^2)$ simplifies the

equation to:

$$(1 - .592/\lambda_e^4) \text{Exp} \left[m(\lambda_e^2 + .592/\lambda_e^2 - 1.31) \right] = (.65/Am)(pr_o/h_o) \quad (19)$$

Using the in-vitro aorta site values of r_0 and h_0 given in Table 1*, the values of the coefficients A and m determined previously, and the pulsatile pressures of 140, 155, and 170 cm H₂O, equation (19) can be solved by numerical iteration technique to obtain the approximate in-vivo values of the tangential extension ratio, λ_e , corresponding to the physiologic pulsatile flow condition. The results of these calculations are tabulated below for each of the three thoracic aorta locations.

Pressure	UPPER (Z = 5 cm)	MIDDLE (Z = 12 cm)	LOWER (Z = 20 cm)
p = 140 cm H ₂ O	1.59	1.24	1.14
p = 155 cm H ₂ O	1.67	1.31	1.18
p = 170 cm H ₂ O	1.72	1.34	1.20

Conclusion

Based on the results of the above analytical approximation of the in-vivo tangential extension ratios, λ_e , the biaxial specimen test program will be conducted for those combinations of λ_z and λ_e shown in Table 2 on the following page at each of the three thoracic aorta sites. Each specimen will be tested for a total of nine strain combinations. Details regarding the biaxial testing are contained in the following chapter.

*Average values for axial specimens numbers 4, 13, and 16 were used. These values are not contained in Table 1 due to the loss of the measurement records.

TABLE 2 - PRINCIPAL EXTENSION RATIO COMBINATIONS
FOR BIAxIAL SPECIMEN TESTING

Location	λ_z	λ_e
UPPER (Z = 5 cm)	1.25 1.30 1.35	} 1.60, 1.70, 1.80
MIDDLE (Z = 12 cm)	1.25 1.30 1.35	} 1.20, 1.30, 1.40
LOWER (Z = 20 cm)	1.25 1.30 1.35	} 1.15, 1.20, 1.30

CHAPTER V

BIAXIAL TEST

Introduction

Fourteen steer thoracic aortas were used for the biaxial test program with three specimens removed from each as shown in Figure 4, page 21. Figure 12 is a schematic diagram of the test set-up for each specimen and shows the orientation of the specimen relative to the loading fixtures, the instrumentation used to measure the predetermined extension (λ) ratios, and the instrumentation used to measure the biaxial loads, P_e and P_z , needed to obtain the test extension ratio values for each of the two principal directions.

The purpose of the biaxial testing of the aorta material described herein is to obtain stress-strain data so that the steady state or passive two-dimensional (plane stress) constitutive equations ($\sigma - \epsilon - E$) for the material can be analytically described in Chapter VI and so used in the physiologic analysis of the in-vivo blood vessel, Chapter VII. Similar testing could be conducted in the future under the conditions of cyclic loading (1 to 25 Hertz) so as to determine the constitutive equations applicable to the viscoelastic character of the aorta material.

Test Specimen, Set-Up, Instrumentation

Each specimen was cut from the aorta (Figure 14) using an aluminum template having a 1.75 cm diameter hole in the center. The overall specimen size was square, 5 X 5 (± 1 mm) cm, and a thin ring of 1.75 diameter

RIGID SUPPORT

BUCKLE (2)

3PIECE GRIP-PULLEY
FITTINGS (8)

-1 LOADING BAR (2) -
LONGITUDINAL

-2 LOADING BAR (2) -
TANGENTIAL

CABLE

TO LOADING
PLATFORM

P_z

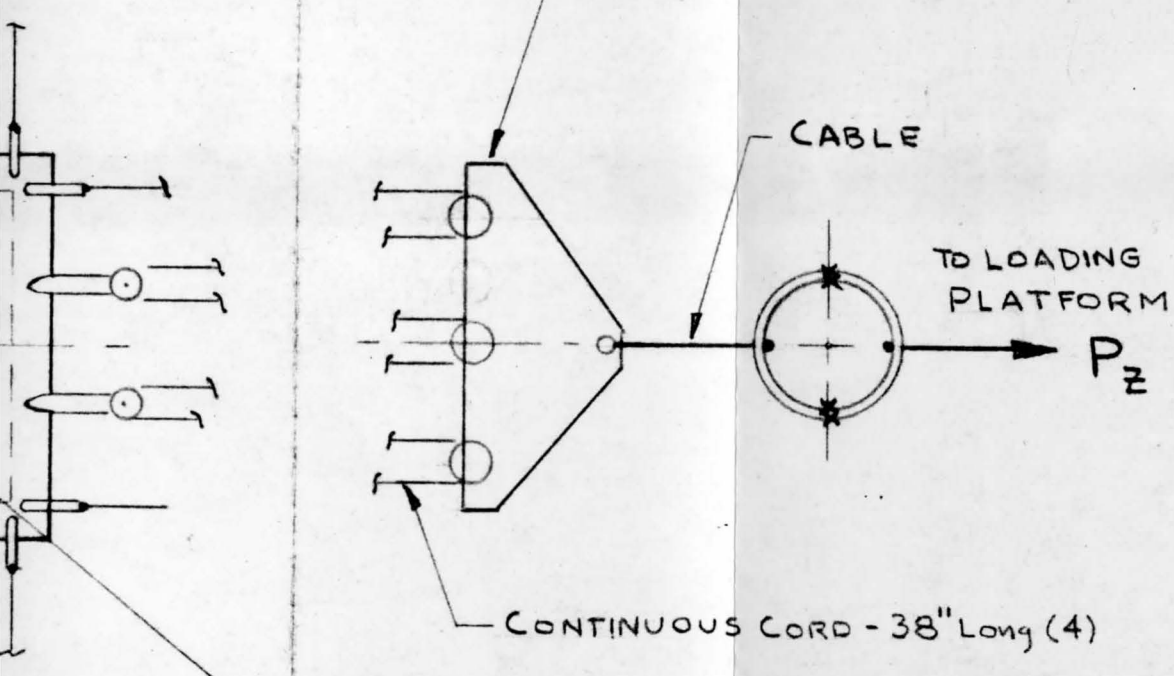
CONTINUOUS CORD - 38" Long (4)

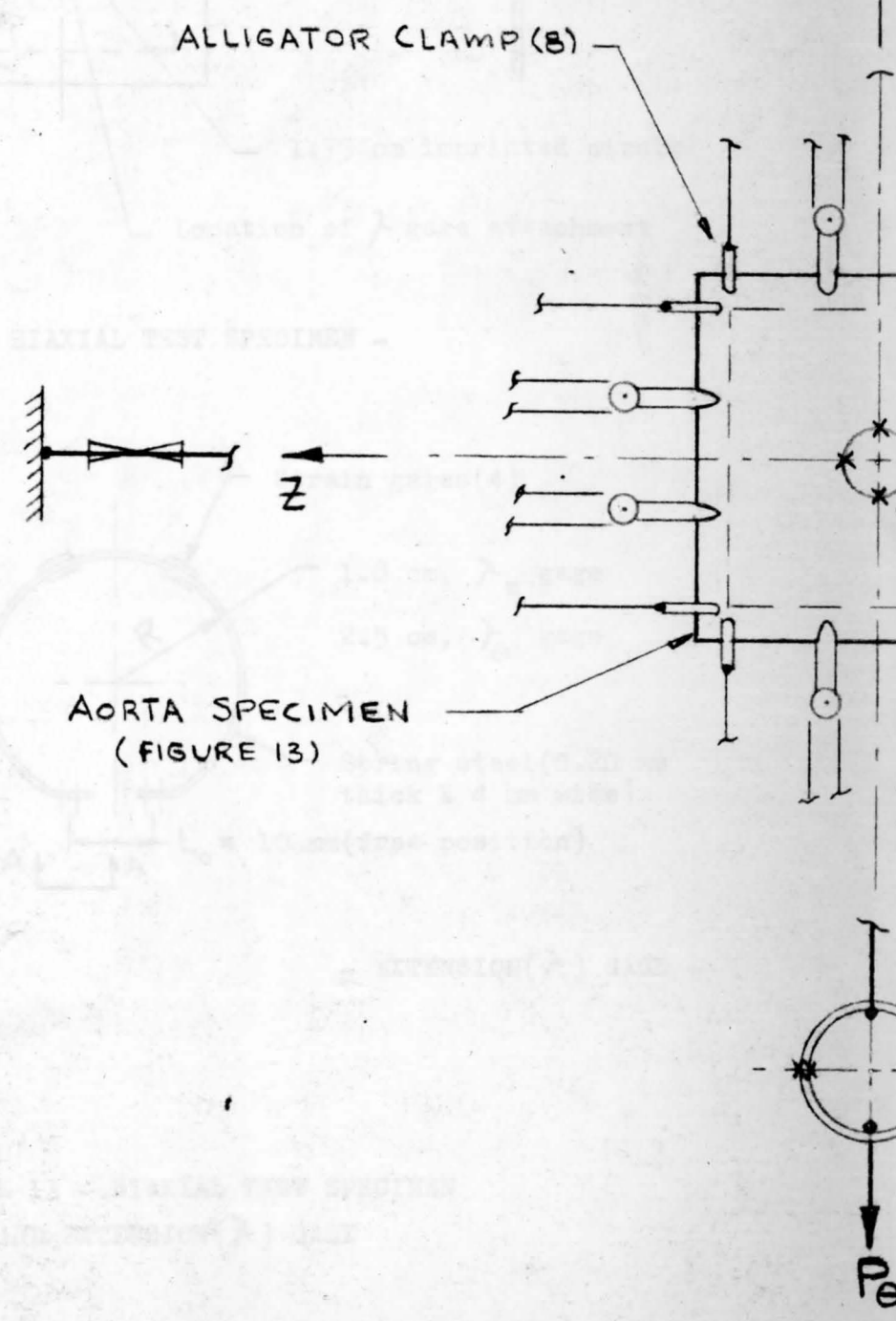
LOCATION OF EXTENSION GAGES
(FIGURE 13)

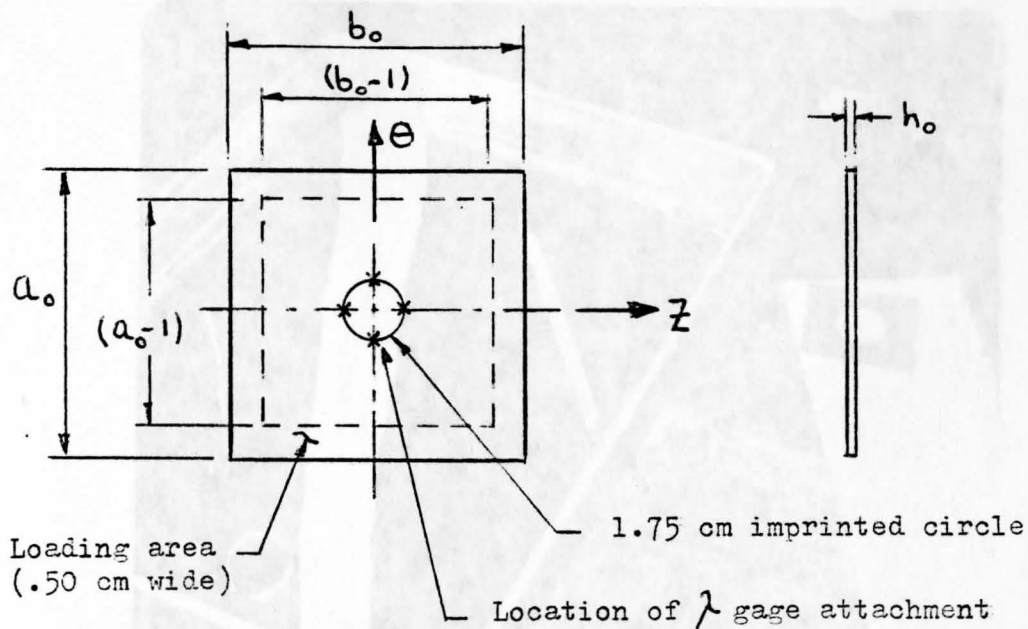
LOAD CELL (2)

LOADING PLATFORM

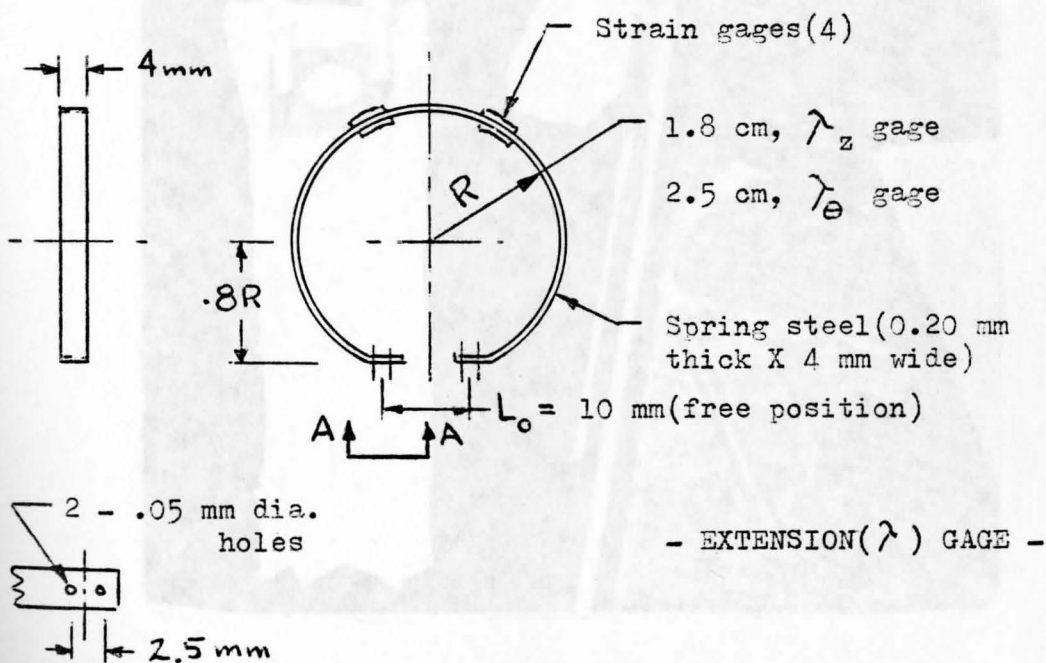
FIGURE 12 - DIAGRAM OF
BIAXIAL TEST SET-UP







- BIAXIAL TEST SPECIMEN -

- EXTENSION (λ) GAGE -

View A-A

FIGURE 13 - BIAXIAL TEST SPECIMEN
AND EXTENSION (λ) GAGE

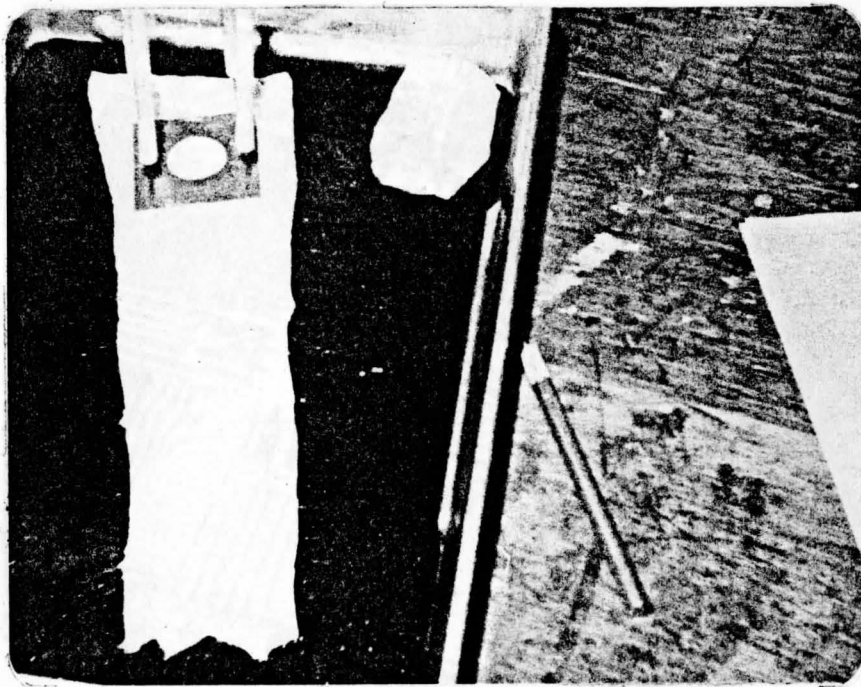
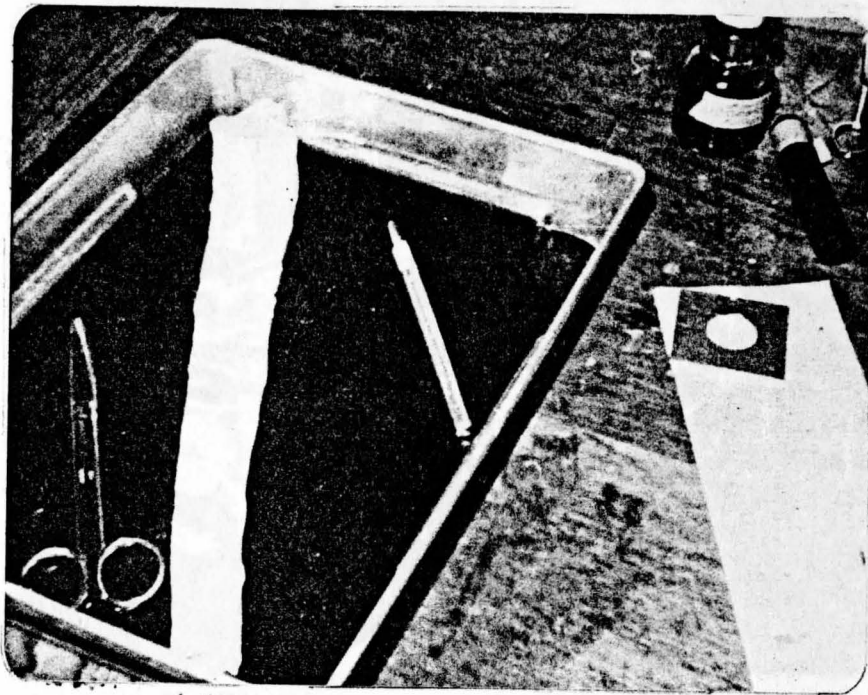


Figure 14 - Photographs of Specimen and
Biaxial Test Set-Up

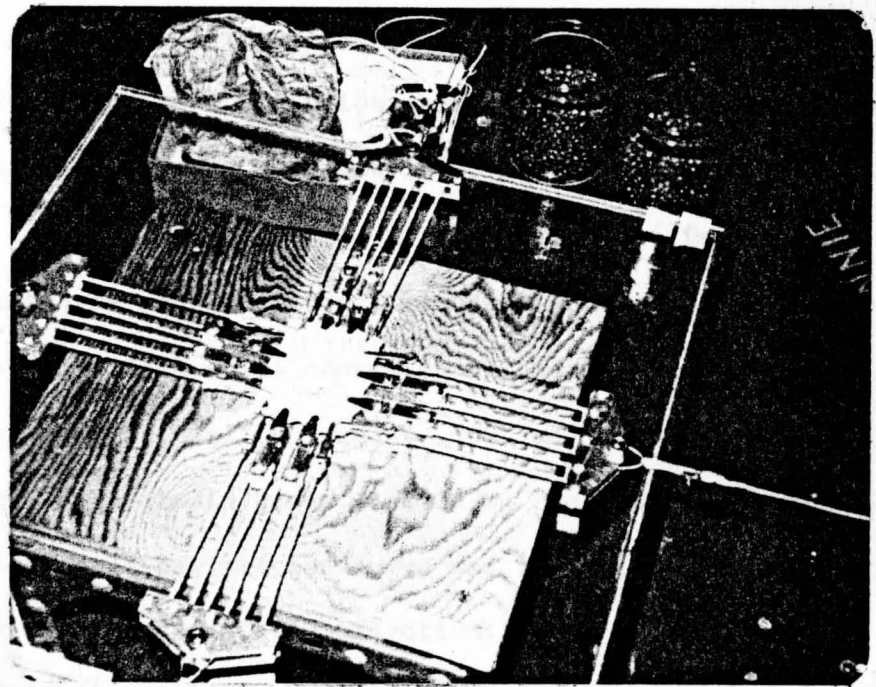
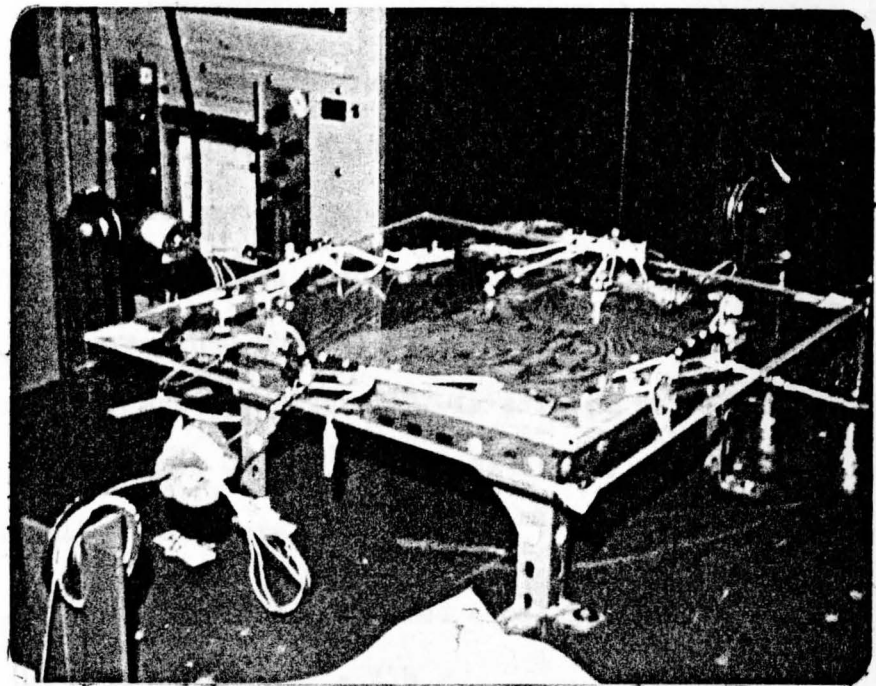


Figure 14 - continued

was impressed on it using non-toxic azurae A, methylene blue (phosphate buffered) dye. Figure 13 depicts the geometry of the test specimen. Each of the two types of loading fixtures (the alligator clamps and the special grip-pulley fittings) gripped the specimen within 5 mm of the edge of the specimen. A square loaded test section of dimensions $(a_o - 1) \times (b_o - 1)$ remained where the stress distribution due to the directional loads P_e and P_z , Figure 12, is assumed to be uniform at the center of the specimen and within the locale of the dye-imprinted circle. The true principal stresses are

σ = applied load/deformed cross-sectional area

$$\text{or } \sigma_z = 454 P_z \lambda_z / (a_o - 1) h_o, \text{ gm/cm}^2 \quad (20a)$$

$$\text{and } \sigma_e = 454 P_e \lambda_e / (b_o - 1) h_o, \text{ gm/cm}^2 \quad (20b)$$

where a_o , b_o , and h_o refer to the measured unstressed dimensions, λ_e and λ_z are the controlled test extension ratios, and P_e and P_z are the measured applied loads. The constant, 454, is required for the purpose of converting the load from pound to gram units. This is required since the loading platforms used fractional pound weights and lead shot of varying quantities. The load cells consisted of heat-treated aluminum rings (1.250" inside diameter, wall thickness .100" and .250" wide) with four active miniature foil strain gages mounted on the inside and outside diameters. The load cell calibration curve was in units of pounds force vs voltage output, or recorder scale deflection.

The preparation of the test specimen and the maintained specimen environment described in Chapter III was adhered to. Prior to installing the test specimen on the test fixture table (Figure 14) the extension ratio gages, λ gages, shown in Figure 13, were sewed to the specimen using black nylon thread. The legs of the λ gages were sewed such that the unstressed

gage length (L_0) was within the 1.75 diameter circle. The purpose of the circle was principally for λ gage location and to visually observe if shear deformation of the circle (or ellipse) occurred during the loading of the tissue.

The λ gages were designed to have a very low spring constant so as to have negligible affect on the applied strain and stress within the test section. Spring rate tests conducted showed the spring constant to be less than 15 grams/cm for both gages. The gages were of two different sizes so that the 90° relative orientation of each could be facilitated with both gages sewed on the upper (inside surface of the vessel wall) or lumen surface of the specimen. The weight of the spring steel gages was negligible but the instrumentation wires were supported during the test so as to minimize vertical (or radial) loading of the specimen.

The load cell and λ gages were wired to a four channel Hewlett-Packard recorder unit, Figure 14. All calibrations were conducted using this recorder unit and the sensitivity of each recorder channel was adjusted so that unit recorder scale deflection readings were directly converted to either load (pounds) or extension ratio (λ) values. This feature facilitated direct readout of information thereby assuring proper test procedure without sacrificing measurement accuracy and testing time. Also data reduction time was minimized.

The calibration of the load cells was conducted the day before each test run and rechecked either following the specimen test or on the following day. This calibration could be conducted on the actual test fixture table using a 5 X 5 cm dummy rubber specimen (tire tube patch material) and was considered to be necessary since the test rig was not totally free of frictional effects between the location of the load cell and the loading platform. A similar calibration and calibration check of the λ gages was

conducted (using the Hewlett-Packard recorder) but had to be made using the Tensilon test machine where changes in the gage length, L_0 , could be accurately measured. The load cells were calibrated to 12 pounds (maximum) and the λ gages to an extension ratio of 1.6 and 2.0 for the z and θ directions, respectively.

For all specimens, the attachment of the small individual loading fixtures was made within the .50 cm wide loading area and the fixtures were equally spaced along the length direction. A continuous string-pulley arrangement was used as shown in Figures 12 and 14 so as to assure equal loading at each fixture attachment. To minimize the non-parallel alignment of the loading strings during stretching of the specimen, the center to center location of the pulleys of the two different loading bars were designed to λ values of 1.30 and 1.50 for the longitudinal and tangential loading bars, respectively. Also, the length of the string was as long as practical so as to keep angular variation of the loading strings to less than 2 degrees. All parts were made from aluminum alloy bar stock and cadmium plated hardware was used. Thus, corrosion due to the use of the saline solution was minimized including the possible contamination of the test specimen tissue.

Since the extension ratios ranged from 1.0 to 1.80 and also varied with respect to the two principal directions two small turn-buckles, shown in Figure 12, were used to maintain the specimen in an approximate fixed but adjustable position on the test table so as to maintain the required 90° angle between the two principal loading directions.

Test Procedure

Each specimen when initially mounted in the test set-up was pre-conditioned by application of four cycles of loading in the longitudinal

direction to the value of $\lambda_z = 1.25$ and approximately simultaneously the four cycles of loading required to give the lowest value of λ_e . Since the pre-conditioning and the final test loadings were essentially manually controlled care was used to assure that the specimen was not strained to a value of less than 1.0 in any direction, i.e., compressive strains were avoided. After a two minute rest period, the biaxial test was initiated and test loadings were conducted to increasing values of λ_e for a given value of λ_z . As each test combination of λ_e and λ_z was reached, the tissue was allowed to stress relax for a period of one to two minutes and the values of the loads, P_e and P_z , were then recorded. The test schedule of λ loading is given in Chapter IV, Table 2. If any specimen was inadvertently unloaded or partially unloaded in any direction due to tearing or slipping of the tissue at one or more grip clamps, the test was terminated at that point. This occurred a few times for the "upper" specimens due to the large tissue thickness, the extreme softness of the tissue, and the significant λ_r deformation caused by the high value of the tangential extension ratio imposed on the specimen during the test.

After each test, the specimen was allowed to soak for two hours in the saline solution. The values of a_o and b_o were measured and found to agree with the originally measured values within a variation of +0 to +0.2 cm. Visual inspection of the tissue thickness indicated a probable reduction in thickness (especially for the upper site location) and is probably due to the reduction in the tissue liquid content caused by the high stretch deformation that the tissue was exposed to during testing.

Test Data

Excluding the measuring of the physical dimensions of each test specimen, the test data consisted primarily of recording the measured

loads, P_{θ} and P_z , associated with the predetermined strains, λ_{θ} and λ_z , as given in Table 2, Chapter IV. Using equations (20a and 20b) the principal stresses, σ_{θ} and σ_z , can be determined. Table 3 lists the values of these stresses associated with each combination of strain and is applicable to the aorta middle site location. Similar test data was obtained for the upper and lower site locations. Included in the table is the number of specimens (N), the value of the mean or average stress ($\bar{\sigma}$), and the value of the standard error of the mean (SEM).

An immediate observation of the stress data is the large degree of specimen to specimen variation. The high to low scatter, or variation, about the mean is approximately ± 30 to 40% of the sample mean stress. This significant variation was previously observed in the axial specimen test results (Figures 9 thru 11) of Chapter III and is typical of that found for biological materials and is the reason why the sample size (N) should not be less than nine specimens. The analysis of the data in Chapter VI is thus based on the mean observed values. The values of the SEM are considered to be normal and are generally equal to 5 to 10% of $\bar{\sigma}$. The value of the SEM is a statistical quantity. It is a measure of the confidence level and variation of the sample mean.

In his development of the non-linear elastic theory for the rheology of large blood vessels, Vaishnav^{18,3} equates the differential change in internal strain energy of the principal stress element (Figure 1) to the change in external work done to the arterial segment caused by a differential increment of internal pressure and longitudinal force. For an incompressible material in which the strain energy function (W) is a function of the strains ϵ_{θ} and ϵ_z , the derivation by Vaishnav concludes with a three dimensional relationship between the difference in principal stresses and

the strain energy gradients as

$$\sigma_{\theta} - \sigma_r = (1 + 2\varepsilon_{\theta}) \frac{dW}{d\varepsilon_{\theta}}$$

$$\sigma_z - \sigma_r = (1 + 2\varepsilon_z) \frac{dW}{d\varepsilon_z}$$

where the strain (ε) is defined as the non-linear (Kirchoff) strain given by equation (9).

For the condition of plane stress (biaxial stress) the value of σ_r is equal to zero and the above equations reduce to the generalized form of:

$$\frac{dW}{d\varepsilon_n} = \sigma_n / (1 + 2\varepsilon_n); \quad n = \theta, z \quad (21)$$

Consequently, the stress data given in Table 3 can be transformed to the strain energy gradient of the strain energy density function (W) of the material. Table 4 contains the test data represented by equation (21).

MIDDLE LOCATION, $Z=12$ CM

			$\lambda_z = 1.35$					
			$\lambda_e = 1.20$		1.30		1.40	
σ_e	σ_z	σ_e	σ_z	σ_e	σ_z	σ_e	σ_z	σ_e
669	1025	2044	1050	884	1238	1406	1419	2288
676	414	1133	522	414	538	824	491	1091
825	415	1212	430	485	460	900	491	1291
848	688	1310	744	544	869	886	898	1470
836	885	1401	863	544	1008	1180	1008	1449
819	561	943	658	371	658	658	658	943
866	710	1588	645	540	668	901	660	1199
917	651	1261	711	639	729	1003	824	1529
927	446	1567	730	434	782	800	782	1163
836	705	1216	731	330	859	661	859	978
833	719	1066		552		867		1299
896		1299						
2	11	12	10	11	10	11	10	11
30	656	1337	708	518	781	916	809	1336
71	58	84	54	43	72	66	86	111

TABLE 3 - BIAXIAL TEST STRESS DATA*

$\lambda_z = 1.25$						$\lambda_z =$			
$\lambda_e = 1.20$		1.30		1.40		$\lambda_e = 1.20$			
σ_z	σ_e	σ_z	σ_e	σ_z	σ_e	σ_z	σ_e	σ_z	
644	738	681	1250	819	1963	906	950	938	
343	414	343	750	704	1133	370	414	429	
328	485	342	893	385	1170	415	485	388	
618	614	631	959	631	1310	643	281	658	
550	544	735	1180	735	1450	885	621	888	
415	299	415	656	471	892	504	336	562	
542	555	527	901	534	1360	553	758	558	
514	733	546	1247	530	1584	601	498	639	
368	546	368	836	429	1275	382	639	387	
532	320	629	744	655	1040	677	417	677	
535	657	626	996	626	1255	625	356	636	
							552		
N	11	11	11	11	11	11	12	11	
$\bar{\sigma}$	490	537	531	947	593	1312	595	526	613
SEM	33	45	43	62	41	87	55	56	55

* gm/cm²

LOCATION, $Z=12$ CM

		$\lambda_z = 1.35$							
		1.40		$\lambda_e = 1.20$		1.30		1.40	
ϵ_e	$\frac{dW}{d\epsilon_z}$	$\frac{dW}{d\epsilon_e}$	$\frac{dW}{d\epsilon_z}$	$\frac{dW}{d\epsilon_e}$	$\frac{dW}{d\epsilon_z}$	$\frac{dW}{d\epsilon_e}$	$\frac{dW}{d\epsilon_z}$	$\frac{dW}{d\epsilon_e}$	
10	607	1043	576	586	679	832	779	1167	
20	245	578	286	288	295	488	269	557	
38	246	618	236	337	252	533	269	659	
52	407	668	408	378	477	524	493	750	
72	524	715	478	378	553	698	553	739	
96	332	481	361	258	361	389	361	481	
120	420	810	354	375	366	533	362	612	
143	385	643	390	444	400	594	420	780	
168	264	799	401	301	429	473	429	593	
195	417	620	401	229	471	391	471	499	
214	425	544		383		513		663	
230		663							
	11	12	10	11	10	11	10	11	
30	388	682	389	360	429	542	444	682	
42	34	43	30	30	40	39	47	57	

TABLE 4 BIAXIAL TEST $\frac{dw}{d\epsilon_n}$ * DATA, MIDDLE

$\lambda_z = 1.25$						$\lambda_z =$			
$\lambda_\theta = 1.20$		1.30		1.40		$\lambda_\theta = 1.20$			
$\frac{dw}{d\epsilon_z}$	$\frac{dw}{d\epsilon_\theta}$	$\frac{dw}{d\epsilon_z}$	$\frac{dw}{d\epsilon_\theta}$	$\frac{dw}{d\epsilon_z}$	$\frac{dw}{d\epsilon_\theta}$	$\frac{dw}{d\epsilon_z}$	$\frac{dw}{d\epsilon_\theta}$	$\frac{dw}{d\epsilon_\theta}$	
412	513	435	740	524	1001	536	660	555	
220	288	220	444	450	578	219	288	254	
210	337	219	528	247	597	246	337	228	
396	426	404	567	404	668	380	195	380	
352	378	471	698	471	740	524	431	524	
266	208	266	388	302	455	298	233	332	
347	385	337	533	342	694	315	526	328	
329	509	350	738	339	808	356	346	370	
236	379	236	495	275	651	226	444	226	
341	222	403	440	419	531	401	290	401	
343	456	401	589	401	640	370	247	370	
							383		
N	11	11	11	11	11	11	12	11	
$\overline{\frac{dw}{d\epsilon_n}}$	314	373	340	560	380	669	352	365	
SEM	23	31	28	36	26	44	32	39	

* gm/cm²

CHAPTER VI

ANALYSIS AND RESULTS OF BIAXIAL TESTING

Introduction

The purpose of this chapter is to determine from the biaxial test data, the two-dimensional relationships of stress and strain (σ vs ϵ, λ) for the anisotropic aorta material under a state of plane stress, $\sigma_r = 0$. Secondary to this goal is to determine the characteristics of the material elastic tangent modulus (E) with respect to direction and strain and the general equation for the radial strain (ϵ_r) as a function of the tangential and longitudinal strains.

Since the detailed analysis and calculations are lengthy for each aorta test location, the analysis in the following section will be based on the test data of Table 4 which is applicable to the middle site location. The method and techniques outlined below are also applicable to the analysis of the biaxial test data at the upper and lower site locations. The final results of such analysis at each of the three locations will be presented in summary form, both graphically and tabular, and will be used in Chapter VII for the in-vivo physiologic analysis of the aorta blood vessel.

Analysis

Strain Energy Gradient:

The biaxial test data for the middle site location presented in Table 4 is plotted in Figures 15 and 16 for the tangential and longitudinal directions of the biaxial specimen loading combinations given in Table 2.

The test mean values and the range of the standard error of the mean (SEM) for the strain energy gradients ($dW/d\epsilon_e$ and $dW/d\epsilon_z$) are plotted against the non-linear strain (ϵ_e and ϵ_z) defined by equation (9) and the extension ratio (λ_e and λ_z) defined by equation (6) for each biaxial test combination of strain loading. The graphs show in general that the mathematical relationship of $dW/d\epsilon_n$ vs ϵ_n is essentially non-linear particularly since the strain energy gradient must be equal to zero for the state of zero strain, ϵ_e or ϵ_z . This boundary condition suggests and is satisfied by a general second order polynomial equation of the form

$$dW/d\epsilon_n = A_n \epsilon_e + B_n \epsilon_z + C_n \epsilon_e \epsilon_z + D_n \epsilon_e^2 + E_n \epsilon_z^2 \quad (22)$$

where $n = e, z$. Using the method of least squares, and the mean values of the test data shown in Figures 15 and 16, the coefficients, A thru E, of this equation can be evaluated via matrix algebra. Thus, the mathematical relationship can be determined using equation (22), or variations of it, providing that the "best fit" is achieved which satisfies the accepted criteria that the statistical correlation coefficient (r) must be ≥ 0.94 . Another criteria to be used is that the general form represented by equation (22) should be reduced to its simplest form (i.e., as few terms as possible) provided that the correlation coefficient criteria is satisfied.

The graph of Figure 15 shows clearly that the strain energy gradient ($dW/d\epsilon_e$) with respect to the tangential strain is independent of the longitudinal strain. Thus, assuming that the coefficients B, C, and E are zero or very small, equation (22) reduces to

$$dW/d\epsilon_e = A_e \epsilon_e + D_e \epsilon_e^2 \quad (\epsilon_z = 0 \text{ to } 0.42) \quad (23)$$

and applying the test mean values to the method of least squares the coefficients A and D are calculated to be equal to +1920 and -1034 respec-

Figure 15 - Strain Energy Gradient $\frac{dW}{d\epsilon_0}$
 -vs-
 Tangential Strain ϵ_0

Middle - z = 12 cm

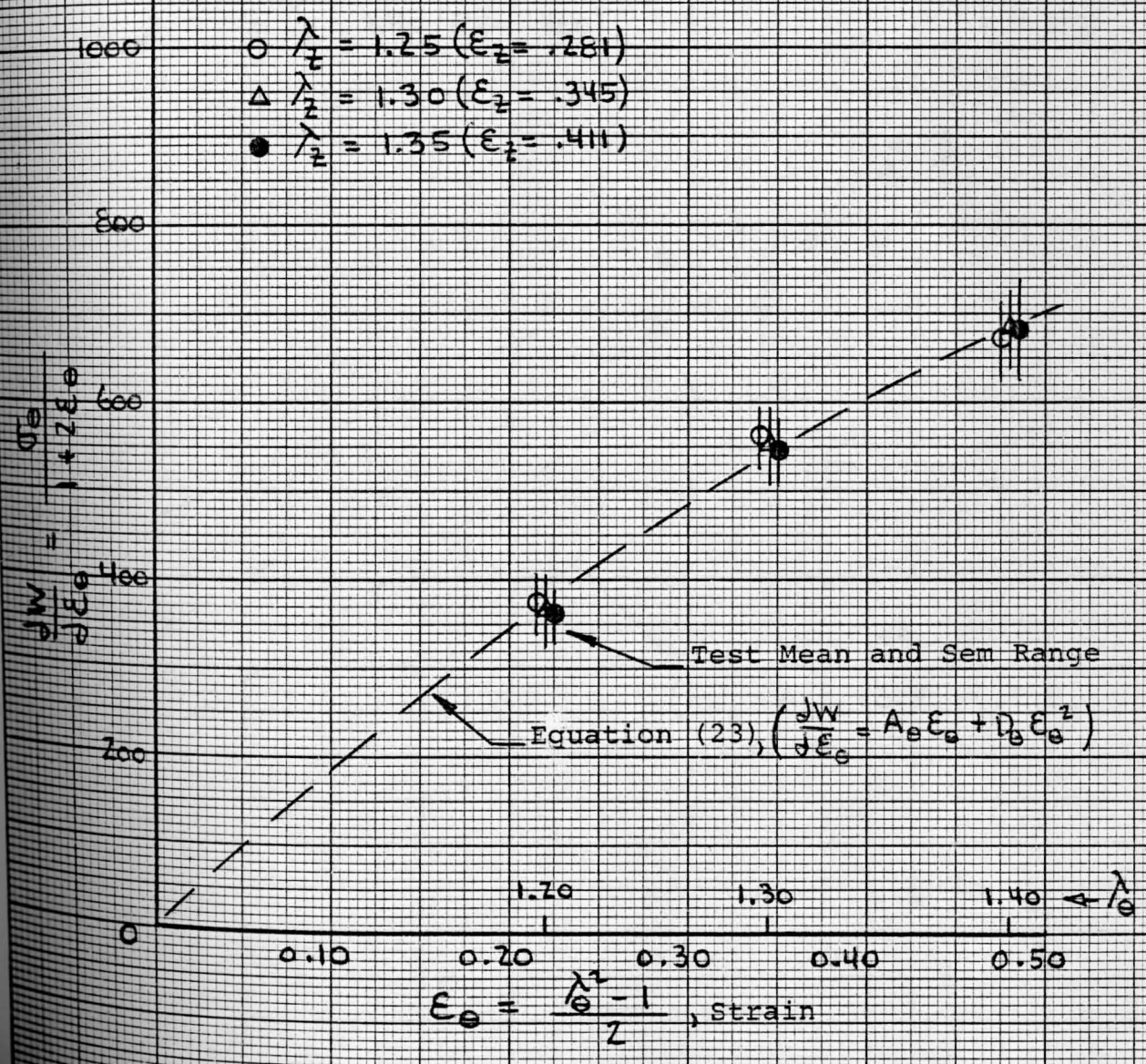
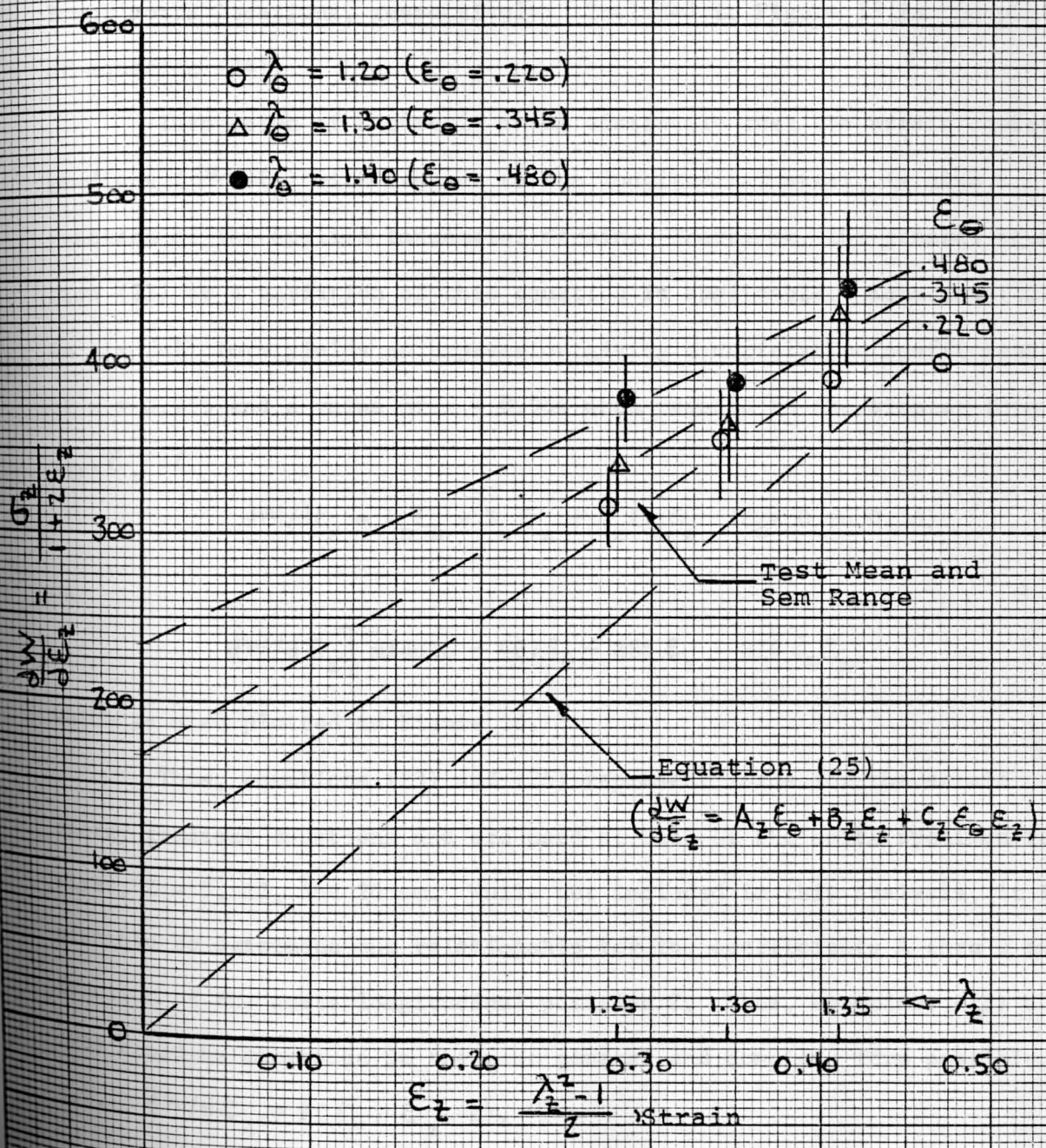


Figure 16 - Strain Energy Gradient $\frac{dW}{d\epsilon_z}$
 -vs-
 Longitudinal Strain ϵ_z

Middle - z = 12 cm



tively, or

$$\left. \frac{dW}{d\epsilon_e} \right]_{\text{middle}} = 1920 \epsilon_e - 1034 \epsilon_e^2 \quad (24)$$

for the middle specimen location. The corresponding correlation coefficient (r) is calculated to be 0.996 indicating approximately 100% agreement between the test data and the empirical equation. Thus, the use of equation (23) for the tangential strain energy gradient is justified, and it also yields r values of 0.970 and 0.981 for the upper and lower aorta locations, respectively. Included in Figure 15 is the plot of equation (24).

Inspection of Figure 16 shows distinctly that the strain energy gradient ($dW/d\epsilon_z$) with respect to the longitudinal strain is also a function of the applied tangential strain. Therefore, the general equation (22) or a variation of this equation is applicable. Equation (22) in its full form yields an expression giving a correlation coefficient of $r = 0.955$ and a value of $r = 0.964$ when reduced to the simpler form in ϵ_e, ϵ_z of

$$\frac{dW}{d\epsilon_z} = A_z \epsilon_e + B_z \epsilon_z + C_z \epsilon_e \epsilon_z \quad (\epsilon_e = 0 \text{ to } 0.50) \quad (25)$$

or

$$\left. \frac{dW}{d\epsilon_z} \right]_{\text{middle}} = 487 \epsilon_e + 885 \epsilon_z - 814 \epsilon_e \epsilon_z \quad (26)$$

which is also plotted in Figure 16.

Thus, equations (23) and (25) represent forms for the strain energy gradient functions and are used at each of the aorta specimen test sizes, $Z = 5, 12, \text{ and } 20$ cm. While not included in this analysis, it is possible to determine the relationship for the coefficients A thru D as a function of the aorta longitudinal position Z . Thus, equations (23) and (25) could be expressed in the most general and complete form possible, i.e., $\frac{dW}{d\epsilon_n} = F(\epsilon_e, \epsilon_z, Z)$.

Stress-Strain Relations:

Having determined the tangential and longitudinal strain energy gradient equations (24 and 26) for the middle thoracic aorta location as functions of the finite non-linear strain, the equations for the true tangential and true longitudinal stresses (based on the deformed geometry) as functions of the two-dimensional strains can be determined. Using equation (21) in conjunction with equations (24) and (26) we obtain

$$\begin{aligned}\sigma_e &= 1920 \epsilon_e + 2806 \epsilon_e^2 - 2068 \epsilon_e^3 && (\text{gm/cm}^2) \\ \sigma_z &= 487 \epsilon_e + 885 \epsilon_z + 180 \epsilon_e \epsilon_z + 1770 \epsilon_z^2 - 1628 \epsilon_e \epsilon_z^2\end{aligned}\quad (27)$$

which represents the relationship of stress and strain applicable to the biaxial loading of the principal stress element at the middle site location.

The biaxial stress test data (test mean and SEM range) of Table 3 is plotted in Figures 17 and 18 for the tangential and longitudinal stresses respectively. The derived curves represented by equation (27) are also shown for direct visual comparison with the test values. The "best fit" of these equations as measured by the correlation coefficient (r) is the same as previously noted for the strain energy gradients (SEG) since stress and SEG are not independent of each other. Extrapolation of equations (27) or the plotted curves beyond a strain of 0.50 is not advisable.

Included in Figure 18, σ_z vs ϵ_z, ϵ_e , is the curve for $\epsilon_e = 0$. This should not be assumed to be the stress-strain curve for uniaxial longitudinal loading since the strain in the tangential direction for such loading would be less than zero or compressive strain, i.e., $\epsilon_e < 0$. As would be expected, Figure 18 shows that for a given longitudinal strain, the corresponding longitudinal stress increases as the mutually perpendicular strain ϵ_e (or loading) is increased. Also notice, for both Figures 17 and 18, that the stress-strain curves are very close to being linear

Figure 17 - True Tangential Stress
-vs-
Tangential Strain

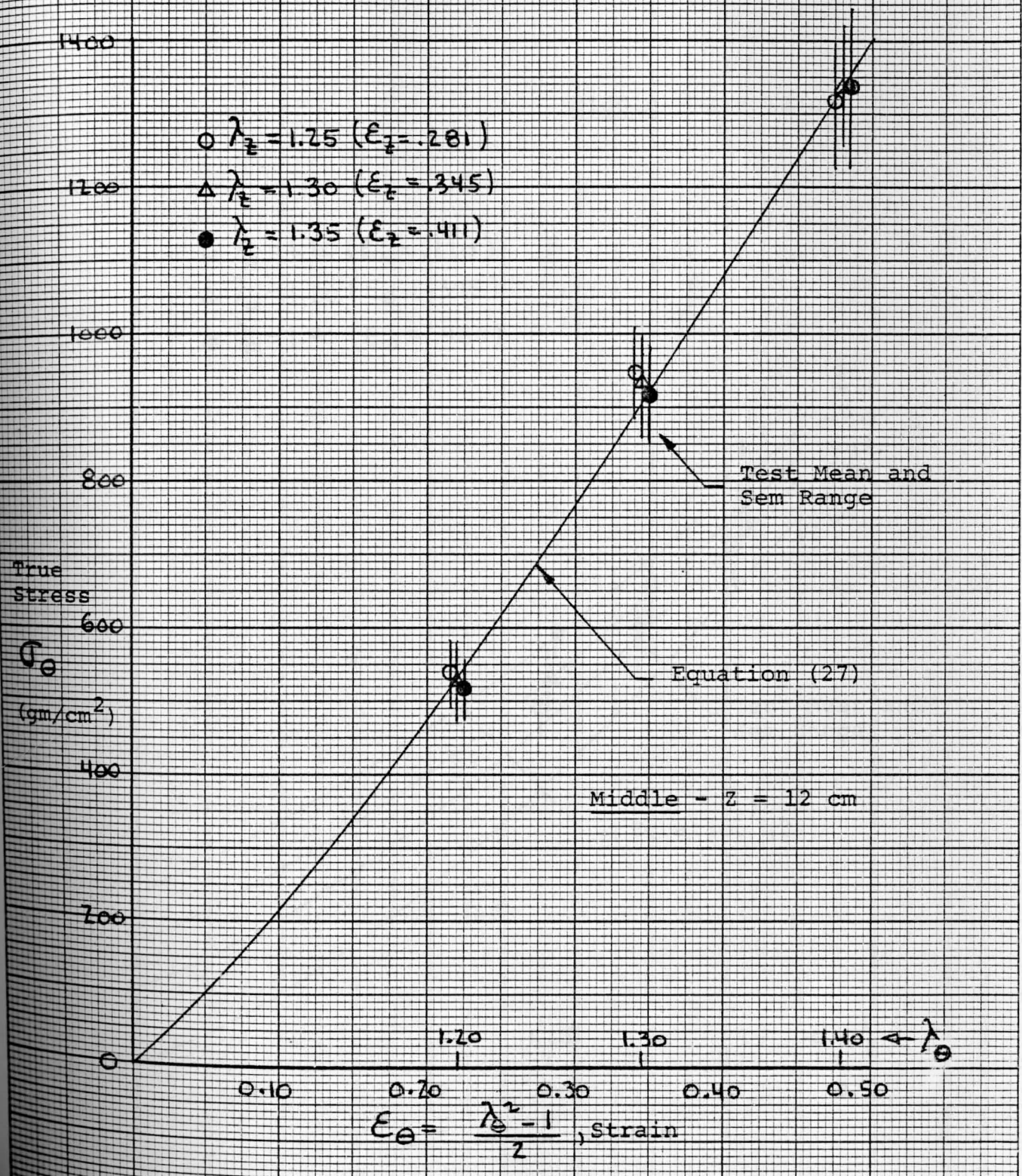
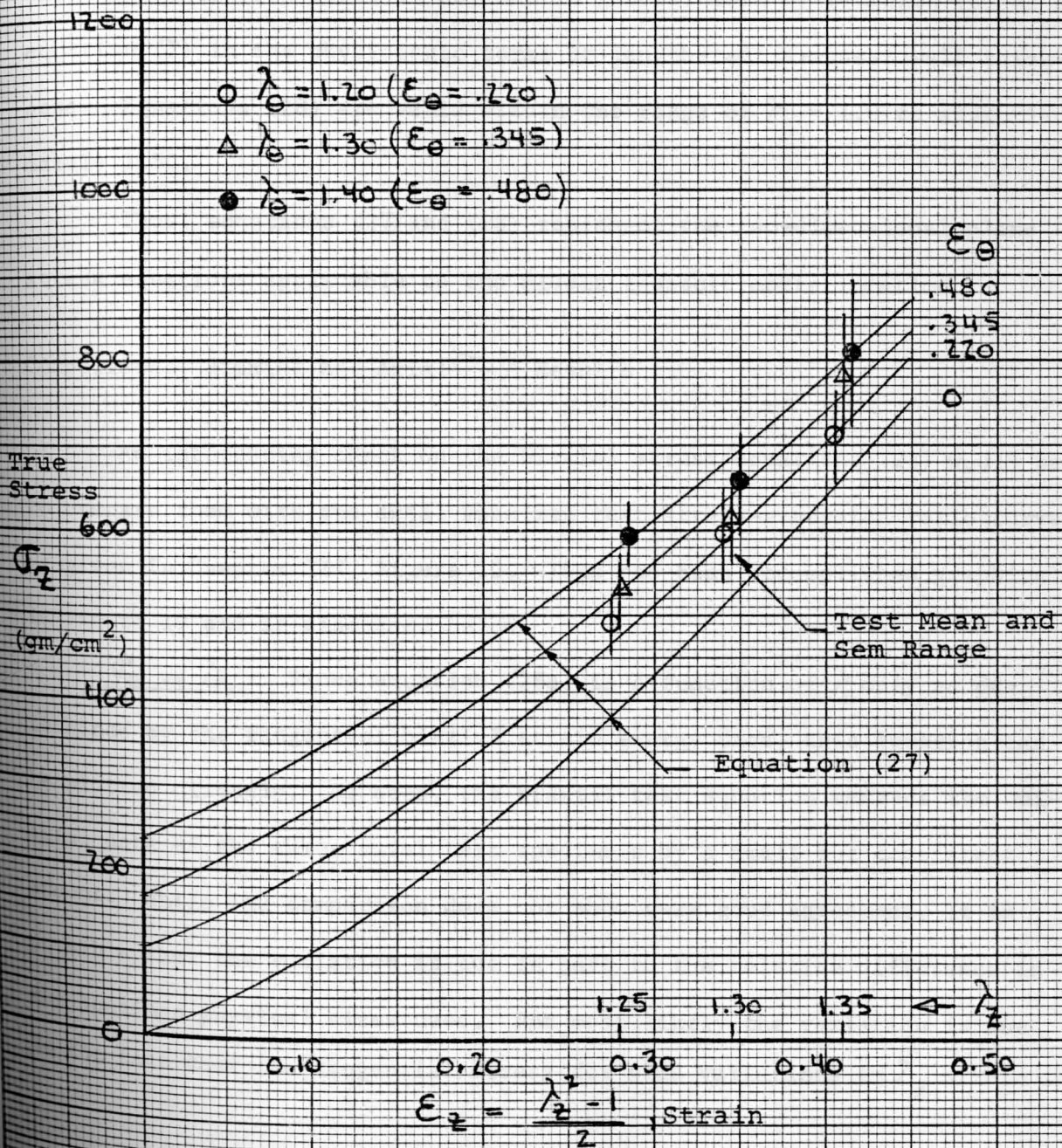


Figure 18 - True Longitudinal Stress

-vs-

Longitudinal and Tangential Strain

Middle - $z = 12$ cm



within the tested ranges of the extension ratios of λ_z and λ_e .

The above equations can be converted to the more practical (in-vivo notation) form of $\sigma_n = f(\lambda_n)$ using the non-linear strain vs extension ratio relationship of equation (9). Or:

$$\sigma_e = 1477 \lambda_e^4 - 1219 \lambda_e^2 - 259 \lambda_e^6 \quad (\text{gm/cm}^2) \quad (28a)$$

$$\sigma_z = 653 \lambda_z^4 + 466 \lambda_e^2 \lambda_z^2 - 908 \lambda_z^2 - 210 \lambda_e^2 \lambda_z^4 \quad (28b)$$

where the extension ratio is defined in general form by equation (6) or by equation (7) in the physiologic terms of length-radius-vessel wall thickness. Equations (28) are valid within the range of $\lambda_n = 1.0$ to approximately 1.50.

Thus, equations (27) and (28) represent the two-dimensional plane stress equations applicable to the middle thoracic aorta location.

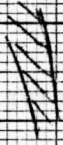
Comparison: Biaxial and Axial σ - λ Results

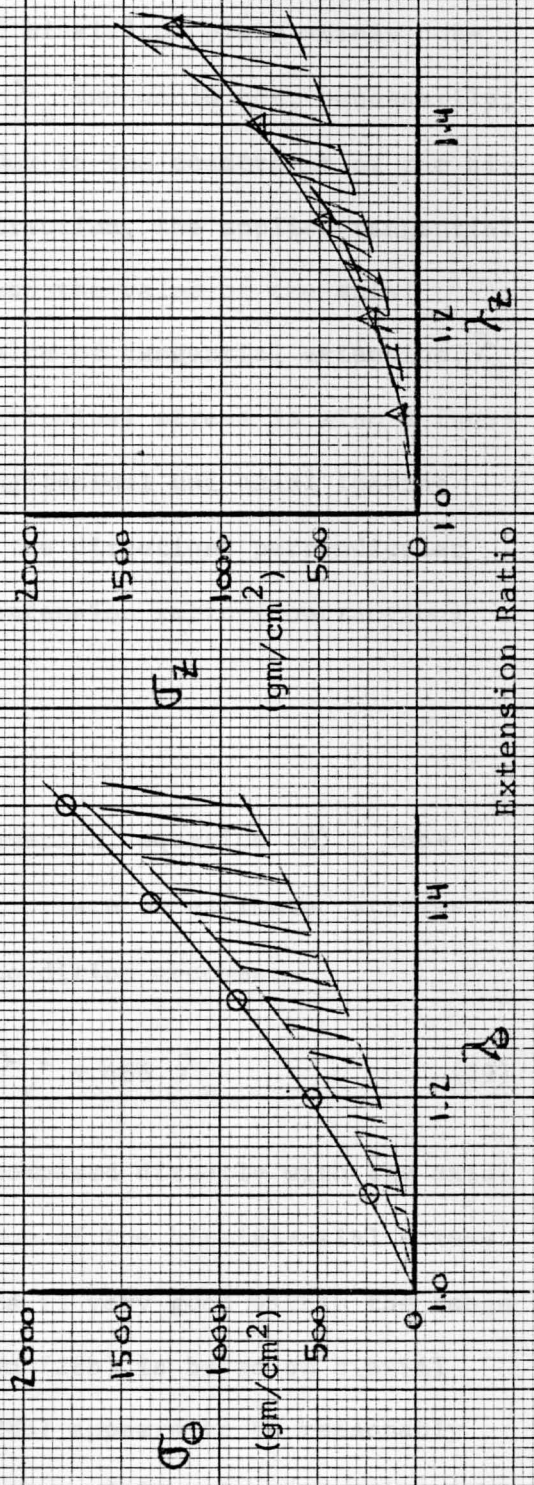
An interesting check on the biaxial stress equations (28) would be to compare them with the axial specimen test stress-extension ratio curves as given in Chapter III, Figure 10. This has been accomplished graphically in Figure 19 and is discussed below.

σ_e vs λ_e : Since equation (28a) is a function of λ_e only as determined by the tangential biaxial strain energy data, this equation can be plotted directly. As seen, the biaxial test equation exceeds the uniaxial data of the three axial test specimens by a small but consistent amount. While the comparison does not show very good agreement, it is possible that the variation is due in part to the relative difference in the specimen physical sizes used. But most likely the variation is due to the fact that the tangential stress for wide variations in λ_z strain is

Figure 19 - Comparison of Biaxial Test Stress-Strain Equations with Axial Test Specimen Data

Middle - Z = 12 cm

Code:  Axial Specimen Test Range (3 specimens)
 O—O Biaxial Test: Equation (28a)
 A—A Biaxial Test: Equation (29)



not actually independent of λ_z . In tangential uni-axial stress loading the extension ratio λ_z would be considerably smaller than unity in comparison with the biaxial test range of $\lambda_z = 1.25$ to 1.35 . On this basis, equation (28a) is representative of biaxial or plane stress conditions over a relatively narrow range of λ_z and would not, necessarily, be representative of uni-axial loading. Due to the constraint of the biaxial test specimen in the longitudinal direction, the applied tangential stress, as shown in Figure 19, should exceed the value of the axial specimen tangential stress for the same value of tangential extension, λ_e .

σ_z vs λ_z : Equation (28b) for longitudinal stress is also a function of the tangential strain λ_e . For longitudinal uni-axial loading where the material is free to contract in the directions perpendicular to the loading axis, the free tangential extension ratio (contraction) is given by

$$\lambda_e = \lambda_r = 1/\sqrt{\lambda_z}$$

which is based on the incompressibility equation, equation (8). Substituting this into equation (28b) the appropriate or estimated stress-strain equation for the uni-axial stress condition becomes

$$\sigma_z = 653 \lambda_z^4 - 210 \lambda_z^3 - 908 \lambda_z^2 + 466 \lambda_z \quad (29)$$

which is plotted in Figure 19 and can be compared directly with the axial test specimen data. As seen, the comparison of the biaxial-axial stress equation vs axial specimen test stress data is very good within the range of $\lambda_z = 1.0$ to 1.40 . Thus, while equation (28b) is based on biaxial test λ_e values of 1.20 to 1.40 , equation (28b) appears to be reasonably valid for tangential extension ratios as low as 0.80 . Consequently, it

would appear that specimen size difference affects are negligible or non-existent.

Similar graphic comparisons, as discussed above, were made for the upper and lower specimen site locations. The upper site comparison results were almost identical with those discussed above for the middle location. The comparison at the lower site for both the tangential directions were exceptionally good. Thus, a reasonable measure of confidence level has been achieved between the two widely different types of testing and the analytical results obtained from the biaxial test program. This would indicate that specimen preparation, testing, and the analytical techniques used have been consistent and valid.

Strain-Stress Relations:

In the theory of elasticity, developed by Navier and Cauchy⁷, a set of functions characterizing the state of stress is shown to be linearly related to a set of functions characterizing the state of deformation or strain; and, conversely, the state of strain is linearly related to a set of functions characterizing the state of stress. For a homogeneous elastic isotropic material the linear relationship is identified as Hooke's Law and contains two elastic constants which define the dependence of normal and shear stress relative to infinitesimal normal or shear deformations or strains.

Since the aorta blood vessel wall material is neither isotropic, nor linearly elastic throughout the range of finite or large deformations which the material is normally subjected to, the relationship of stress and strain defined by equation (27) and (28) is not a set of linear

functions but are of the non-linear form:

$$\begin{aligned}\sigma_{\theta} &= F(\epsilon_{\theta}, \epsilon_{\theta}^2, \epsilon_{\theta}^3) \\ \sigma_z &= G(\epsilon_{\theta}, \epsilon_z, \epsilon_{\theta}\epsilon_z, \epsilon_z^2, \epsilon_{\theta}\epsilon_z^2)\end{aligned}\quad (30)$$

or

$$\begin{aligned}\sigma_{\theta} &= F'(\gamma_{\theta}^2, \gamma_{\theta}^4, \gamma_{\theta}^6) \\ \sigma_z &= G'(\gamma_z^2, \gamma_{\theta}^2\gamma_z^2, \gamma_z^4, \gamma_{\theta}^2\gamma_z^4)\end{aligned}\quad (31)$$

where strain is defined by equations (9), (6) or (7). The two dimensional non-linear form of these plane stress "stress-strain" equations cannot be altered to yield an explicit relationship of plane stress "strain-stress" equations as is the circumstance for materials whose behavior can be identified as being isotropic and Hookean.

The biaxial testing (plane stress condition) does not yield the general relationship of

$$\begin{aligned}\sigma_r &= I(\epsilon_r^l, \epsilon_{\theta}^m, \epsilon_z^n) \\ &= I'(\gamma_r^{l'}, \gamma_{\theta}^{m'}, \gamma_z^{n'})\end{aligned}\quad (32)$$

which would exist for a state of three-dimensional stress or loading.

This relationship would be nonlinear and thus the powers of l , m , n are shown but cannot be defined at this point.

Although the strains, ϵ_{θ} , ϵ_z , and ϵ_r cannot be simply and explicitly defined as functions of stress by use of equations (27), (28) or (30), (31) the radial strain ϵ_r can be defined as a function of the tangential and longitudinal strains using the incompressibility, equation (8),

or

$$\gamma_r = 1/\gamma_{\theta}\gamma_z \quad (33)$$

where the extension (strain) ratios are defined by equations (6) and (7).

By rewriting equation (9), the definition of the non-linear or Kirchoff measure of strain, in the form of

$$\lambda_n^2 = 2\epsilon_n + 1$$

and substituting this into (33), after squaring both sides of (33), we obtain after rearrangement

$$\epsilon_r = 1/2 \left[\left[\frac{1}{(2\epsilon_\theta + 1)(2\epsilon_z + 1)} - 1 \right] \right] \quad (34)$$

This is a general relationship for the non-linear strain, ϵ_r , as a function of the tangential and longitudinal strains. As such it is applicable to an incompressible material.

Modulus of Elasticity:

In the classical theory of elasticity for linear infinitesimal strains, the modulus of elasticity, or tangent modulus, is defined as the slope of the stress-strain curve at a stated value of stress or strain. In general, mathematical terms:

$$E_n = d\sigma_n / d\epsilon_n \quad (35)$$

which for most engineering materials is a unique constant with the proportional limit of the material. This same relationship has been used for the description of the modulus of elasticity of biological materials subject to both finite small and large linear and non-linear elastic deformation, Bergel³ and Mirsky⁸, and will be used also for the aorta blood vessel wall material.

Examination of the middle specimen tangential and longitudinal stress-strain diagrams of Figures 17 and 18 show a distinct, but not pronounced, variation of the slope of the curves over the range of strain from 0 to 0.50 and a definite initial or unstressed modulus of elasticity (E_{n_0}) for the unstressed conditions of $\epsilon_z = \epsilon_\theta = 0$.

Differentiating the σ vs ϵ equations (27) per equation (35) the expression for the in-vitro tangential and longitudinal modulus at the middle location becomes

$$\begin{aligned} E_\theta &= 1920 + 5612 \epsilon_\theta - 6204 \epsilon_\theta^2 \\ E_z &= 885 + 180 \epsilon_\theta + 3540 \epsilon_z - 3256 \epsilon_\theta \epsilon_z \end{aligned} \quad (\text{gm/cm}^2) \quad (36)$$

and the unstressed modulus in the tangential and longitudinal directions are 1920 and 885 grams/cm², respectively. Thus, in the unstressed condition, the initial modulus of elasticity at the middle location is approximately 117% stiffer in the tangential direction as compared to the longitudinal direction. Examination of Figure 10 for the axial test specimen shows this same characteristic.

Equations (36) represent the magnitude and the variation of the modulus of elasticity with respect to strain and can be expressed relative to the extension ratios, λ_θ and λ_z , by substituting equation (9) into (36) thereby yielding

$$\begin{aligned} E_\theta &= f(\lambda_\theta) = -2437 + 5908 \lambda_\theta^2 - 1551 \lambda_\theta^4 \\ E_z &= g(\lambda_z, \lambda_\theta) = -1814 + 2609 \lambda_z^2 + 929 \lambda_\theta^2 - 839 \lambda_z^2 \lambda_\theta^2 \end{aligned} \quad (37)$$

which for the unstressed condition, $\lambda_n = 1.0$, yields the same values for the unstressed modulus of elasticity.

Equations (36) are plotted in Figure 20 and are discussed below.

E_{θ} vs ϵ_{θ} :

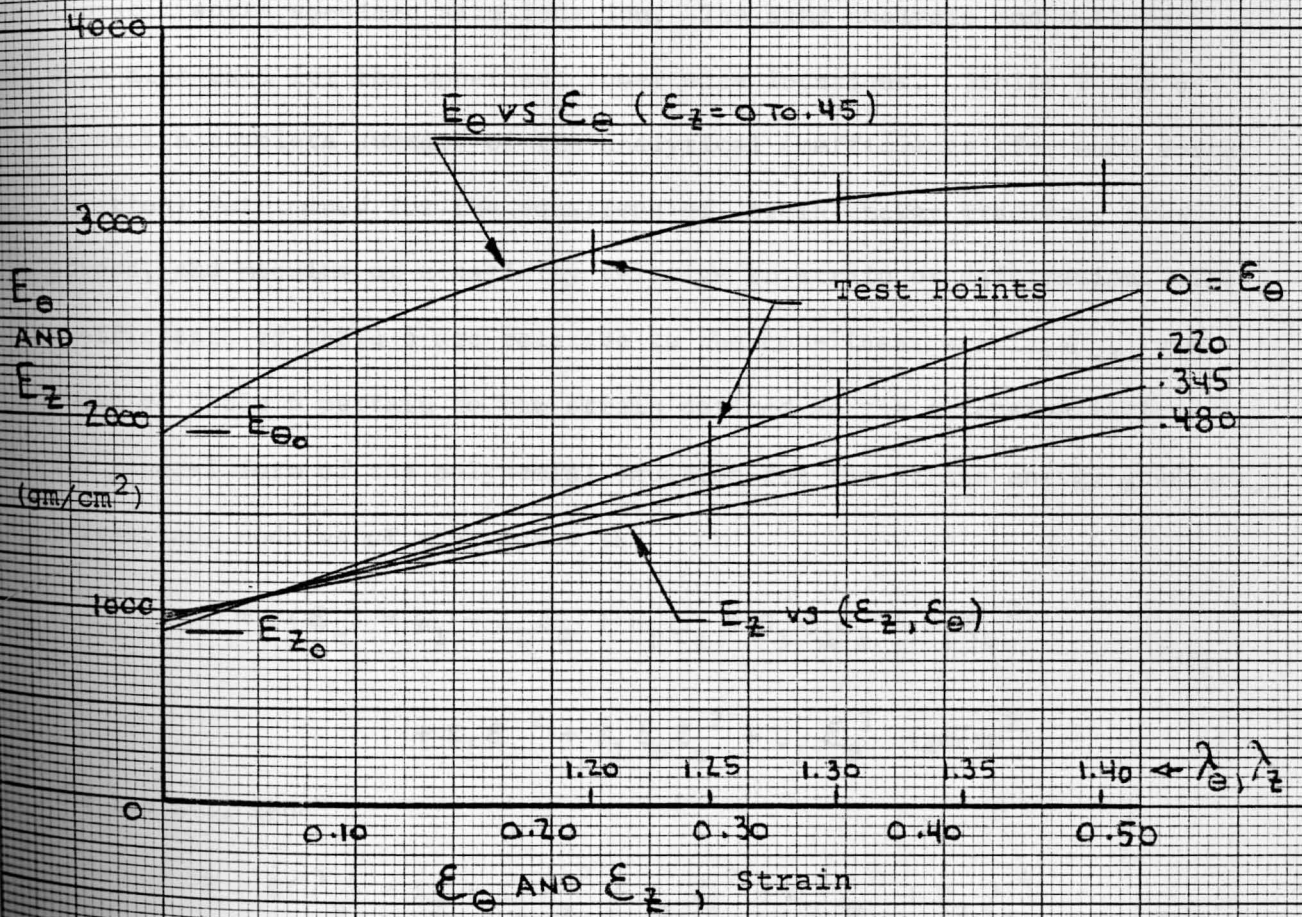
Within the initial strain range of ϵ_{θ} from 0 to 0.22 ($\lambda_{\theta} = 1.0$ to 1.2) the stiffness of the material increases significantly and at $\epsilon_{\theta} > 0.22$ ($\lambda_{\theta} > 1.20$) the tangential modulus of elasticity tends to level off to a maximum value of approximately 3200 gm/cm^2 or a 67% increase in elasticity (stiffness) compared to the unstressed or initial modulus. Within the probable physiologic range of $\epsilon_{\theta} = 0.20$ to 0.50 the value of E_{θ} is approximately constant having a mean value of 3100 gm/cm^2 . This is significant since for analytical purposes analysis and calculations could be simplified, if so desired, with a minimum sacrifice in accuracy. However, the aorta material in the tangential direction for unrestricted strain magnitudes cannot be considered to have a constant value of tangent modulus, E_{θ} as is commonly the case for engineering materials. This point has been displayed in the axial test results of Chapter III.

E_z vs $\epsilon_z, \epsilon_{\theta}$:

In the longitudinal direction, the aorta material again cannot be considered to have a constant value of tangent modulus, E_z , E_z varies linearly with respect to longitudinal strain and is also dependent on the tangential strain. Within the test ranges of ϵ_z from 0.28 to 0.41 ($\lambda_z = 1.25$ to 1.35) and ϵ_{θ} from 0.22 to 0.48 ($\lambda_{\theta} = 1.2$ to 1.4) the average value of E_z is approximately 1800 gm/cm^2 . This value, if assumed constant for the stated range of strains, represents little sacrifice in analytical accuracy and indicates that the material stiffness doubles in magnitude as compared to its initial or unstressed elastic value of 885 gm/cm^2 .

Figure 20 - Tangential and Longitudinal Modulus of Elasticity - vs - Strain

Middle - $z = 12$ cm



The above comments of this section pertain to the in-vitro characteristics of the material modulus of elasticity, or stiffness, relative to strain or deformation at the middle aorta location. It should not be assumed that the in-vivo elastic properties of the aorta wall material are in complete agreement with those discussed above. Such differences will be discussed in the following chapter.

Summary and Discussion of Results

The previous sections of this chapter pertained to the analysis and methods of analysis of the biaxial test data applicable to the middle thoracic aorta specimen site location. The same analysis and methods were also used for the upper and lower site locations. Tables 5 and 6 present a complete summary of the analytical coefficients (for each aorta location) determined for the equations of strain energy gradient, true stress, and modulus of elasticity relative to strain or deformation. The coefficients of Table 5 are relative to the non-linear strain, ϵ_n , and those of Table 6 pertain to the strain defined as the extension ratio, λ_n . The general form of the polynomial equation for the strain energy gradient, stress, and modulus of elasticity is:

$$Y = F(\epsilon_n) = K_1 + A_1 \epsilon_\theta + B_1 \epsilon_z + C_1 \epsilon_\theta \epsilon_z + D_1 \epsilon_\theta^2 + E_1 \epsilon_z^2 + F_1 \epsilon_\theta \epsilon_z^2 + G_1 \epsilon_\theta^3 \quad (\text{gm/cm}^2) \quad (38)$$

for Table 5, and

$$Y = G(\lambda_n) = K_2 + A_2 \lambda_z^2 + B_z \lambda_\theta^2 + C_2 \lambda_\theta^4 + D_2 \lambda_z^4 + E_2 \lambda_\theta^2 \lambda_z^2 + F_z \lambda_\theta^6 + G_2 \lambda_\theta^2 \lambda_z^4 \quad (\text{gm/cm}^2) \quad (39)$$

POLYNOMIAL

$\epsilon_{\theta} \epsilon_z^2$	ϵ_{θ}^3	r	ϵ_n (MAX.)	
		.970	$\epsilon_{\theta} = 1.15$ $\epsilon_z = .45$	U P P E R $z = 5$ cm
		.943		
	-600			
1098				
		.996	$\epsilon_{\theta} = .50$ $\epsilon_z = .45$	M I D D L E $z = 12$ cm
		.964		
	-2068			
1628				
		.981	$\epsilon_{\theta} = .45$ $\epsilon_z = .45$	L O W E R $z = 20$ cm
		.995		
	1326			
232				

TABLE 5 - SUMMARY OF COEFFICIENTS FOR EQUATION (38)

	Y (gm/cm^2)	K_1	E_θ	E_z	$E_\theta E_z$	E_θ^2	E_z^2
U P P E R $z = 5$ cm	dW/dE_θ		1043			-300	
	dW/dE_z		319	818	-539		
	σ_θ		1043			1786	
	σ_z		319	818	99		163
	E_θ	1043	3572			-1800	
	E_z	818	99	3272	-2156		
M I D D L E $z = 12$ cm	dW/dE_θ		1920			-1034	
	dW/dE_z		487	885	-814		
	σ_θ		1920			2806	
	σ_z		487	885	180		177
	E_θ	1920	5612			-6204	
	E_z	885	180	3540	-3256		
L O W E R $z = 20$ cm	dW/dE_θ		1721			663	
	dW/dE_z		569	1080	-616		
	σ_θ		1721			4105	
	σ_z		569	1080	522		216
	E_θ	1721	8210			3978	
	E_z	1080	522	4320	-2464		

Table 6 - Summary of Coefficients for Polynomial Equation (39)

	Y (g_m/cm^2)	K_z	λ_z^2	λ_θ^2	λ_θ^4	λ_z^4	$\lambda_\theta^2 \lambda_z^2$	λ_θ^6	$\lambda_\theta^2 \lambda_z^4$	λ_n (max)
U P P E R Z=5cm	σ_θ			-597	672			-75		$\lambda_\theta =$ 1.80
	σ_z		-702			544	293		-135	
	E_θ	-1193		2686	-450					$\lambda_z =$ 1.35
	E_z	-1407	2175	589			-539			
M I D D L E Z=12cm	σ_θ			-1219	1477			-259		$\lambda_\theta =$ 1.40
	σ_z		-908			653	466		-210	
	E_θ	-2437		5908	-1551					$\lambda_z =$ 1.35
	E_z	-1814	2609	929			-839			
L O W E R Z=20cm	σ_θ			-695	529			166		$\lambda_\theta =$ 1.30
	σ_z		-979			694	439		-154	
	E_θ	-1390		2116	995					$\lambda_z =$ 1.35
	E_z	-1957	2776	887			-616			

for Table 6 with the coefficients listed in each table under the appropriate variable. Each table lists the recommended maximum value of ϵ_n or λ_n for which the equation is considered to be valid. Analytical extrapolation beyond these values is not recommended. Table 5 also includes the "best fit" or statistical correlation coefficient, r , which is a measure of the agreement between the test data and the empirically derived equation.

Stress-Strain:

The equation of tangential and longitudinal stress vs strain, given by equation (38) and Table 5, are plotted in Figures 21 and 22 for each thoracic aorta location including the corresponding mean biaxial test values for purposes of direct comparison. Figures 21 and 22 distinctly show both the non-linear relationship of stress-strain, as is expected, as well as the anisotropic-orthotropic nature of the material which was discussed in Chapter II and observed in the axial specimen test results of Chapter III. Of particular interest is the variation of the tangential stress, for a given tangential strain, with respect to longitudinal location in view of the large mean wall thickness variation shown in Figure 2. The lower site wall thickness is very thin compared ($\approx 40\%$) to that of the upper site location and the lower tangential stress is approximately 100% greater than the upper location at a tangential strain of $\lambda_e = 1.30$. The reduced elastin content, and the increase in the stiffer collagen fibers at the lower location, contribute to a significant increase in the stiffness or modulus of elasticity at the lower location as shown by the higher stress level and the slope of the $\sigma_\theta - \epsilon_\theta$ curve.

For the wide range in the tangential strains ($\epsilon_\theta = 0.22$ to 0.78) used in the σ_z vs ϵ_z curves of Figure 22, it is remarkable that the

Figure 21 - Tangential Stress-Strain
-vs-
Thoracic Aorta Location

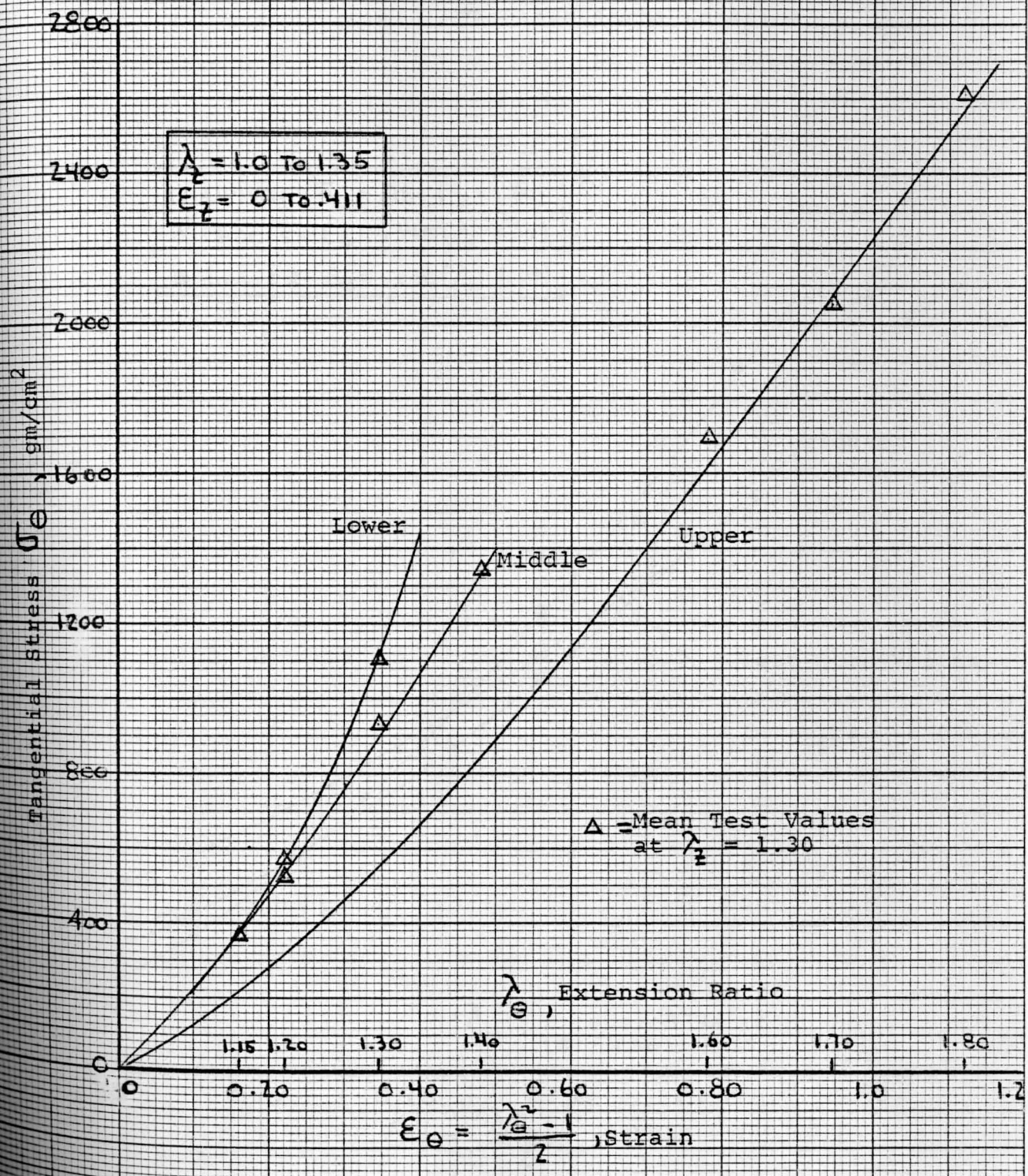
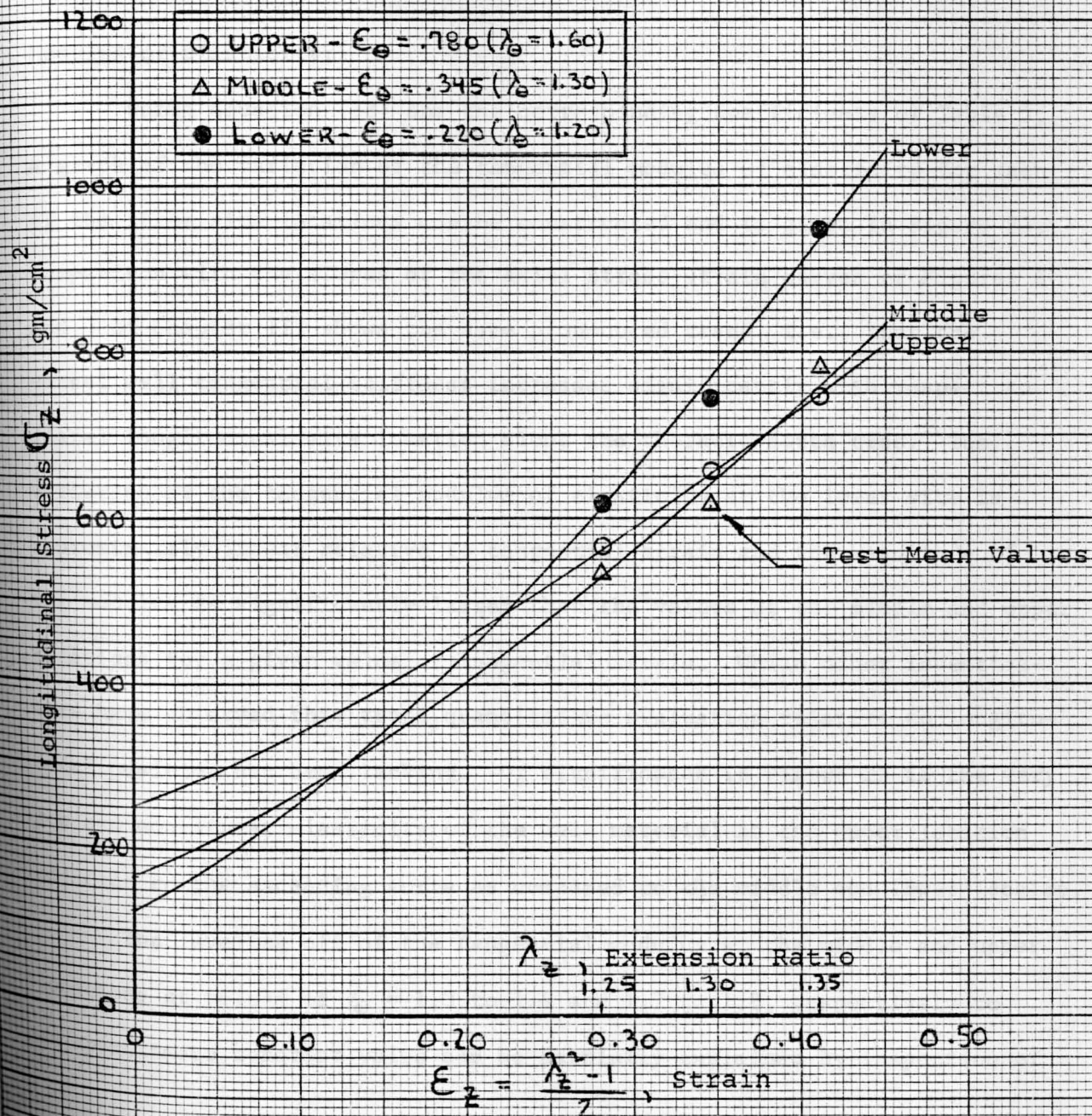


Figure 22 - Longitudinal Stress-Strain

-vs-

Thoracic Aorta Location



variation in longitudinal stress is so small relative to aorta location. Essentially it appears that for a given value of longitudinal strain, say $\lambda_z = 1.30$, a longitudinal stress variation of 600 to 800 gm/cm² would imply that the longitudinal stress is approximately constant relative to longitudinal location. This perhaps is the intended physiologic environment for the in-vivo vessel since one would not expect significant variations in the longitudinal tethering forces.

Modulus of Elasticity:

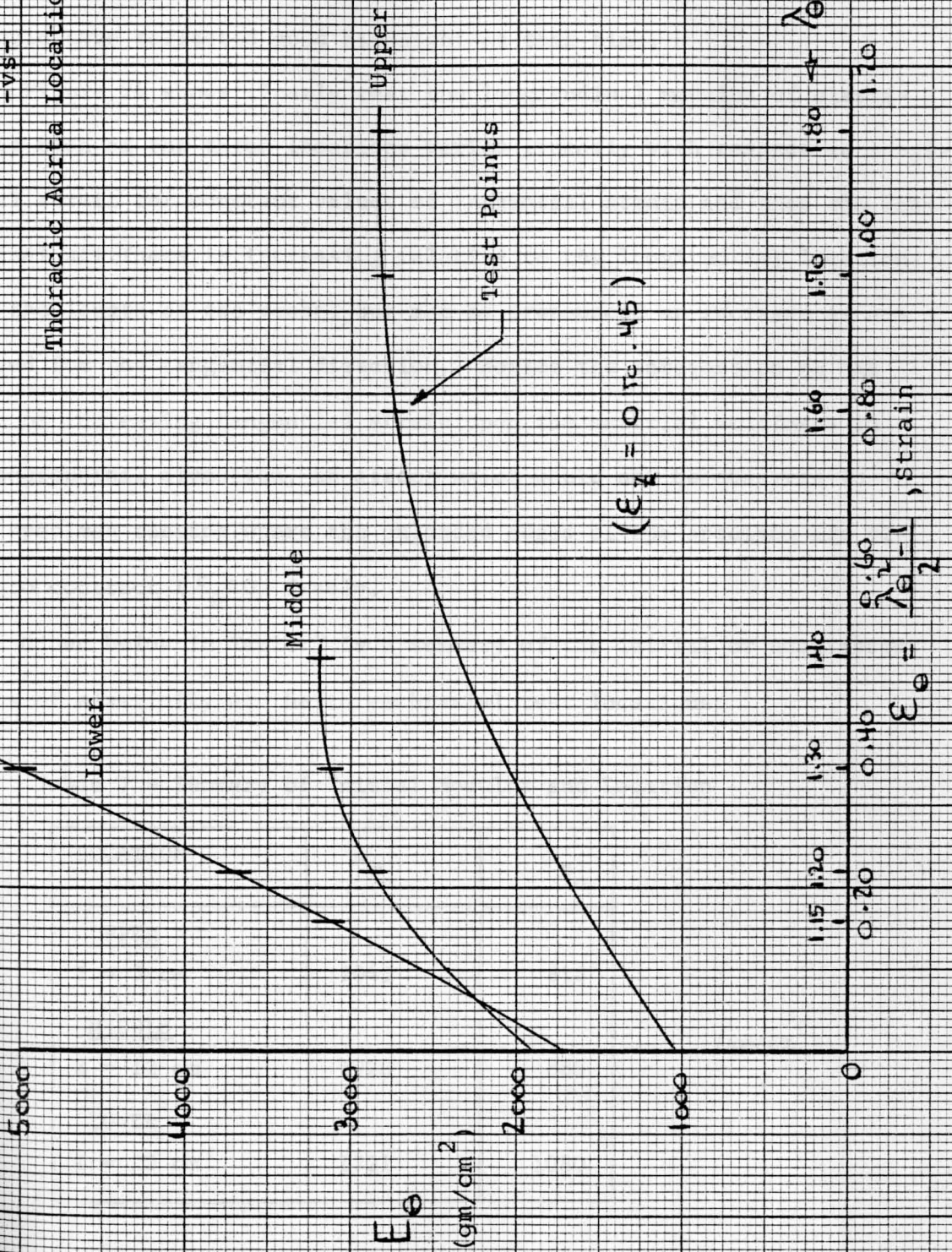
Using equation (38) and the corresponding coefficients of Table 5, a graph of the variation of the tangential modulus of elasticity for each of the three site locations can be constructed and is given in Figure 23. Comparison with the slopes of the axial stress-strain curves of Figures 6 and 7 of Chapter III shows the same pronounced trend, i.e., that the vessel wall tangential stiffness increases significantly with respect to distal longitudinal site location along the thoracic aorta tree. The variation of the tangential modulus of elasticity at the lower site is approximately linear relative to tangential strain and the magnitude of the modulus is significantly larger than the values at the middle and upper locations for a given value of tangential strain. While other investigators have observed this trend, quantitative evaluation relative to longitudinal position has been lacking. Of significance in Figure 23 is the very low and non-linear elasticity of the wall material at the upper location adjacent to the ascending aorta as compared to the middle and lower locales.

The leveling off of the tangential modulus at the middle and upper locations at values of $\lambda_e = 1.3$ to 1.4 and 1.7 to 1.8, respectively to an approximate constant value can be partially explained by inspection of

Figure 23 - Tangential Modulus of Elasticity

-vs-

Thoracic Aorta Location



$(E_{\lambda} = 0.7e - 45)$

$E_{\theta} = \frac{\lambda_e^2 - 1}{2}$, strain

Figure 7 but still raises the question as to why this occurs at the middle location for a low value of $\lambda_{\theta} = 1.40$. It appears that additional biaxial testing at a value of 1.50 for this location would have been of value. Also, testing the upper specimen at an extension ratio of 1.3 or 1.4 would have reflected good hindsight at this time.

Figure 24 shows clearly that the longitudinal modulus of elasticity at each of the three locations varies linearly with respect to longitudinal strain for constant values of tangential strain, and that the longitudinal stiffness is increasing relative to the longitudinal location along the length of the vessel, but not as pronounced an increase as was observed for the tangential direction. Notice the interaction or the affect of increasing tangential strain upon the material stiffness in the longitudinal direction, an affect which would not be observed in axial specimen testing where the unloaded edges of the specimen are allowed to contract ($\epsilon_{\theta} < 0$) freely.

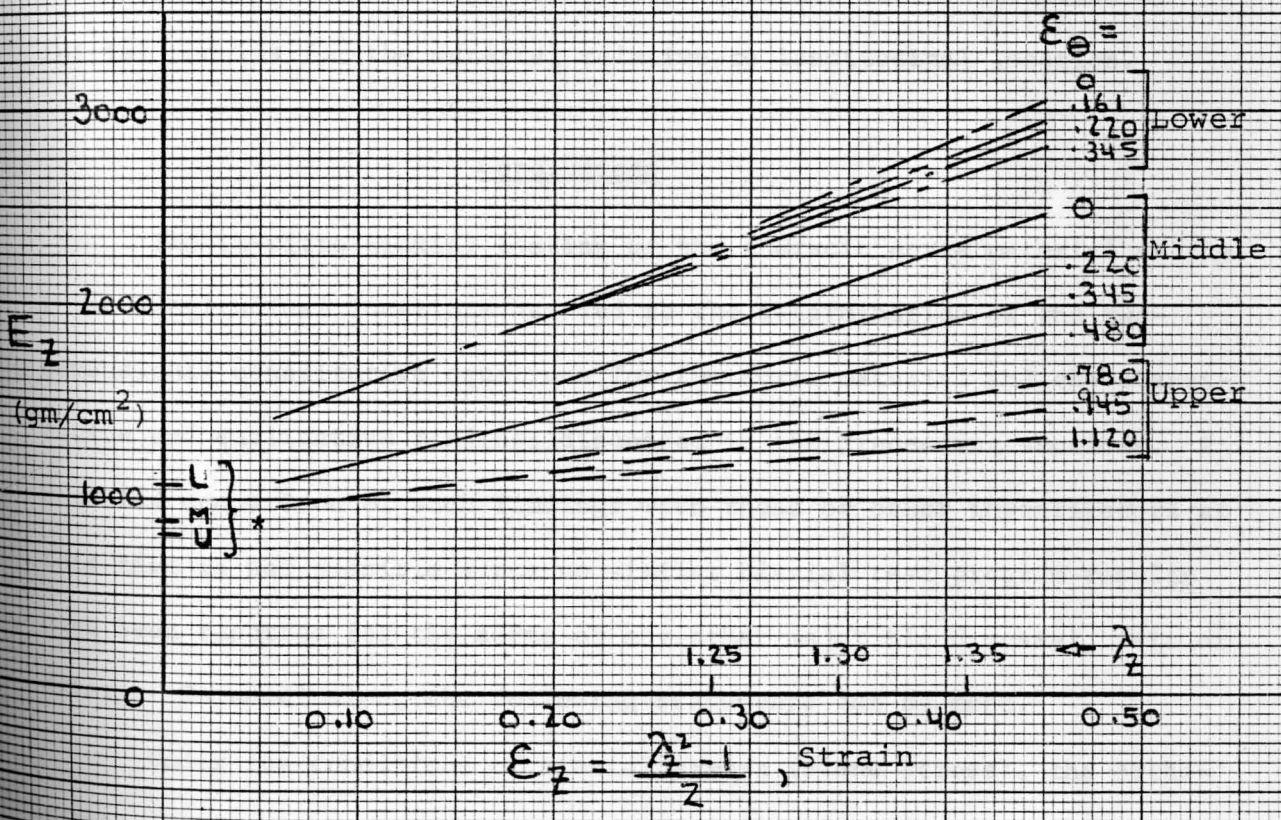
Given below in Table 7 is a summary of the initial or unstressed modulus of elasticity at the three biaxial test locations.

Table 7 - Summary of Initial Modulus and Location

LOCATION	E_{e_o}	E_{z_o}
<u>UPPER</u> Z = 5 cm	1043	818
<u>MIDDLE</u> Z = 12 cm	1920	885
<u>LOWER</u> Z = 20 cm	1721	1080

(gm/cm²)

Figure 24 - Longitudinal Modulus of Elasticity
 -vs-
 Thoracic Aorta Location



*Unstressed Modulus at
 $E_z = E_\theta = 0$

This data is plotted in Figure 25 relative to the longitudinal location along the thoracic aorta vessel. A linear regression analysis was used to determine the degree of linear variation of modulus with respect to location. The equations for the initial modulus are

$$E_{\theta_0} = 43.54Z + 1024$$

$$E_{z_0} = 17.63Z + 710$$

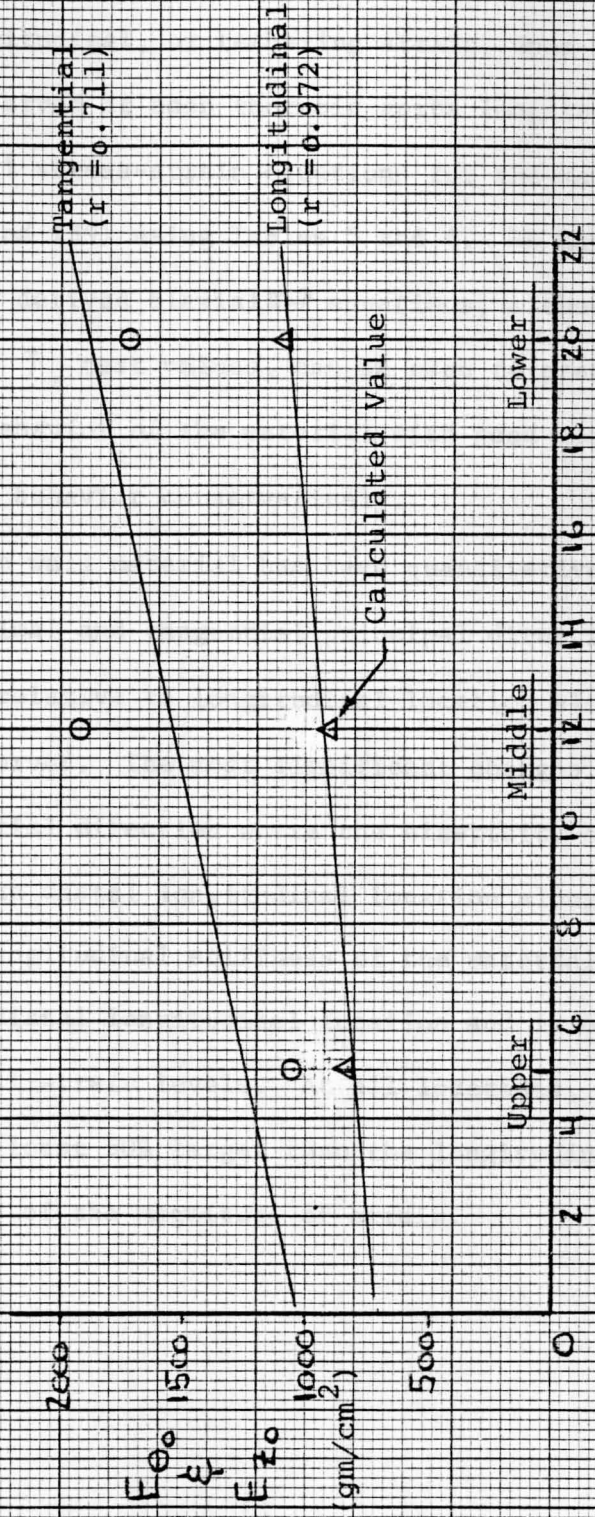
and are shown compared with the calculated test data points. The correlation coefficient of 0.972 indicates a definite linear variation of the longitudinal initial material modulus relative to longitudinal location along the thoracic aorta vessel. The low coefficient of 0.711 for the tangential direction indicates a distinct non-linear variation of initial modulus for the material relative to longitudinal location.

Conclusions

The in-vitro biaxial testing of the thoracic aorta material at the three longitudinal locations has led to the determination of the two-dimensional constitutive equations for the aorta material and the quantitative and qualitative findings discussed in the preceding sections. A detailed comparison of such findings with those of other investigators at this time is not possible since no similar biaxial test program results have been reported for the aorta or any other major blood vessel, vein or artery. In conclusion, the following statements can be made.

Under the conditions of biaxial stress (plane stress), the orthotropic non-linear stress-strain characteristics of the tissue in the two principal directions of loading have been analytically described and further

Figure 25 - Variation of Initial Modulus
-vs-
Aorta Longitudinal Position



Longitudinal Location Z - cm.

confirms the non-linear characteristic of the material as previously reported using axial specimen tests, Chapter III. The interaction of longitudinal and tangential strains upon the longitudinal stress and the relative independence of longitudinal, or tethering strain, upon the tangential stress has been observed at each thoracic aorta longitudinal location. The two-dimensional stress-strain equations for the material are defined by equations (38) and (39) using Tables 5 and 6. We have also seen that these empirically derived biaxial σ - λ equations, although based on a small range of λ_{θ} and λ_z test values, can be used to predict the uniaxial longitudinal σ - λ behavior of the material with good accuracy and the uniaxial tangential σ - λ behavior conservatively.

The elasticity of the wall material has been quantitatively defined for both the longitudinal and tangential principal directions and the variation of stiffness relative to longitudinal location along the thoracic aorta has been observed. The most significant changes in elasticity occurs in the tangential direction where the elasticity of the tissue increases rapidly with distal longitudinal location along the thoracic aorta tree. The longitudinal stiffness of the material increases moderately with respect to distal longitudinal location and is only slightly dependent upon the tangential strain levels. At all locations, the tangential modulus, E_{θ} , is at least 50% larger than the longitudinal modulus of elasticity regardless of the magnitude of strain.

CHAPTER VII

PHYSIOLOGIC ANALYSIS

Introduction

Having determined the mathematical stress-strain relationships of the thoracic aorta material at each of the three locations, it is now possible to determine the in-vivo blood vessel parameters such as diameter and wall thickness changes and the state of principal stresses and strains under the influence of the physiologic loading of pulsatile pressure. The analysis which follows is based on the following assumptions.

1. The longitudinal, or tethering, state of strain (λ_z) is approximately constant and equal to $\lambda_z = 1.30$. This has been discussed in Chapter II and the assumption is based on the in-vivo measurements made by other investigators for the steady state situation.
2. It is assumed that the in-vitro material characteristics based on the biaxial testing are applicable to those of the tissue in the in-vivo state. This assumption and its affects will be discussed further at length.
3. It was initially assumed that the tangential wall stress distribution is uniform based on the assumption that the vessel is "thin wall." Correction factors will be applied to the calculated value of σ_e where the r_m/h value is less than 10.0.
4. For the reasons stated in Chapter II, the radial wall stress due to internal pressure is assumed to be negligible and thus has no influence on the tangential or longitudinal strains.

Analysis

The aorta geometry data given in Table I of Chapter III for vessel wall thickness (h_o) and circumference (c_o) is applicable to the in-vitro condition where the blood vessel is completely unstressed and the deformation is zero; $\lambda_n = 1.0$. Based on assumption No. 1 above, the "unstressed in-vivo" condition is defined as being the in-vivo blood vessel condition where the internal blood pressure is equal to zero ($p = 0$) and the vessel is pre-stressed longitudinally (tethering condition) to a longitudinal extension ratio of $\lambda_z = 1.30$ resulting in a tangential extension ratio (λ_e) of .877 relative to the in-vitro state. For this in-vivo condition the upper, middle, and lower specimen locations shown in Figure 4 are now located at $Z = 6.5, 15.6,$ and 26 cm, respectively, relative to the ascending-thoracic aorta reference location of $Z = 0$. Similarly, the in-vitro values of h_o and c_o given in Table 1 must now be corrected, using the incompressibility equation, for the in-vivo condition. The "unstressed in-vivo" values for the aorta blood vessel are given below:

Location	h_o (cm)	c_o (cm)
UPPER, $Z = 6.5$ cm	0.474	6.402
MIDDLE, $Z = 15.6$ cm	0.325	5.350
LOWER, $Z = 26$ cm	0.184	4.828

and are applicable to the physiologic unstressed condition $p = 0,$

$$\lambda_z = 1.30.$$

The following method of analysis pertains to the middle thoracic aorta location and is also applicable to the upper and lower aorta locations using the appropriate equations of Chapter VI and the aorta in-vitro geometry given in Table 1 of Chapter III.

The aorta wall tangential stress due to internal pressure loading is given by equation (1) and has been redefined by equation (16) as a function of the internal pressure, the unstressed geometry, and the strains defined as extension ratios. Rewriting equation (16) in terms of the vessel unstressed mean diameter, d_o , we obtain

$$\sigma_{\theta} = (pd_o/2h_o) \lambda_z \lambda_e^2, \quad \text{gm/cm}^2 \quad (40)$$

and from Chapter VI, equation (39) - Table 6, the plane stress equation for the middle thoracic aorta tangential stress is given as

$$\sigma_{\theta} = 1477 \lambda_e^4 - 1219 \lambda_e^2 - 259 \lambda_e^6 \quad (41)$$

Equating equations (40) and (41), rearranging and simplifying gives

$$\lambda_e^4 - 5.70 \lambda_e^2 = -4.71 - .0019 (d_o/h_o) p \lambda_z$$

which can be further reduced by substituting the values of the unstressed wall thickness and diameter at the middle location given in Table 1 and the value of $\lambda_z = 1.30$. Thus, we obtain

$$\lambda_e^4 - 5.70 \lambda_e^2 = 4.71 - .0132p \quad (42)$$

the relationship of the tangential strain with respect to the internal pressure p . Substituting various values of blood pressure into (42) allows

the corresponding in-vivo tangential strain to be determined. Using equation (7b), the corresponding mean vessel wall diameter is

$$d = d_o \lambda_e \quad , \quad \text{cm} \quad (43)$$

Transposing equation (7c) and using the incompressibility equation, equation (8), the in-vivo wall thickness can be expressed as

$$h = h_o / (\lambda_z \lambda_e) = .77h_o / \lambda_e \quad , \quad \text{cm} \quad (44)$$

where the value of λ_e in this equation and equation (43) is based on the value obtained from equation (42) for a given value of internal pressure.

At this point, the ratio of in-vivo mean wall radius to wall thickness ratio can be calculated so as to determine if the thin wall assumption is valid. Or:

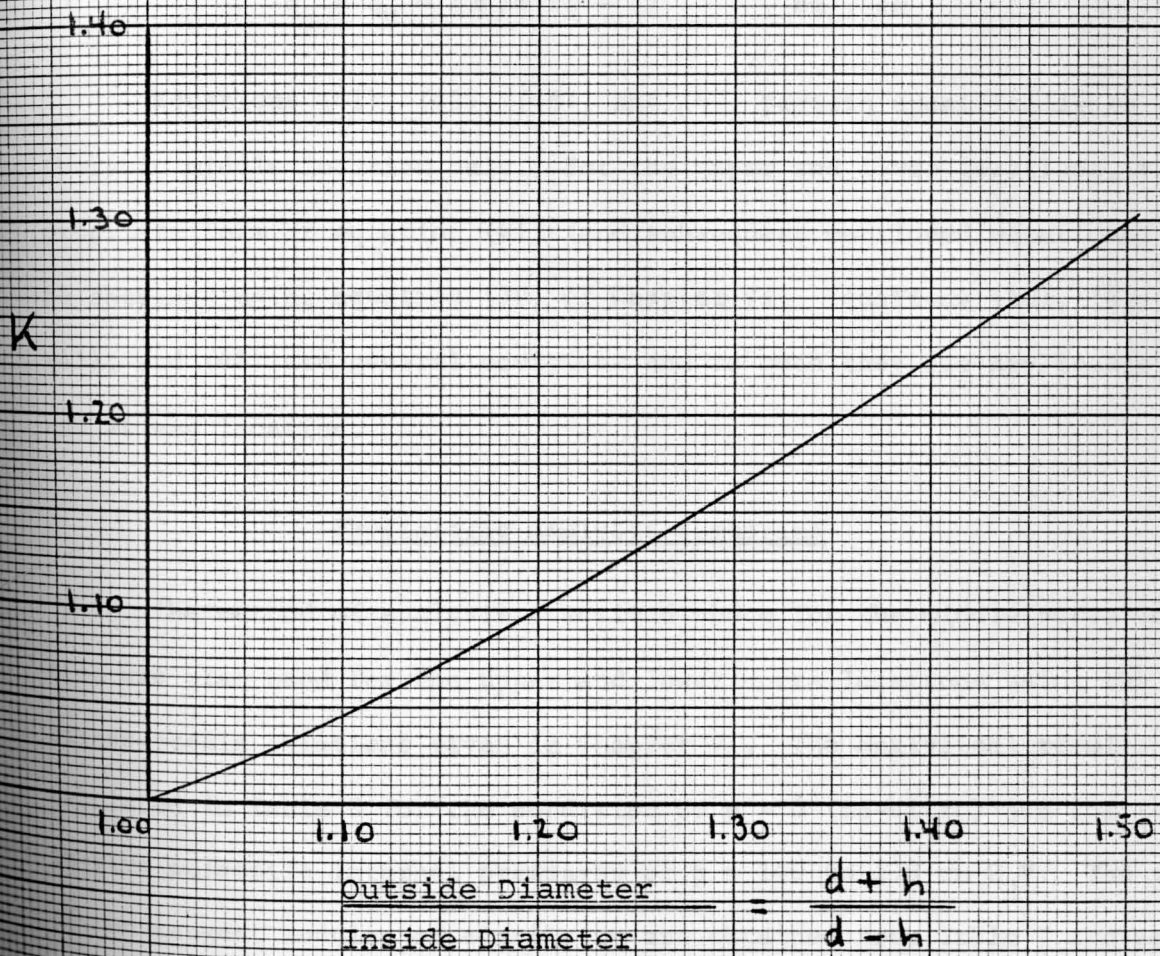
$$r_m/h = d/2h \quad (45)$$

If the value is ≥ 10 , the tangential wall stress is often assumed to be uniform across the thickness of the wall material. The magnitude of the tangential stress can be determined using equation (41). For r_m/h values less than 10 (thick wall cylinder), the maximum value of the tangential wall stress at the inside or lumen surface of the vessel is

$$\sigma_e = K(1477 \lambda_e^4 - 1219 \lambda_e^2 - 259 \lambda_e^6) \quad (46)$$

where the correction factor K is given in Figure 26. Use of equation (46) is recommended and is based on the Theory of Elasticity, Sokolnikoff⁷, of thick walled isotropic cylinders. Since the aorta wall is non-linear anisotropic, equation (46) is recommended over the use of equation (41).

Figure 26 - Thick Wall Cylinder Tangential
Stress Correction Factor K



The longitudinal wall stress at the middle location is given by equation (39) and Table 6, and is

$$\sigma_z = 653 \lambda_z^4 + 466 \lambda_z^2 \lambda_e^2 - 908 \lambda_z^2 - 210 \lambda_z^4 \lambda_e^2$$

or

$$\sigma_z = 331 + 188 \lambda_e^2 \quad (47)$$

A parameter of general hemodynamic interest and which will be discussed further is the internal fluid flow cross-sectional area (q_A , cm^2) or the flow volume per unit longitudinal length (q_V , cm^3) of the vessel wall. Or:

$$q_A = q_V = (\pi/4)(d - h)^2, \text{ cm}^2, \text{ cm}^3 \quad (48)$$

Equations (41), (42), (46), and (47) pertain specifically to the thoracic middle location only. For the upper and lower locations, the appropriate form of equation (41) (and subsequent mentioned equations) must be obtained using equation (39) of Chapter VI. Equations (40), (43), thru (45), and (48) are general equations and as such they are applicable for use at any location.

Physiologic Analysis Summaries

The method of analysis described above for the middle aorta location was also used for the upper and lower aorta locations using the stress-strain relations given in Chapter VI. The analytical results are tabulated in Table 8 for the condition of $p = 0$ (in-vitro) and for the in-vivo pulsatile internal pressures of $p = 140$ to $170 \text{ cm H}_2\text{O}$. The values of the tangent modulus of elasticity are obtained from Table 7 and equation (38), or Figures 23 and 24 of Chapter VI.

PHYSIOLOGIC DATA

UPPER z = 15.6 cm			LOWER z = 26 cm			
PRESSURE			INTERNAL PRESSURE			
	155	170	0 *	140	155	170
5	1.295	1.325	1.00	1.330	1.355	1.380
1	.3385	.3778	0	.3845	.4180	.4522
4	2.512	2.571	1.750	2.328	2.371	2.415
	.220	.214	.210	.121	.119	.117
6	5.70	6.12	4.19	9.71	9.88	10.10
2	4.126	4.363	1.890	3.826	3.983	4.148
0	971	1101	0	1412	1610	1829
	646	661	0	809	827	848
	3100	—	1721	—	5450	—
	1800	—	1080	—	2400	—

R COMPARISON

TABLE 8 - SUMMARY C

PARAMETER	UPPER z = 6.5 cm				M
	INTERNAL PRESSURE				INTE
	0 *	140	155	170	0 *
λ_{θ}	1.00	1.365	1.405	1.445	1.00
ϵ_{θ}	0	.4316	.4870	.5540	0
d	2.320	3.167	3.260	3.352	1.940
h	.540	.304	.296	.287	.370
r_m/h	2.15	5.28	5.43	5.78	2.63
q_A, q_V	2.520	6.438	6.900	7.378	1.940
σ_{θ}	0	813	950	1095	0
σ_z	0	573	584	597	0
E_{θ}	1043	—	2350	—	1920
E_z	818	—	1633	—	885

* IN-VITRO DATA SHOW

Figures 27 thru 29 graphically depict for each aorta location, the analysis results as a function of the internal pressure over the range of $p = 0$ to $p = 200$ cm H₂O assuming a constant value of the longitudinal or tethering strain of $\lambda_z = 1.30$. Plotted on each graph is the relationship of mean wall diameter of the vessel (d), the tangential ($\bar{\sigma}_\theta$) and longitudinal wall stress ($\bar{\sigma}_z$), and the hemodynamic parameters (q_A , q_V) vs the internal blood pressure (p). The change in each physiologic variable with respect to pressure at each location is seen on each figure and a comparison between each aorta location can be made using the figures. Superimposed on each diameter curve are the values of r_m/h and the tangential strain at the three pressures of 100, 155, and 200 cm H₂O.

Figure 30 presents the distensibility curves of the blood vessel or the relationship of mean wall diameter and internal pressure relative to the in-vivo longitudinal location along the length of the aorta. Superimposed on the mean pressure (155 cm H₂O) curve is the cyclic change in diameter for the pulsatile pressure values of 140 and 170 cm H₂O.

The summaries of the in-vivo physiologic variables presented in Figures 27 thru 30 are based on the in-vitro biaxial testing of the aorta tissue and are a first time comprehensive evaluation of each variable over a wide range of internal pressure.

A detailed analysis of the variables at each location and a "location to location" comparison will be made in the following discussion including a comparison of the results of this study with the information available in the literature.

Figure 27 - Physiologic Data at Upper Location

-vs-
Internal Pressure

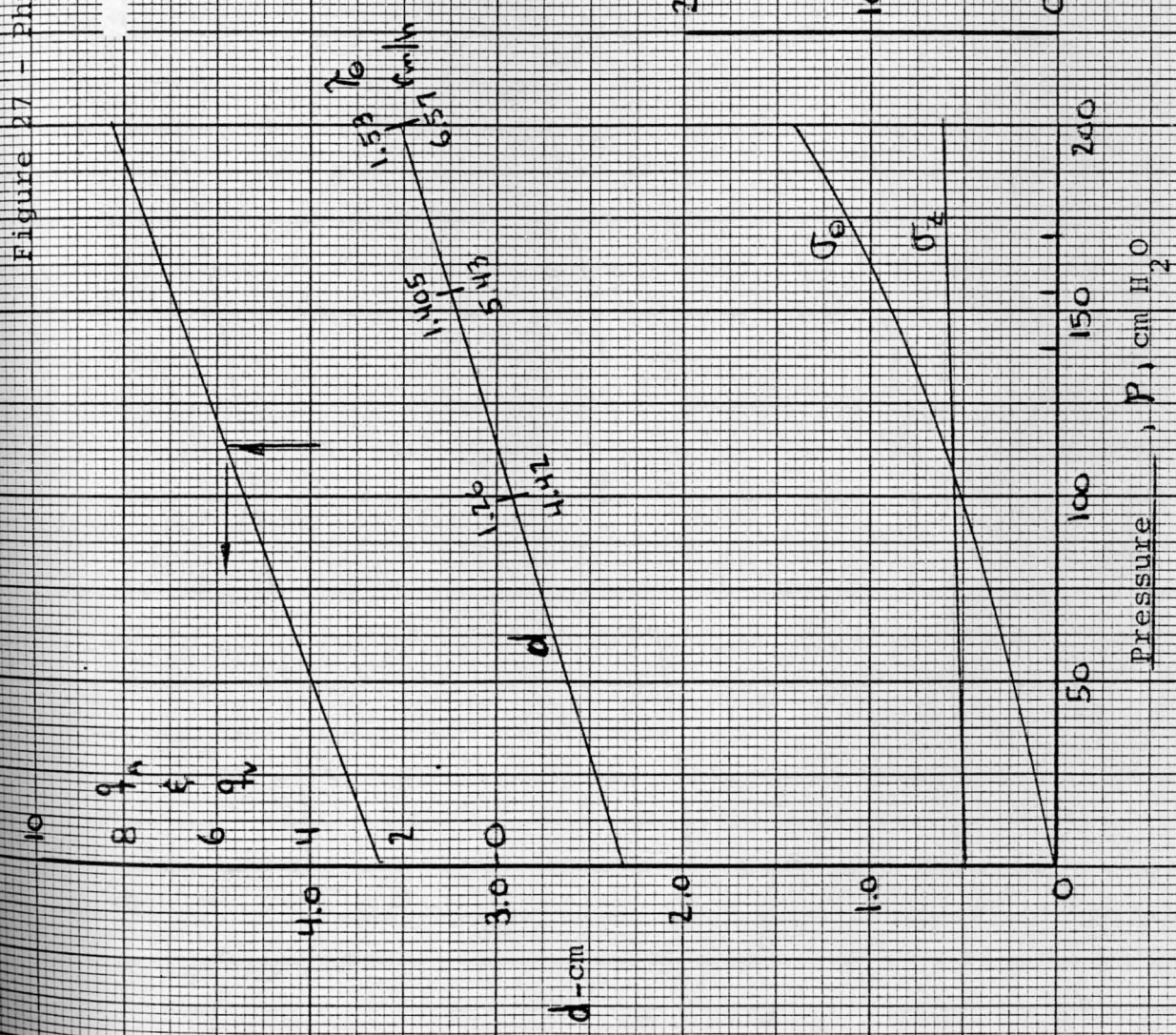


Figure 28 - Physiologic Data at Middle Location

-v\$-
Internal Pressure

$$[\gamma_z = 1.30]$$

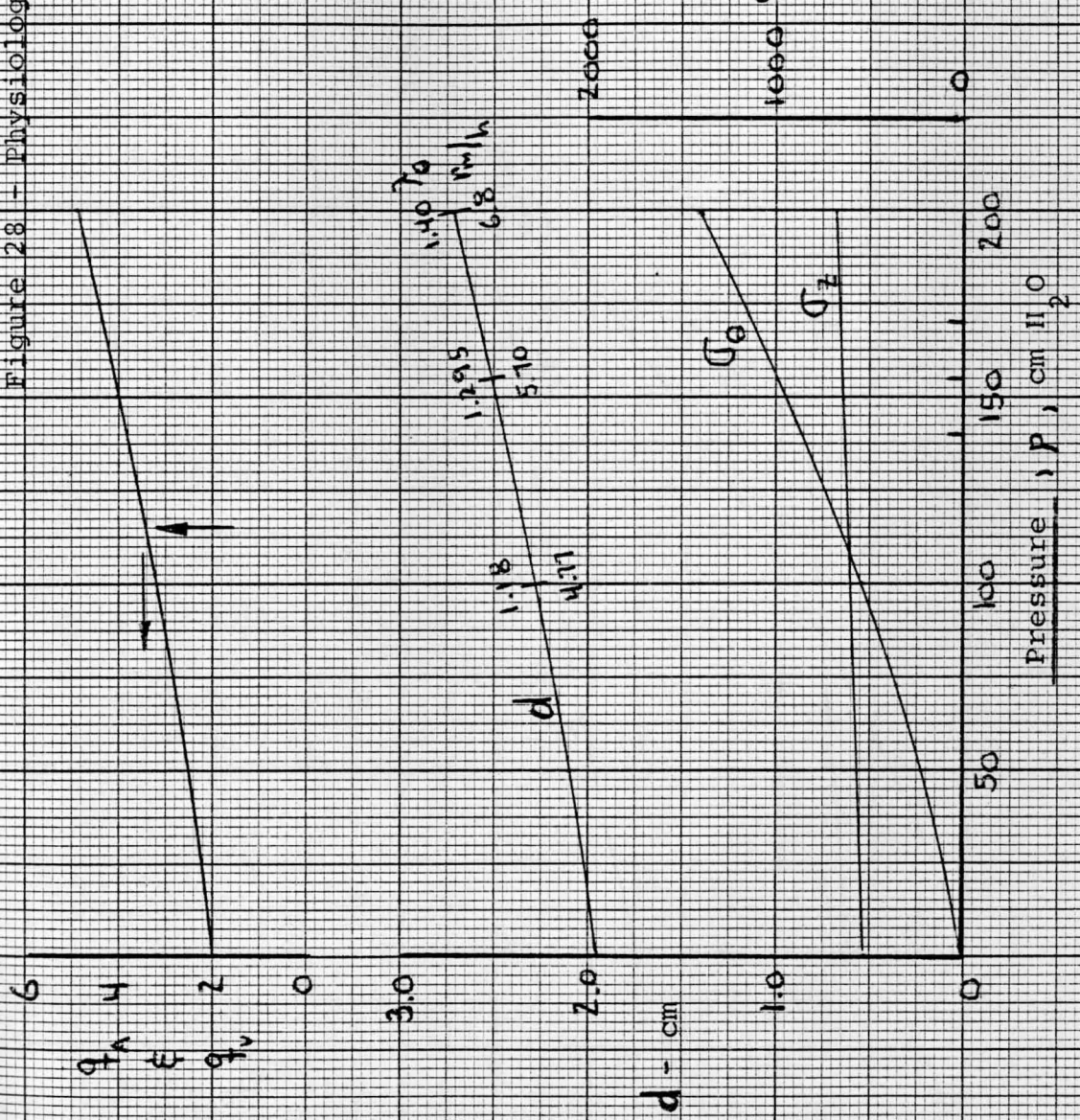


Figure 29 - Physiologic Data at Lower Location

-v/s-
Internal Pressure

$$\left[\lambda_z = 1.30 \right]$$

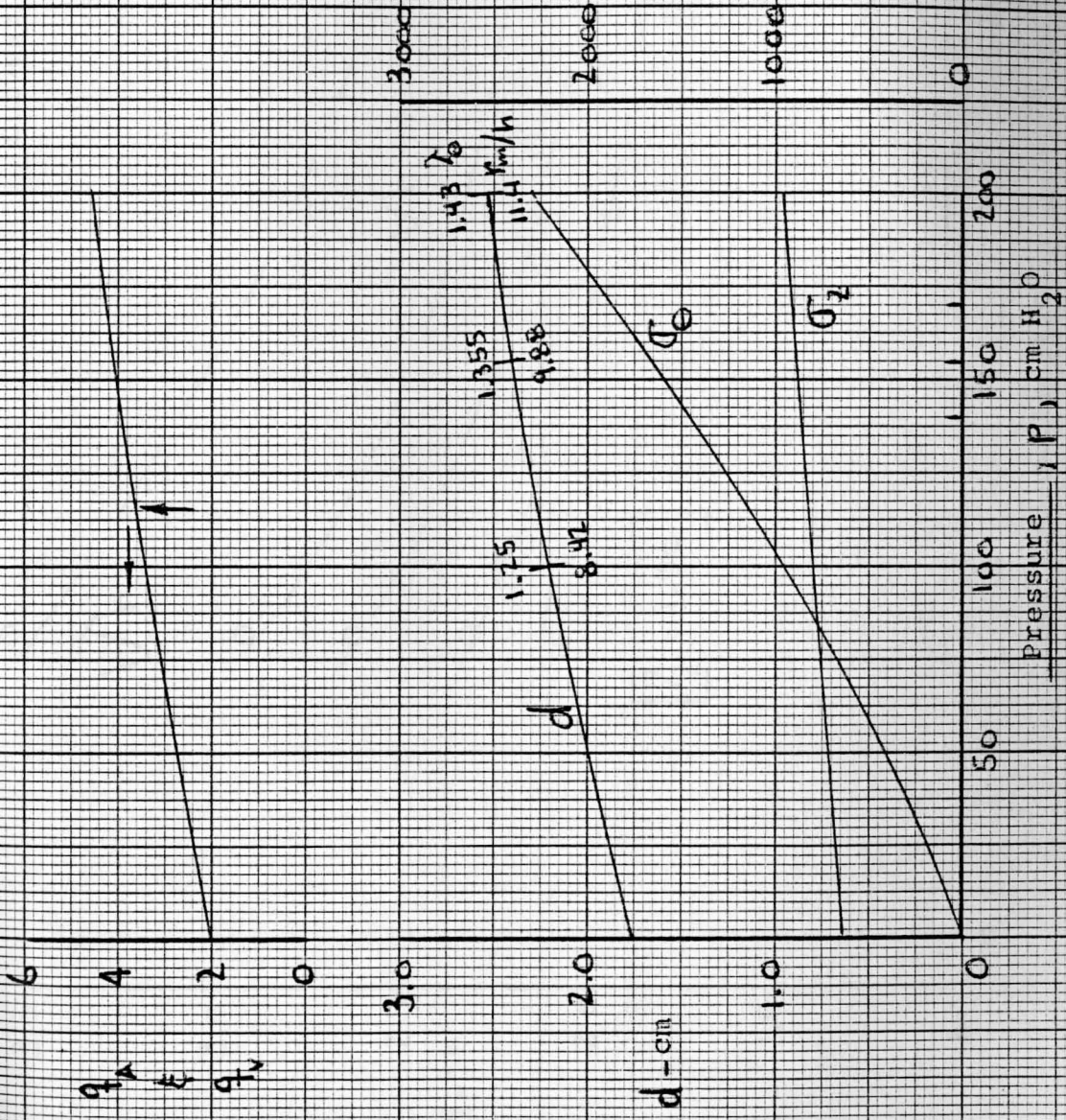
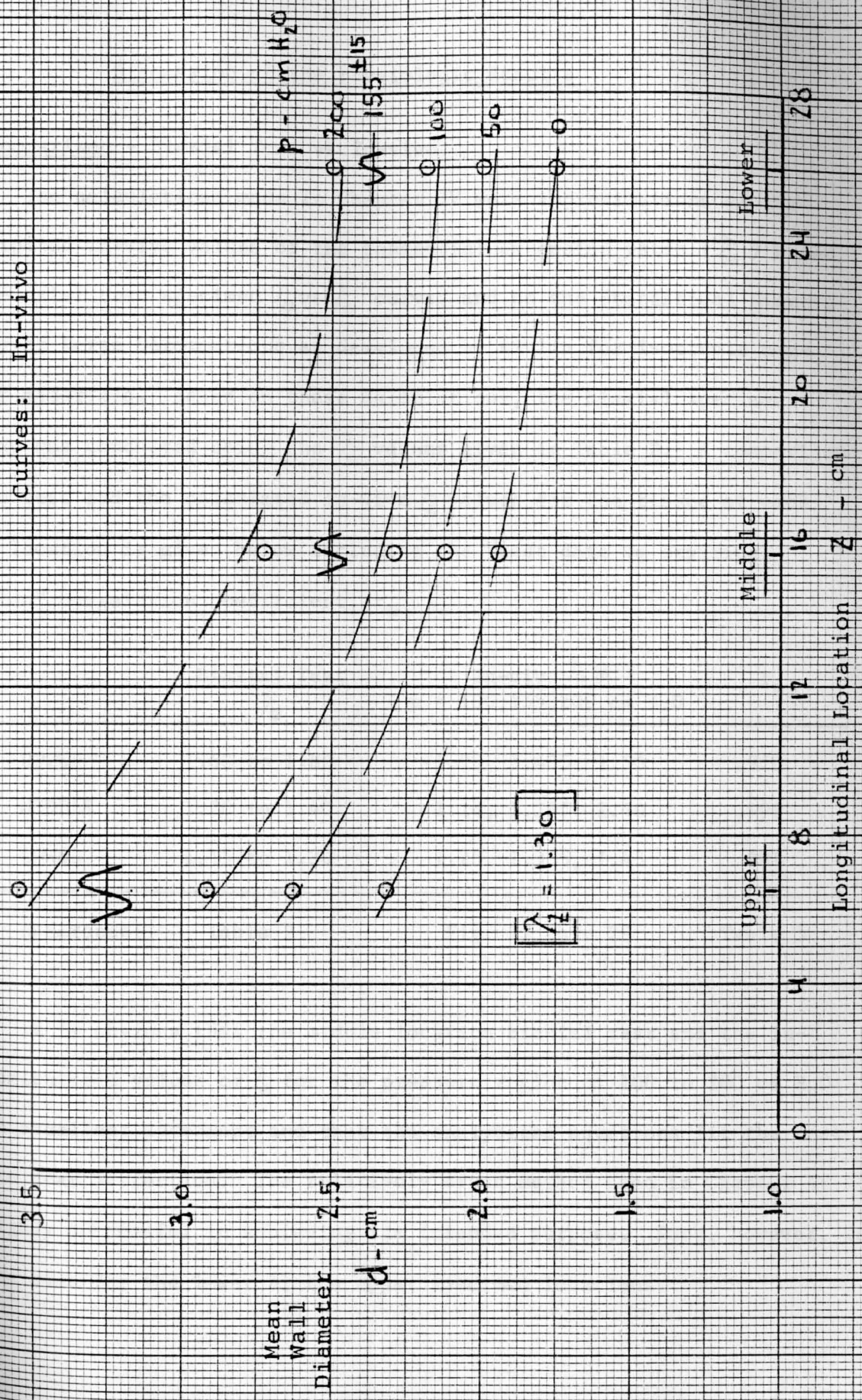


Figure 30 - Thoracic Aorta Distensibility
Curves: In-vivo



Mean Wall Diameter

d - cm

Longitudinal Location Z - cm

Upper

Middle

Lower

$\lambda_z = 1.30$

Discussion of the Physiologic Results

λ_e Comparison - Biaxial Test vs In-vivo

The calculations made in Chapter IV were approximations of the anticipated in-vivo values of the tangential extension ratio (λ_e) based on the axial test specimen $\bar{\sigma}_e$ vs λ_e curves and on the Statistical Kinetic Theory of Large Deformations as developed by Rivlin for isotropic non-linear materials. Based on these calculations, the biaxial specimen testing was conducted using the λ_e values given in Table 2. A comparison of the test and the calculated in-vivo λ_e values for the tissue at each aorta location is given below including the "test data vs empirical equation" correlation coefficient, r_e .

	<u>Biaxial Test</u> λ_e	<u>In-vivo λ_e @</u> p = 100, 155, 200 cm H ₂ O	r_e
UPPER	1.60 to 1.80	1.26, 1.405, 1.53	.970
MIDDLE	1.20 to 1.40	1.18, 1.295, 1.40	.996
LOWER	1.15 to 1.30	1.25, 1.355, 1.43	.981
Reference:	Table 2	Fig. 27 thru 29	Table 5

It is obvious that the middle location biaxial test and the in-vivo calculated values of λ_e for the pressure region of 100 to 200 cm H₂O are in excellent agreement and that the analytical equations fit the test data to near perfection. The relatively crude method used in Chapter IV was highly successful in achieving its intended purpose. Such, however, is not the case for the lower or the upper specimen locations.

At the lower location, the biaxial test λ_{\ominus} values used are slightly below the in-vivo calculated values and thus the derived $\sigma - \lambda$ equations based on the test results had to be extrapolated beyond the test region of $\lambda \leq 1.30$. While this extrapolation of the test data equations is not considered to be serious no estimation of the accuracy of such extrapolation is possible to make. Inspection of the lower location tangential curves (σ_{\ominus} and E_{\ominus}) of Figures 21 and 23 would indicate no serious harm since the extrapolated region is not large and the curves are continuous smooth functions.

In the case of the upper location, the in-vivo values of λ_{\ominus} , Table 8, lie well below the test range of 1.60 to 1.80. It is obvious in this case (as mentioned in Chapter VI) that the test should have included a data point at $\lambda_{\ominus} = 1.40$, or that the testing should have been conducted at values of 1.30, 1.40, and 1.50. The method used in Chapter IV appears to have the affect of assuming the elasticity of the material as being too low in magnitude and thus it has predicted values of λ_{\ominus} in excess of the probable in-vivo values. It is also very possible that the use of only three axial specimens (Figure 9) at this location gave a poor representation of the animal to animal variation since the three stress-strain curves show only minor variation in the tangential loading direction. Consequently, the test data and the resulting equations ($r = 0.970$) had to be interpolated between $\lambda_{\ominus} = 1.0$ and 1.60 in the physiologic analysis. It is likely that this interpolation is not harmful, but without a biaxial test data point within this range conjecture of the effect is strictly speculative.

As a whole, the method used in Chapter IV has achieved its purpose without apparent serious harm to the final physiologic analysis results.

It is apparent, however, that the most accurate analysis of the aorta tissue must be based on the actual biaxial testing of the material. Based on the above observations, the conduct of any further testing of the thoracic aorta material should be made using the tangential extension ratios listed below and experimental results should include measurement of tissue thickness. A fourth test point has been added to improve the accuracy of the test program and its results.

Location	λ_e
UPPER	1.25, 1.35, 1.45, 1.55
MIDDLE	1.15, 1.25, 1.35, 1.45
LOWER	1.20, 1.30, 1.40, 1.50

Incompressibility-Accuracy

All previous analysis has been based on the assumption that the aorta tissue is an incompressible material as noted in Chapter II based on the experimental investigations of Carew¹⁴. A measure of the accuracy of the biaxial test results and the resulting in-vivo physiologic data contained in Table 8 (which is based on the incompressible assumption) is to calculate using the data of Table 8 the actual value of Poisson Ratio (ν) of the material at each of the three aorta locations. From the Theory of Elasticity, the value of ν is a function of the material volumetric or bulk modulus (k) and the modulus of elasticity (E). Or:

$$\nu = (3k - E)/6k$$

where the bulk modulus is defined as the ratio of the hydrostatic stress divided by the volumetric strain of the vessel wall material under loading

measured relative to the original or unstressed volume of the material. The modulus of elasticity in this case is defined as the principal tangential modulus, E_{θ} , at the mean pulsatile pressure. Using the nomenclature of Table 8:

$$k = - \frac{\bar{\sigma}_m}{\Delta V/V_0} = - \frac{1/3(\bar{\sigma}_e + \bar{\sigma}_z + \bar{\sigma}_r)}{(d_o h_o - dh \bar{\lambda}_z)/(d_o h_o)}, \quad \text{gm/cm}^2$$

Substituting the data of Table 8 into the above equations, the values of the material Poisson Ratios are

$$\left. \begin{array}{l} \text{UPPER} - .50096 \\ \text{MIDDLE} - .50083 \\ \text{LOWER} - .49795 \end{array} \right\} .49991 \text{ (average)}$$

which is within +.2 to -.4% deviation from the theoretical value of $\nu = .50000$ for an incompressible elastic material.

Vessel Wall Thickness

Table 8 lists the mean wall radius to wall thickness ratios, r_m/h , at each aorta location for the unstressed in-vitro vessel. The values of 2.15, 2.63, and 4.19 for the upper, middle, and lower locations, respectively, show that the steer thoracic aorta is definitely a thick wall cylinder in the in-vitro state. At the in-vivo mean pulsatile pressure, the same location values are 5.43, 5.70, and 9.88, respectively, or the r_m/h criteria commonly used by other investigators is not satisfied for the in-vivo condition of loading. Consequently, contrary to that mentioned in Chapter II, the in-vivo vessel cannot be strictly classified as thin wall until the location distal to the lower specimen location, or at $z > 26$ cm. When considered as a thick wall cylinder, the tangential wall stress at each of the three locations increases from +5 to +10% and represents

the approximate maximum value of stress at the lumen surface of the vessel. This increase is hardly significant and for general stress calculations, the assumption of thin wall is justified such that equation (1) or (46) can be used without the use of the correction factor k . All values of σ_e given in Table 8, however, are corrected values and thus reflect the magnitude of the lumen surface stress.

It is possible that the in-vivo range of $r_m/h = 7.1$ to 16.6 representative of dog and man noted in Chapter II is not typical of the steer due to the large difference in body size and the heart weight to body weight ratio differences.

Figures 27 thru 29 show the variation in r_m/h at each aorta location over the pressure range of 100 to 200 cm H₂O. Calculations assuming a longitudinal extension ratio, $\lambda_z = 1.35$ show only small changes in both vessel mean wall diameter (+2%) and in the r_m/h ratio (+6%).

Hemodynamic Observations

The geometric shape of the aorta at the mean cyclic pressure of 155 cm H₂O shows, from Table 8, that the value of the internal flow cross-sectional area (q_A) at the upper location is 6.90 cm^2 as compared to an approximate constant value of 4.12 cm^2 and 3.98 cm^2 at the two distal locations. Assuming steady state volume flow conditions and negligible wall frictional losses in the length of the aorta these values of q_A indicate that the fluid velocity increases by approximately 70% between the upper and middle locations and remains approximately constant between the middle and lower locations. Thus, the unstressed geometry of the aorta vessel and its large variance in the tangential modulus of elasticity (Figure 23) with respect to longitudinal location, and under the condition of in-vivo

longitudinal and tangential loading, results in the thoracic aorta at its upper location acting as a velocity accelerator forcing fluid to increase velocity rapidly over a very short longitudinal distance. For the cyclic condition of ± 15 cm H₂O amplitude, the variation of q_A is $\pm 6.8\%$ and $\pm 4\%$ at the upper, middle, and lower locations indicating that the pulse fluid velocity is also magnified significantly.

In Chapter II, the ascending and thoracic aorta was classified as being a flexible tube which due to its low and varying elastic properties aids in the transmission of the blood from the left ventricle to the extremities of the arterial system. As a secondary observation of the analysis of this chapter, the above paragraph crudely, at best, indicates that such is the circumstance for the upper or proximal region of the thoracic aorta. It is unfortunate that four thoracic specimens, or at least one specimen from the ascending aorta, had not been used in this study as the observations noted above would have been more conclusive. Consequently, only the probable fluid flow characteristics can be recognized.

Table 8 further shows that the wall diameter variation for pulsatile flow condition ranges from $\pm 3\%$ to $\pm 2\%$ and that the wall thickness changes by approximately $\pm 5\%$. Thus, the cyclic radial wall velocity of the lumen surface is undoubtedly small relative to the longitudinal velocity of the fluid. Also, the dynamic wall boundary condition, in the strictest sense, cannot be assumed to be rigid without further assessment of the actual in-vivo performance of the blood vessel wall and the measurement of the fluid flow properties along the length of the vessel.

Longitudinal Characteristics

The aorta vessel is a flexible elastic tube subjected to an approximate constant longitudinal tethering strain ($\lambda_z = 1.30$) with a superimposed longitudinal loading caused by the in-vivo mean pressure of 155 cm H₂O. Figures 27 thru 29 show that the magnitude of the longitudinal stress increases slowly and linearly with pressure and consequently the total longitudinal load in the vessel wall is due to tethering load plus the superimposed loading due to the radial deformation of the elastic tube caused by the internal pressure. As the internal pressure causes radial deformation of the vessel, a positive longitudinal load results due to the vessel wall resisting the longitudinal contraction which would occur if the vessel had no longitudinal constraint. Thus, the total longitudinal load (F_L) in the wall is equal to the sum of the tethering force (F_t) and the induced longitudinal force (F_p) caused by the pressure loading. Or:

$$F_L = F_t + F_p \quad (49)$$

From this relationship, one can calculate the magnitude of the induced longitudinal load in the vessel due to the internal pressure and compare it relative to the total load in the vessel wall at the mean in-vivo pressure of 155 cm H₂O. Using equations (49) and (2)

$$F_p = F_L - F_t \quad (50)$$

$$= \pi [dh \sigma_z]_{\lambda_z = 1.30}^p = 155 - \pi [dh \sigma_z]_{\lambda_z = 1.30}^p = 0; \text{ grams}$$

Using equation (50) the magnitude of the longitudinal forces at each aorta location can be determined. The results are summarized below:

- LONGITUDINAL FORCES -

	<u>Total</u> F_L - gms	<u>Tethering</u> F_t - gms	<u>Pressure</u> F_p - gms	$(F_p/F_L) \times 100$
UPPER Z = 6.5 cm	1770	1448	322	18.2%
MIDDLE Z = 15.6 cm	1122	901	221	19.7%
LOWER Z = 26 cm (r)	733 (.983)	558 (.986)	175 (.969)	23.9%

Using linear regression analysis, we find that all three forces vary linearly with location (Z) and decrease in magnitude along the vessel distal length. Also, the induced load due to the radial pressure loading of the vessel is approximately 20% of the total longitudinal load at each location.

In the discussion of Figure 22 of Chapter VI, it was observed that for an assumed constant value of tethering strain ($\lambda_z = 1.30$) the variation in the longitudinal stress was found to be relatively small ($\sigma_z = 600$ to 800 gm/cm^2) for wide variations in the tangential strain ($\epsilon_\theta = 1.22$ to 0.78 .) This prompted the statement that -- "one would not expect significant variations in the longitudinal tethering forces" -- for the in-vivo physiologic environment. This statement is true only if the descending aorta blood vessel was reasonably straight, had constant cross-sectional area, and was well removed from the ascending aorta.

Table 8 shows at $p = 155 \text{ cm H}_2\text{O}$ that the in-vivo longitudinal stress, as expected, varies from 584 to 827 gm/cm^2 with respect to distal longitudinal location along the thoracic descending aorta but the above longitudinal force summary table shows that the magnitude of the forces (tethering, pressure, and total) are not constant at the three longitudinal aorta locations. The varying cross-sectional geometry of the aorta and the non-linear stress-strain behavior of the material prohibits the forces from being equal regardless of the manner of loading; constant tethering strain, or constant pressure loading. To better understand the longitudinal forces shown in the above table, and the effects of these forces, Figures 31a thru c depict the internal wall loading at each location and the average balancing shear forces which act between each aorta location so as to maintain the required longitudinal equilibrium of the blood vessel. The difference in the longitudinal load acting at the upper and middle locations and acting between the middle and lower locations is balanced by longitudinal shear forces (\bar{q} - force per unit of longitudinal length) which act between the outside surface of the vessel wall and the perivascular tethering tissue. These average shear forces are converted to average values of shear stress, $\bar{\sigma}_s$ - gm/cm^2 . A discussion of each of the three longitudinal loading figures follows.

Figure 31a: This figure represents the complete physiologic situation of both tethering ($\lambda_z = 1.30$) and the mean physiologic pressure loading of the blood vessel in its normal distended longitudinal and radial configuration. The average shear stresses acting between the outside surface of the blood vessel and the perivascular tethering tissues are 7.2 and 4.6 gm/cm^2 . These in-vivo values are very low in magnitude as might be

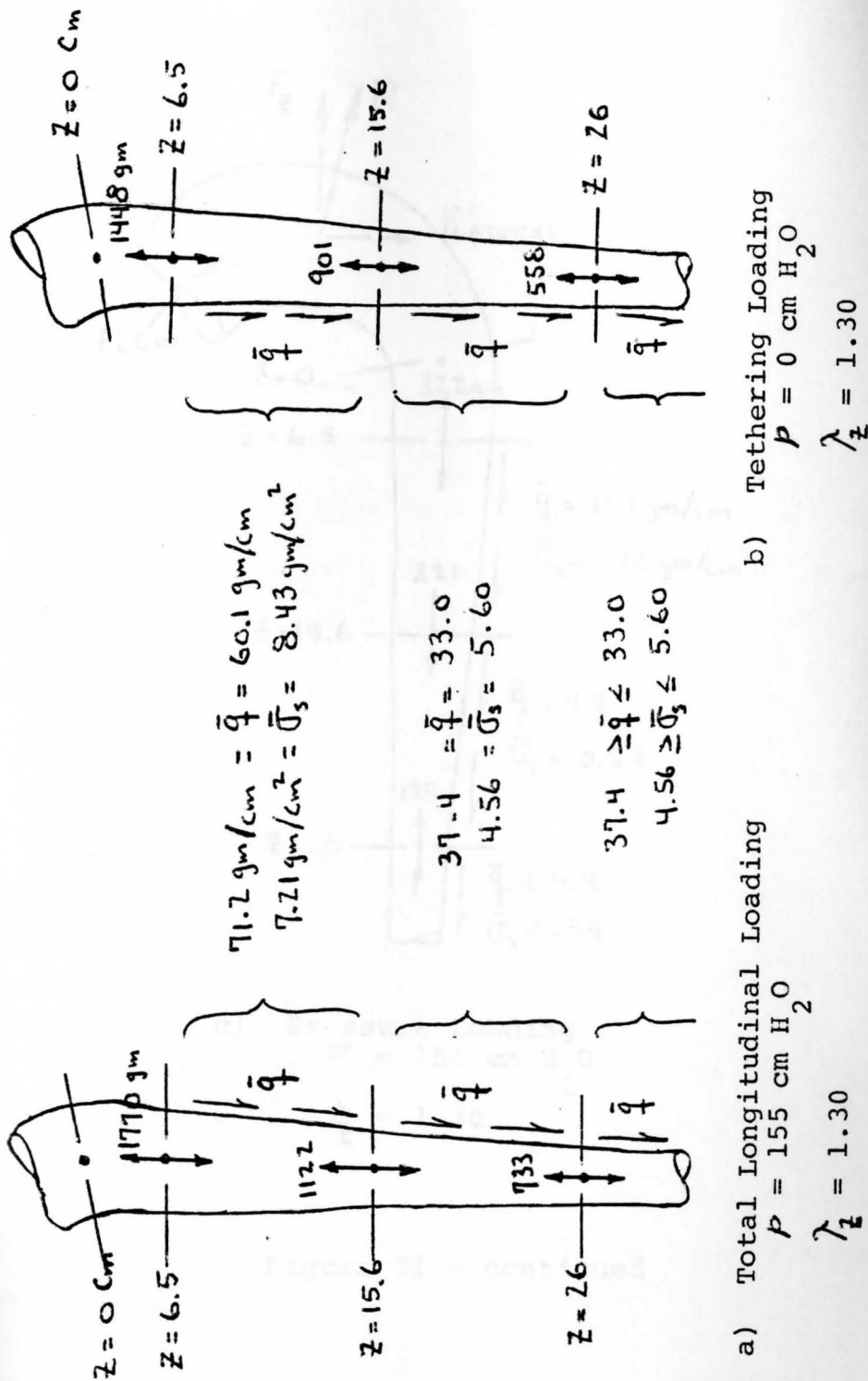
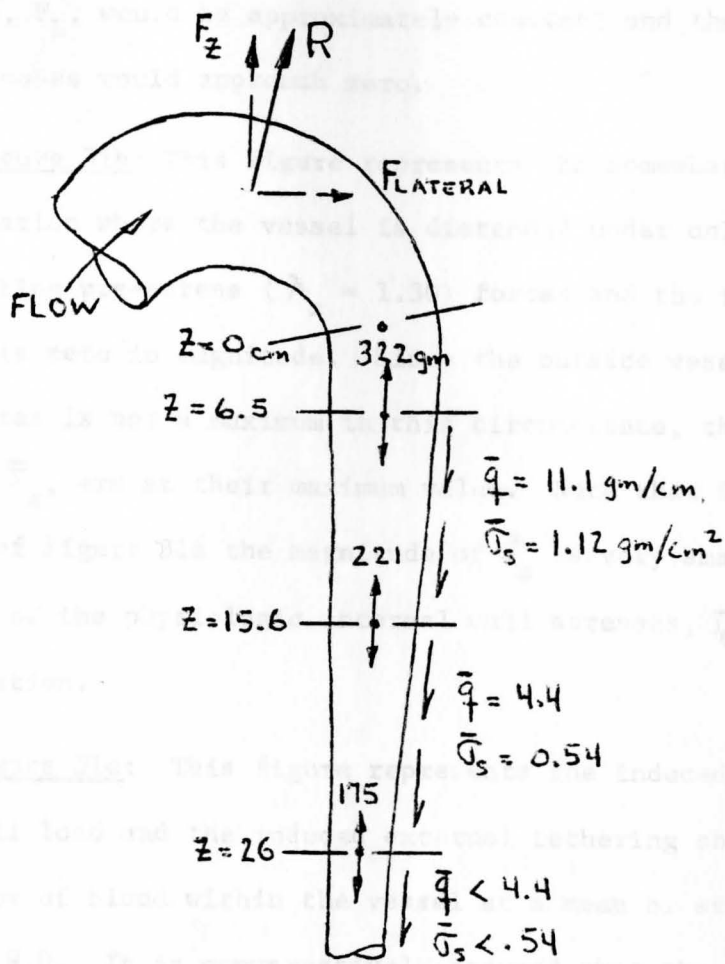


Figure 31 - Longitudinal Loading of the Descending Thoracic Aorta



- c) Pressure Loading
 $P = 155 \text{ cm H}_2\text{O}$
 $\lambda_z = 1.30$

Figure 31 - continued

expected since the tethering tissues are essentially fatty-viscous matter. At some point distal to the lower location, $Z > 26$ cm, either within the length of the thoracic aorta or within the abdominal aorta, the longitudinal force, F_L , would be approximately constant and thus the tethering shear stresses would approach zero.

Figure 31b: This figure represents the somewhat unrealistic in-vivo situation where the vessel is distended under only the influence of the tethering pre-stress ($\lambda_z = 1.30$) forces and the internal blood pressure is zero in magnitude. Since the outside vessel diameter and surface area is not a maximum in this circumstance, the tethering shear stresses, $\bar{\sigma}_s$, are at their maximum value. Note that for both this loading and that of Figure 31a the magnitude of $\bar{\sigma}_s$ is very small compared to the magnitude of the physiologic internal wall stresses, $\bar{\sigma}_\theta$ or $\bar{\sigma}_z$, at any aorta location.

Figure 31c: This figure represents the induced longitudinal internal wall load and the induced external tethering shear stresses caused by the flow of blood within the vessel at a mean or steady state pressure of 155 cm H₂O. It is conservatively assumed that the shear stress acting between the flowing fluid and the lumen surface of the vessel are negligible in magnitude. This assumption is based on the observation of Patel²⁰ who states that during a cardiac cycle, with maximum volume flow, the internal surface shear stresses would be -- "much lower than 1 gm/cm²." Consequently, the values of \bar{q} and $\bar{\sigma}_s$ shown in the figure are most likely to be maximum values.

The question raised by Figure 31c is -- "what causes the large longitudinal load (322 gm) acting at the upper location of $Z = 6.5$ cm?" The

answer lies in the fact that a force R acts on the ascending aorta (a curved pipe) and is due to the time rate of change of the flowing pressurized fluid within the ascending aorta. As shown in the figure, the resulting force R can be resolved into longitudinal and lateral force components. The longitudinal component F_z , directed upward, acts as a tension force within the wall of the descending aorta. If the descending aorta was unsupported by tethering tissue this force, F_z , would be constant throughout the length of the blood vessel. The change in cross-sectional geometry of the blood vessel and the inherent perivascular tissue resistance in effect reduces or dampens the effect of the steady state and pulsatile loading acting within the ascending aorta. The lateral force component at the ascending aorta is assumed to be resisted locally or by the heart and its supporting envelope since the bending resistance of the descending aorta must be negligible.

We see in Figures 31a thru 31c that the perivascular tissue plays a significant role in not only the application of the in-vivo tethering pre-stress condition but also in maintaining the necessary longitudinal equilibrium of the ascending and descending aorta blood vessel. Furthermore, it is not likely that the shear stress between the blood vessel and the tissue exceeds 10 gm/cm^2 under normal and healthy circumstances.

Table 8 and Figures 27 thru 29 also show that the cyclic longitudinal stress variation for the pulsatile pressure loading is approximately $\pm 2\%$, $\pm 2.3\%$, and $\pm 2.5\%$ of the mean stress at the upper, middle, and lower locations, respectively. It is possible to convert these cyclic variations of stress, using the equations of Chapter VI, into cyclic strains ($\pm \lambda_z$) or to cyclic longitudinal deformations per unit of longitudinal length of the vessel. Using the middle location ($Z = 15.6 \text{ cm}$) as

an example, the calculations yield a longitudinal cyclic deformation or displacement of $\pm .10$ mm/cm of vessel length at the in-vivo pressure of $155 \pm^{15}$ cm H₂O. Patel²⁰ reports the in-vivo measurement of aorta displacement of approximately $\pm .15$ mm/cm for the dog at a location of $Z = 14$ cm distal to the ascending aorta for pulsatile pressure of $180 \pm^{15}$ cm H₂O. While the two animals and the locations used are similar, but not identical, reasonable agreement exists between the in-vivo experiments and the analytical results based on the biaxial testing of the tissue. Consequently, the longitudinal cyclic stresses and strains are very small and contribute little to the structural or hemodynamic mechanics of the thoracic aorta. The primary consideration in these areas of study are the circumferential or radial displacement of the vessel wall.

Tangential Stress and Strain

The tangential stress curves of Figures 27 thru 29 show the characteristic non-linear increase of wall stress with respect to pressure loading from 0 to 200 cm H₂O similar to that displayed in Figure 21 for the basic material stress-strain relationship. Of interest is the fact that the σ_e vs p curves for the upper and middle locations are almost identical over the full range of pressure while at the lower location the value of the tangential stress is considerably higher for any given pressure. Examination of the pulsatile tangential stresses listed in Table 8 shows that at the upper and middle locations, the pulsatile stresses range from 800 to 1100 gm/cm² as compared to 1412 to 1829 gm/cm² at the lower location. The reason for this significant variance over a relatively short longitudinal distance (10 cm) is shown in the ratio of the mean wall radius to wall thickness ratios and the values of the in-vivo wall thickness itself. At the lower aorta location, the vessel wall thickness is approximately 50%

thinner and can definitely be classified as "thin wall." Thus, we see that a significant change in vessel geometry, and consequently tangential wall stress, occurs between $Z = 15.6$ to 26 cm distance indicating that "location" is an important factor when discussing any comparative data between investigations, or investigators. The graphs also show that the point of equal tangential and longitudinal stress is at 90 to 110 cm H_2O . Above this pressure, the tangential stress exceeds the longitudinal stress and at the mean pulsatile pressure the value of σ_e is approximately 50 to 100% higher than σ_z depending on aorta location.

It was pointed out in Chapter II that the radial wall stress (equation 4) has generally been found from other investigators to be approximately an order of magnitude lower than the tangential or longitudinal stress and is generally considered to be negligible. Table 8 shows that:

$$\begin{aligned}\sigma_r &= 78 \text{ gm/cm}^2 @ p = 155 \text{ cm H}_2\text{O} \\ \sigma_z &\cong 584 \text{ gm/cm}^2 @ p = 155 \text{ cm H}_2\text{O} \\ \sigma_e &\cong 950 \text{ gm/cm}^2 @ p = 155 \text{ cm H}_2\text{O}\end{aligned}$$

which clearly verifies that point made previously. While Table 8 does not list the value of the radial strain (compressive), the value can be determined from equations (33) or (35).

If the values of the physiologic tangential stress and extension ratios given in Table 8 at the upper, middle, and lower locations, for the mean normal pulsatile pressure of 155 cm H_2O , are plotted on Figures 9 thru 11, respectively, we see that the rheologic condition of the blood vessel lies within the initial characteristic region of the tissue uniaxial stress-strain diagram. This is to say that the normal in-vivo tangential wall stresses and strains of the aorta blood vessel lie comfortably to the left of the characteristic "knee" of the material axial

stress-strain diagram. Under the abnormal physiologic condition of 200 cm H₂O, or higher pressures, such as would be found in cases of hypertension or vessel constriction, the tissue material is functioning adjacent to or to the right of the knee of the curves. It is within this region that the physiologic wall stresses are not only higher in magnitude but the variation in wall stress from subject to subject can be very large. It should also be noted that the elasticity or stiffness of the blood vessel material is considerably higher under such circumstances.

In conclusion, we observe that in the normal physiologic state, the blood vessel tangential wall stresses and strains lie comfortably within the low stress-strain region of the characteristic non-linear stress-strain curve of the material. It is within this region where the low elasticity elastin fibers are carrying the largest share of the vessel tangential wall loading.

Patel¹¹, conducted in-vivo experiments using 14 living dogs. A 7.5 cm length segment of the middle descending thoracic aorta was isolated in each dog and by-passed from the main systemic circulation with dissection of the local tethering tissue being kept to a minimum so as not to alter the longitudinal in-vivo characteristics of the blood vessel. Tests were performed under pulsatile conditions at mean values of 145 to 162 cm H₂O so as to measure tangential incremental values of physiologic stress and strain. Incremental stress (P_e) and incremental strain (e_e) are defined as follows:

$$P_e = (\bar{T}_e)_p = 170 - (\bar{T}_e)_p = 140 \quad , \text{ gm/cm}^2 \quad (51)$$

$$e_e = \frac{(d)_p = 170 - (d)_p = 140}{(d)_p = 155} \quad , \text{ cm/cm} \quad (52)$$

Applying these definitions of incremental stress and strain to the phy-

siologic steer thoracic aorta data of Table 8, we obtain

$e_e = .057$ - UPPER -	$P_e = 282$
$= .047$ - MIDDLE -	$= 251$
$= .037$ - LOWER -	$= 417$

which are applicable to the pulsatile conditions of 155 ± 15 cm H₂O and are based on the in-vitro stress-strain determinations of Chapter VI.

For the mean pulsatile pressures of 145, 154, and 162 cm H₂O, Patel reports for the dog middle descending thoracic aorta segment in-vivo values of .038 to .045 cm/cm and 260 to 330 gm/cm² for the incremental tangential strain and stress, respectively. These values for the dog indicate good agreement with the middle and lower in-vivo calculated values listed above based on the in-vitro experimental biaxial testing of the steer tissue. The experiments of Patel also yield mean values of $\bar{\sigma}_e$ ranging from 1170 to 1630 gm/cm² as compared with the 950 to 1610 gm/cm² values given in Table 8.

Such agreement is significant, since it clearly indicates that the in-vivo predictions of this study are within good agreement and thus the advantage of in-vitro biaxial specimen testing is further enhanced. However, it is possible that "animal to animal" variations exist more than is indicated by the above comparison and that "location" of the specimen and measurements can also be an important factor. The data of Patel cannot be classified as being location, or point, properties since vessel wall geometry may have varied significantly within the 7.5 cm length of the isolated vessel. The fact remains though that, on average, the correlation of the calculated data of Table 8 with the in-vivo testing by Patel is certainly encouraging.

Wall Deformation and Distensibility

The non-linear tangential stress-strain relationship of equations (38) and (39) as depicted in Figure 21 for each aorta biaxial test specimen location and the non-linear form of equation (41) applicable to in-vivo loading would ordinarily be expected to yield a similar non-linear relationship between blood vessel internal pressure and mean wall diameter since the extension ratio strain λ_{\ominus} is related to vessel diameter. However, in Figures 27 thru 29 for each aorta location, the pressure-diameter (p - d) curves are approximately linear with only slight non-linearity in evidence. In fact, using pressures of p = 0, 50, 100, 150, and 200 cm H₂O and linear regression analysis, the curves of p - d shown can be very closely approximated by the following equations which display excellent correlation coefficients.

$$\left. \begin{array}{l} \text{UPPER - } d = .0061p + 2.320 \quad , r = .999 \\ \text{MIDDLE - } d = .0038p + 1.925 \quad , r = .988 \\ \text{LOWER - } d = .0037p + 1.785 \quad , r = .981 \end{array} \right\} \begin{array}{l} p = 0 \text{ to } 200 \\ \text{cm H}_2\text{O} \end{array}$$

Patel²¹, and Patel and Janicki²² also report the finding of linear p - d relationships for the main pulmonary artery, the left coronary circumflex artery, and the common carotid artery in dog by both in-vitro and in-vivo blood vessel segment testing. Thus, the finding of the linear calculated in-vivo p - d characteristic for the steer thoracic aorta in this study, based on in-vitro biaxial testing of the tissue, is confirmed by experimental investigations. It is likely that this linear characteristic is true for all major blood vessels under normal physiologic conditions and in healthy animals.

Figure 30 is a graph of mean wall diameter vs longitudinal location along the thoracic aorta tree for various pressures ranging from p = 0

to $p = 200 \text{ cm H}_2\text{O}$. The curves are distensibility curves since they reflect the variation or change in mean wall diameter with pressure, the rate of change of diameter relative to longitudinal location, and thus give an overall view of the tangential deformation or elasticity of the blood vessel. Superimposed at the mean pulsatile pressure of $155 \text{ cm H}_2\text{O}$ is the cyclic variation of mean wall diameter associated with the pulse pressure of $\pm 15 \text{ cm H}_2\text{O}$. Similar distensibility curves are not found in the literature since in-vitro and in-vivo testing of blood vessel segments precluded the gathering of such extensive data without considerable cost in both instrumentation and test time. This is probably why most experimental investigators have confined themselves to the recording of very local data and data associated generally with the pulse pressure loading of the vessel. Figure 30 is unique in its form.

Two common measures of blood vessel elasticity or distensibility used in reported in-vivo experiments are the percent change in mean wall radius ($\% \Delta R$) relative to the pulse mean pressure and the slope of the pressure-radius relationship, $\Delta R / \Delta p$, for either the pulse pressure range or over the full range of pressure. Using the data of Table 8 and the above equations, the values of $\% \Delta R$ and $\Delta R / \Delta p (\text{cm/cm H}_2\text{O})$ are tabulated below:

	UPPER	MIDDLE	LOWER
$\% \Delta R]_{\text{pulse}}$	± 2.8	± 2.4	± 1.8
$\Delta R / \Delta p]_{\text{pulse}}$	3.1×10^{-3}	1.95×10^{-3}	1.45×10^{-3}
$\Delta R / \Delta p]_{0 - 200}$	3.05×10^{-3}	1.90×10^{-3}	1.85×10^{-3}
V.D.	.487	.394	.280

and clearly indicates the decrease in vessel distensibility (increase in elasticity or stiffness) as the location (Z) increases distal to the ascending aorta. While no similar data exists for the thoracic aorta, Patel²¹, gives values of $\% \Delta R = \pm 8.3\%$ and $\Delta R / \Delta p = 4.0$ to 11.11 (7.45 mean) $\times 10^{-3}$ for the main pulmonary artery under distending pressures ranging from 12 to 27 cm H₂O. Thus, the thoracic aorta vessel is considerably stiffer than the thinner wall and lower pressure main pulmonary blood vessel.

Included in the above table is another index of vessel wall distensibility, volume distensibility (V.D.). Volume distensibility is defined as the percent change in lumen volume vs diastolic volume, per cm H₂O of pulse pressure. In terms of the nomenclature used in Table 8, volume distensibility can be defined as follows:

$$V.D. = \left[\frac{\Delta q_v}{[(q_v)_{140} \Delta P]} \right] \times 100, \quad \% \quad (53)$$

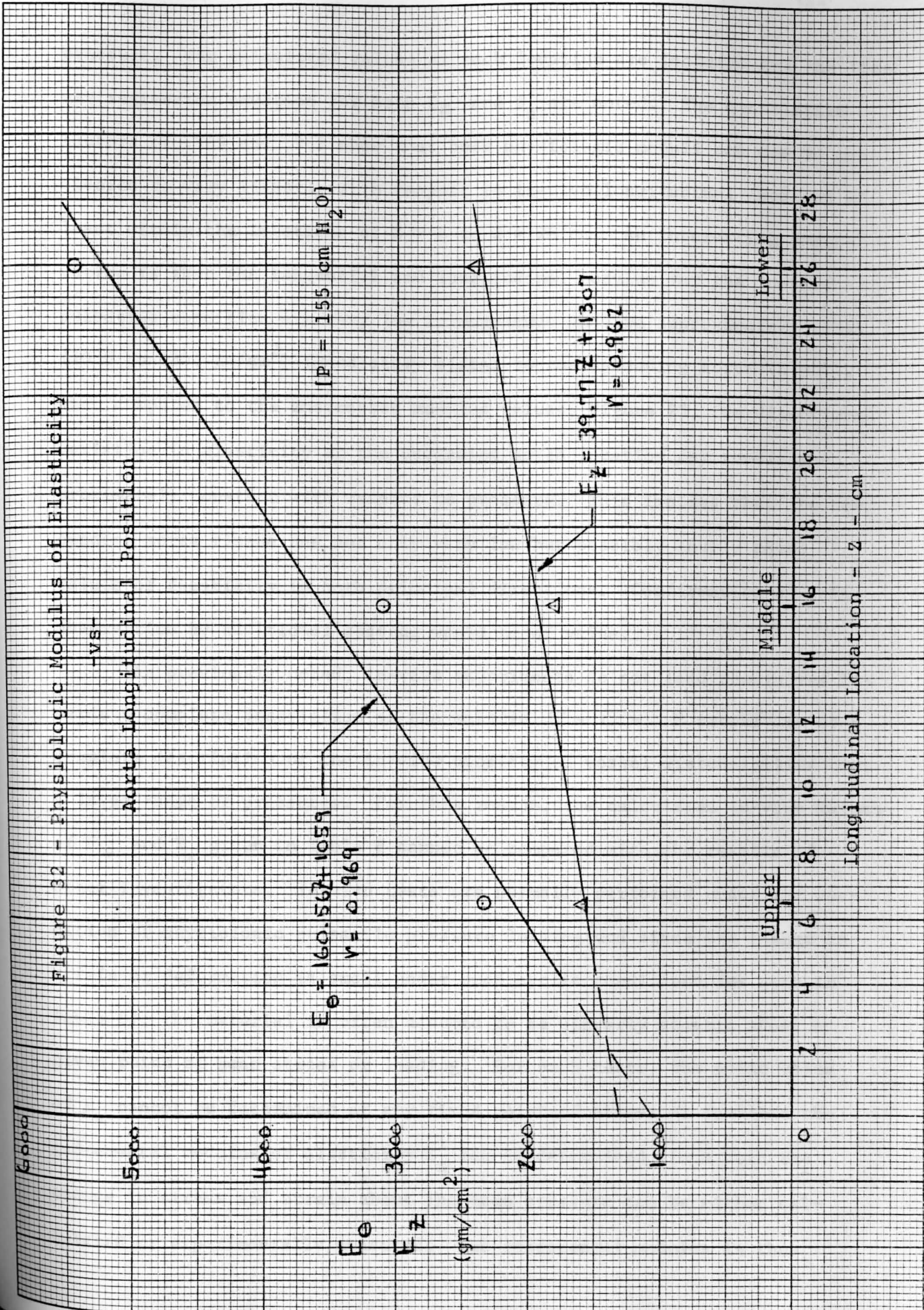
Comparing the in-vivo calculated values at the lower and upper locations, it is seen that the upper thoracic location is approximately 75% more elastic (or distensible) than that of the lower location. The values given above compare very favorably with the value of $.33 \pm .11$ given by Patel²⁰ for a segment of the descending aorta of the dog (in-vivo) at pressures of 140 to 189 cm H₂O. However, Patel²³ reports a value of $.42$ (average) for the ascending aorta which is less than the value of $.487$ given in the table at the location just distal to the ascending aorta. It is generally acknowledged that the ascending aorta is more distensible than the descending thoracic aorta. Using the data given in Table 1 of Patel²³, for ten dogs, the range of V.D. is calculated to be $.246$ to $.599$ for the ascending aorta.

In-vivo Modulus of Elasticity

As discussed in Chapters III and VI, the tangent modulus of elasticity of the aorta material is not a unique value, or a constant, as is normally the case for linear elastic isotropic materials. Rather, due to the non-linear anisotropic and orthotropic characteristic of the material, the modulus of elasticity is more accurately defined as the tangent modulus and is a unique function of the state of stress and its principal direction. To define the value of E as having a value of 3000 gm/cm^2 is meaningless unless the direction and magnitude of the stress or strain is also given since the value of E must be defined as a state point. Table 8 lists the values of E_{θ} and E_z for both the in-vitro and the in-vivo condition of $p = 155 \text{ cm H}_2\text{O}$ mean pulsatile pressure. It is seen from the table that the longitudinal modulus at each aorta location is approximately 100 to 120% larger in magnitude for the physiologic condition and that the tangential modulus increases approximately 125, 160, and 210% at the upper, middle, and lower aorta locations, respectively, when compared to the corresponding in-vitro values. Again, the general trend of increasing stiffness with respect to distal location is obvious but now the tangential percent increase is not constant with respect to location (for a fixed value of loading or pressure) but increases at a faster rate as location Z increases. This could be expected if one reviews the general $\sigma_e - \lambda_e$ and $\sigma_e - \epsilon_e$ curves of Chapters III and VI.

In Chapter VI, it was found, Figure 25, that the unstressed longitudinal modulus, E_z , varied linearly with location and that the unstressed tangential modulus, E_{θ_0} , was distinctly non-linear with respect to location along the aorta length. Figure 32 is a graph of E_{θ} and E_z relative to longitudinal location along the thoracic aorta at the physiologic mean

Figure 32 - Physiologic Modulus of Elasticity
-vs-
Aorta Longitudinal Position



pressure. The calculated values at each location are included and the linear regression equation for both E_{θ} and E_z are noted. The correlation factors of .969 and .962 show that both physiologic moduli can now be considered to vary linearly with respect to in-vivo longitudinal location at least within the locations of $Z = 4$ to $Z = 28$ cm. An interesting observation is that the tangential and longitudinal modulus for the in-vivo pulsatile condition are very low in magnitude and are approximately equal (1000 to 1300 gm/cm^2) immediately distal to the ascending aorta ($Z = 0$). When compared to the unstressed modulus values, Figure 25, the directional variation in elasticity at the ascending aorta location may remain approximately constant with respect to pressure. This implies that the ascending aorta tissue has not only very low but possibly nearly equal values of elasticity in both principal directions. Confirmation of this observation by additional testing would be of value.

As previously noted, in-vivo experiments do not lend themselves towards a complete description of the material $\sigma - \epsilon - E$ properties or a complete description of the in-vivo property of vessel distensibility over a large range of pressures. For this reason, the calculated in-vivo values of E_{θ} and E_z given in Table 8 cannot be compared with the results of other investigators. In-vivo tests are normally performed under the condition of physiologic pulsatile pressure loading and since the change in strain or deformation is small under such cyclic conditions (as seen in Table 8), the material is often assumed to be linearly elastic about a given point of mean stress or loading. For such tests, the point value of E_n cannot be determined at any fixed point of stress or load but the incremental modulus of elasticity E_n^1 can be determined since both the change in stress and strain about the mean pressure can be either calculated or experimentally measured. The incremental modulus is thus

defined as being the change in stress divided by the change in strain over the range of the pulsatile pressure, Δp , or

$$E_n^1 = \left[\Delta \sigma_n / \Delta \epsilon_n \right]_{\Delta p}, \quad \text{gm/cm}^2 \quad (54)$$

Using this definition of the incremental modulus, the value of the tangential incremental modulus, E_θ^1 , can be determined directly from Table 8. The incremental longitudinal modulus, E_z^1 , cannot be calculated since the analysis assumes that the longitudinal or tethering strain, λ_z , is constant and thus $E_z^1 \approx E_z$.

Since the radial stress-strain relations could not be determined from the biaxial test program for the material ($\sigma_r = 0$) the point value of E_r at the mean physiologic pressure also cannot be determined. However, using equation (33) and the values of Table 8, for $\lambda_z = 1.30$, the radial incremental modulus, E_r^1 , can be determined for the average pulsatile radial wall stress of $\Delta \sigma_r = -15 \text{ gm/cm}^2$. Since the incremental modulus is by definition the modulus about a point of changing strain it is also a close approximation of the actual point modulus at the mean state of pulsatile loading; or $E_r \approx E_r^1$.

The calculated values of the three incremental moduli are given below:

	<u>UPPER</u>	<u>MIDDLE</u>	<u>LOWER</u>
$E_\theta^1 =$	2510	3230	6160
$E_z^1 \approx$	1633	1800	2400
$E_r^1 \approx$	877	916	1260

and are applicable to the Kirchhoff measure of strain which is used throughout this study. Since the incremental modulus is a measure of the average

slope of the non-linearly increasing stress-strain characteristic of the material the values of E_{θ}^1 are larger than corresponding values of E_e by approximately 5 to 13%. Of prime interest in this table is the value of the incremental radial modulus E_r^1 which is an approximate measure of the actual point value of E_r at the mean pulsatile pressure. It is seen that the radial wall elasticity is very small relative to both E_{θ}^1 and E_z^1 , a point which is readily observed when attempting to measure the tissue thickness, as mentioned in Chapter III.

The values of the incremental tangent modulus can be compared with the in-vivo experimental results of Patel¹¹ for the middle descending thoracic aorta of the dog when modified to the conventional or Cauchy strain measure ($\bar{E}_e = \lambda_e - 1$) units. The values of the incremental longitudinal and radial modulus when modified cannot be directly compared due to the assumption of constant longitudinal strain used in this analysis, and the test methods used in the Patel experiments. The incremental tangential modulus \bar{E}'_e (Cauchy) using the nomenclature of this report and that of Patel is:

$$\bar{E}'_e = \left[\frac{\Delta \sigma_e}{\Delta \bar{E}} \right]_{\Delta P} = P_e / e_e \quad , \quad \text{gm/cm}^2 \quad (55)$$

The calculated values at each thoracic aorta location are given in the table on the following page where a comparison can be made with the in-vivo tangential values calculated using the Table 1 data contained in Patel's report. Patel measured incremental modulus for two different mean pressures and for two different ranges of the tangential extension ratio by virtue of his experimental set-up technique. The comparable range and mean pulsatile pressure of this study is also given. As previously noted, the test location chosen by Patel would be comparable to the locations of

this study defined as the middle and lower location. With this in mind, we see below that a reasonably good correlation exists between the predicted in-vivo values of 4200 to 8300 gm/cm² for this study, based on the in-vitro biaxial test results, and the experimental in-vivo values of 5800 to 8100 gm/cm² of Patel.

- \bar{E}'_e VALUES -

	UPPER	MIDDLE	LOWER	
Analysis	3525	4183	8340	$\lambda_e = 1.30$ to 1.40 $p = 155$ cm H ₂ O
Patel ¹¹ (Table 1 - group 1)	5805 to 6600 (MDTA)			$\lambda_e = 1.29$ to 1.45 $p = 145$ cm H ₂ O
Patel ¹¹ (Table 1 - group 2)	6631 to 8107 (MDTA)			$\lambda_e = 1.46$ to 1.55 $p = 154$ cm H ₂ O

Conclusion

As a result of the biaxial test program of Chapter V which facilitated the determination in Chapter VI of the in-vitro directional "stress-strain-elasticity" properties of the thoracic aorta tissue, it has been shown that the in-vivo or physiologic characteristics of the aorta blood vessel under the condition of pulsatile blood pressure can be predicted. The physiologic characteristics are defined at each of the three thoracic aorta locations in Table 8 for the pulsatile condition of loading and the variation of each important parameter with respect to internal blood pressure is contained in Figures 27 thru 30. The study of these parameters has resulted in an improved understanding of the affects of the pulsatile pressure loading upon the in-vivo blood vessel (such as a complete

description of vessel distensibility, and information pertaining to the longitudinal forces and shear strains acting between the blood vessel and the supporting perivascular tissue). Such quantitative information has not previously been available in the literature.

Of major significance is the fact that the analytically predicted vessel characteristics have been shown to agree reasonably well with the in-vivo experimental findings of other investigators using segments of the thoracic aorta of dog. The correlation of the calculated in-vivo parameters with the experimental findings reported in the literature implies confidence in the fact that the in-vitro material biaxial specimen test results can be used to predict with reasonable accuracy the in-vivo environment of the actual blood vessel.

CHAPTER VIII

SUMMARY

This study has been confined to three principal areas. Each is briefly discussed below and concluding comments are made.

Biaxial Test Apparatus

A relatively simple and inexpensive biaxial test set-up was designed and is described in Chapter V including the requirements of specimen environment which must be maintained during such in-vitro specimen testing. This experimental design proved adequate in achieving the end result which was the description of the passive or steady state directional stress-strain-elasticity properties of the steer descending thoracic aorta at three longitudinal aorta locations for the condition of plane stress loading. Similar experimental biaxial testing of any blood vessel tissue has not been previously accomplished by other investigators.

The experimental apparatus described in Figures 12 and 14 is adequate for 5 cm square specimens which satisfies the use of large animal blood vessels such as those of the steer. For smaller animals, including man, and for smaller blood vessels having unstressed diameters as small as 0.8 cm the basic design can be scaled down and with minor refinements would be satisfactory for 2.5 cm square specimens. The use of the extension gages (λ gages) of Figure 13 would be impractical for such small specimens as measurement of directional displacements presents a major problem. An optical method is visualized which would be satis-

factory and which would not require photographic techniques.

In-vitro Blood Vessel Tissue Properties

The in-vitro tangential and longitudinal stress-strain-elasticity properties of the non-linear anisotropic blood vessel tissue are contained in Chapter VI and are defined by equations (38) and (39) using the coefficient tables, Tables 5 and 6. The stress-strain, and tangent modulus-strain, properties are given at each of the three thoracic aorta longitudinal locations of Figure 4 and the variation of these tissue properties relative to the longitudinal location along the aorta tree are shown graphically in Figures 21 thru 25. By virtue of the plane stress loading of the specimen the properties of the tissue in the radial direction cannot be defined without testing under tri-axial loading conditions.

In-vivo Physiologic Predictions

Chapter VII has outlined the method whereby the in-vitro tangential and longitudinal plane stress properties of the tissue, determined in Chapter VI, can be used to predict the in-vivo physiologic state of the aorta blood vessel under physiologic pulsatile pressure loading. A summary of the calculated physiologic data is given in Table 8 and is shown graphically in Figures 27 thru 30. This data pertains to the in-vivo blood vessel geometry, wall stresses, elasticity, and the hemodynamic flow characteristics for both the unstressed state and the normal physiologic state of pulsatile pressure loading. A comparison of the calculated in-vivo blood vessel characteristics with the in-vivo experimental findings of other investigators, using blood vessel segments, has shown that the analytical in-vivo predictions

agree reasonably well with the reported experimental findings. The correlation between the two methods, analytical vs. experimental, indicates confidence in the fact that in-vitro biaxial test specimen results can be used to predict the in-vivo characteristics of the blood vessel material.

Notwithstanding the success of this study various improvements and modifications have been recommended in Chapters VI and VII which would more accurately assess the findings of this study. An ideal situation for further study would be a well conceived program supported by computer facilities whereby in-vivo measurements are made on living dogs initially and then followed by the conducting of in-vitro biaxial testing of the blood vessel tissue. Such a program, while costly and time consuming, would not only verify the accuracy of the correlation between the two methods but should also lead to refinements of the analytical techniques so that the need for future in-vivo testing would be minimal. The biaxial testing and the analytical in-vivo predictions based on such work could be extended to the major arteries and veins which constitute the local cardiovascular system supporting the heart and the major vessels of the animal body. Concurrently with the above investigations the variation of the two principal materials, elastin and collagen, with location along the blood vessel length and the affects of these quantitative variations upon the qualitative physical properties should be closely examined. The potential value of such studies, under both normal and abnormal physiologic conditions, is limited only to one's imagination.

BIBLIOGRAPHY

BOOKS

1. H. H. Dukes, The Physiology of Domestic Animals, (Comstock Publishing Associates, 7th edition, 1964) pp. 173.
2. Y. C. Fung, et al, Biomechanics - Its Foundations and Objectives, (Prentice-Hall, Inc., Englewood Cliffs, N. J. 1972) pp. 110.
3. D. H. Bergel, Cardiovascular Fluid Dynamics, (Academic Press, New York, 1972) Chapter 11, Volume II.
4. L. R. G. Treloar, The Physics of Rubber Elasticity, (Oxford University Press, London, 1958).
5. G. L. Humason, Animal Tissue Techniques, (W. H. Freeman Company, San Francisco, 1967).
6. F. R. Eirich, Rheology, (Academic Press, New York, Volume I, Chapter 10, 1956).
7. I. S. Sokolnikoff, Mathematical Theory of Elasticity, (McGraw-Hill Book Company, N. Y., 1956) Chapters I-III.
8. I. Mirsky, et al, Cardiac Mechanics, (John Wiley and Sons, N. Y., 1974) Chapters I and XI.

ARTICLES

9. D. H. Bergel, "The Static Elastic Properties of the Arterial Wall", Journal of Physiology, 156, pp. 445, 1961.
10. D. J. Patel, D. L. Fry, "Longitudinal Tethering of Arteries in Dogs", Circulation Research, XIX, pp. 1011, 1966.
11. D. J. Patel, et al, "Static Anisotropic Elastic Properties of the Aorta in Living Dogs", Circulation Research, XXV, pp. 765, 1969.
12. D. J. Patel, D. L. Fry, "The Elastic Symmetry of Arterial Segments in Dogs", Circulation Research, XXIV, pp. 1, 1969.
13. B. M. Learoyd, M. G. Taylor, "Alterations With Age in the Viscoelastic Properties of Human Aortic Walls", Circulation Research, 18, pp. 278, 1966.

14. T. E. Carew, et al, "Compressibility of the Arterial Wall", Circulation Research, XXIII, pp. 61, 1968.
15. Y. Lanir, Y. C. Fung, "Two-Dimensional Mechanical Properties of Rabbit Skin - I. Experimental System", Journal of Biomechanics, 7, pp. 29, 1974.
16. Y. Lanir, Y. C. Fung, "Two-Dimensional Mechanical Properties of Rabbit Skin - II. Experimental Results", Journal of Biomechanics, 7, pp. 171, 1974.
17. M. G. Sharma, "Viscoelastic Behavior of Conduit Arteries", Biorheology, II, pp. 279, 1974.
18. R. N. Vaishnav, et al, "Nonlinear Anisotropic Elastic Properties of the Canine Aorta", Biophysical Journal, 12, pp. 1008, 1972.
19. R. S. Rivlin and D. W. Saunders, "Large Elastic Deformations of Isotropic Materials", Proceedings of the Royal Society, Vol. 243, pp. 34, 1951.
20. D. J. Patel, et al, "Aortic Mechanics in the Living Dog", Journal of Applied Physiology, 16(2), pp. 293, 1961.
21. D. J. Patel, et al, "Mechanical Properties and Dimensions of the Major Pulmonary Arteries", Journal of Applied Physiology, 15(1), pp. 92, 1960.
22. D. J. Patel, J. S. Janicki, "Static Elastic Properties of the Left Coronary Circumflex Artery and the Common Carotid Artery in Dogs", Circulation Research, 27(2), pp. 149, 1970.
23. D. J. Patel, D. L. Fry, "In Situ Pressure-Radius-Length Measurements in Ascending Aorta of Anesthetized Dogs", Journal of Applied Physiology, 19(3), pp. 413, 1964.